Dissertation

Submitted to the
Combined Faculties for the Natural Sciences and for Mathematics
of the Ruperto-Carola University of Heidelberg, Germany
for the degree
of Doctor of Natural Sciences

presented by

Christian Neufeld, Dipl. Biochem.
born in Ludwigshafen, Germany
Oral-examination: _____

Pex14p and its Ligands,
Structural Basis of the Early Steps of Peroxisomal Protein Import

Referees: Prof. Dr. Irmgard Sinning

Dr. Michael Sattler

Table of contents

Zusammenfassung

Peroxisomaler Proteinimport erfolgt mit Hilfe einer speziellen Translokalisations-Machinerie an der peroxisomalen Membran. Obwohl die beteiligten Proteine während der letzten Jahre identifiziert wurden, sind Details zum Mechanismus der Translokalisation noch nicht bekannt. Aktuelle Ergebnisse lassen auf ein „cycling receptor“ Model schließen, welches aus „cargo recognition“ (der Aufnahme von peroxisomalen Matrixproteinen im Cytosol), dem „docking“, der Abgabe der aufgenommen Proteine ins peroxisomalen Lumen und dem Rezeptor Recycling besteht.

Das membranassozierte Peroxin Pex14p wird im Allgemeinen als eine Hauptkomponente des peroxisomalen „Docking“-Komplexes angesehen. Es interagiert neben einigen membrangebundenen Peroxinen mit den PTS-Rezeptoren Pex5p und Pex7p und besteht aus drei Domänen: einem konservierten N-terminus, einer hydrophoben Region und einer coiled-coil Domäne. Die N-terminale Domäne erkennt sogenannte WxxxF/Y-Motive, konservierte aromatische Sequenzen im PTS1-Rezeptor Pex5p. Obwohl es kein klassisches WxxxF/Y Motiv aufweist bindet Pex19p, ein Protein mit einer Schlüsselfunktion in der peroxisomalen Biogenese, dieselbe N-terminale Domäne von Pex14p wie Pex5p.

In der vorliegenden Arbeit wurden funktionelle und strukturelle Studien am N-terminalen Tel von Pex14p durchgeführt. Die erhaltenen 3-dimensionalen Modelle beschreiben ein 3-Helix Bündel, das eine hydrophobe Interaktionsfläche für amphipatische, helikale Liganden darstellt. Der Vergleich zwischen der Komplexstruktur von Pex14p (aa 16-80W)-Pex5p (aa 116-124) mit der von Pex14p (aa 16-80W)-Pex19p (aa 66-77) zeigt dass beide die gleich Bindestelle besetzen, wobei Pex19p eine unerwartete invertierte Orientierung aufweist. Die Strukturdaten wurden durch NMR Titrations- und ITC-Experimente ergänzt, welche die kompetitive Bindung von Pex5p und Pex19p bestätigten und Pex5p als den stärkeren Liganden charakterisieren. Die so gewonnen Ergebnisse erlauben einen Einblick in die molekularen Abläufe während der frühen Schritte des peroxisomalen Imports und implizieren Voraussetzungen die mögliche Pex14p-Interaktionspartner erfüllen sollten.

Abstract

Peroxisomal matrix protein import is mediated by a distinct translocation machinery at the peroxisomal membrane. Although the components involved have been identified during the last years, details of the translocation mechanism are still unknown. Current evidence favour a cycling receptor model, consisting of cytosolic cargo recognition, docking, cargo release and receptor recycling. The membrane associated peroxin Pex14p has been proposed as a main component of the peroxisomal docking complex. It interacts with the PTS receptors as well as with several membrane-bound peroxins. Pex14p consist of three major domains, e.g. a conserved N-terminus, a hydrophobic region and a coiled coil domain. The N-terminal domain recognizes a conserved aromatic motif which is part of the PTS1 receptor Pex5p and called WxxxF/Y motif (Saidowsky et al 1999). Although the peroxisomal biogenesis factor Pex19p has no classical WxxxF/Y motif, it has been described as interacting with the same N-terminal domain of Pex14p as Pex5p (Fransen et al. 2004). This work presents functional und structural studies of the N-terminus of Pex14p. The obtained 3-dimensional models describe a three-helical-bundle providing a hydrophobic interaction surface for an amphipathic, helical ligand. Comparison of the N-Pex14p-Pex5p and N-Pex14p-Pex19p complex structure shows that both ligands occupy the same binding pocket, wherein Pex19p exerts an unexpected reverse orientation. The structural data was supplemented with NMR titration and ITC data confirming the binding of Pex5p and Pex19p as competitive and characterizing Pex5p as the stronger ligand. These results provide insights into the molecular recognition mechanisms of the early steps of peroxisomal import and might implicate prerequisites for possible interaction partners of Pex14p.

Abbreviations

Å	Ångström ($1x10^{-10}$m)
AAA	ATPases associated with diverse cellular activities
ATP	adenosine tri phosphate
B	strength of an external magnetic field
DNA	desoxyribonucleic acid
E. coli	*Escherichia coli*
EDTA	ethylenediaminetetraacetic acid
ER	endoplasmatic reticulum
HEPES	N-(2-hydroxyethyl)piperazine-N'-2-ethanesulfonic acid
His_6	hexahistidine
H.polymorpha, Hp	*Hansuela polymorpha*
HSQC	heteronuclear single quantum coherence spectroscopy
γ	gyromagnetic ratio
I	spin angular momentum (vector)
I	spin quantum number
IPTG	isopropyl-β-D-thiogalactopyranoside
ITC	isothermal titration microcalorimetry
$\mathbf{K_a}$	molar association constant
$\mathbf{K_d}$	molar dissociation constant
LB	Luria Bertani bacterial growth medium
m	magnetic quantum number
$\mathbf{M_{z,eq}}$	longitudinal magnetization
$\mathbf{M_{x,y}}$	transvers magnetization
mPTS	peroxisomal membrane protein targeting signal
Ni-NTA	nickel nitrilotriacetic acid
NMR	nuclear magnetic resonance spectroscopy
NOE	nuclear Overhauser effect
NOESY	nuclear Overhauser and exchange spectroscopy
PAH2	paired amphipathic helix (domain) 2
PBD	peroxisomal biogenesis disorder
PCR	polymerase chain reaction
PEX	gene encoding peroxin or Pex protein

Pex5p(L)	peroxin 5 protein, long isoform containing 37 extra residues (1-639)
PMP	peroxisomal membrane protein
ppm	parts per million
PTS1	peroxisomal targeting signal type 1
PTS2	peroxisomal targeting signal type 2
R	gas constant, 8.314 J/mol/K
RDC	residual dipolar coupling
RING	really interesting new gene (zinc binding proteins)
RNA	Ribonucleic acid
S.cerevisiae, Sc	*Saccharomyces cerevisiae*
SCP2	sterol carrier protein 2, PTS1 containing protein
SDS-PAGE	sodium dodecyl sulphate polyacrylamide gel electrophoresis
SH3	type three Src homology domain
SRP	signal recognition particle
TAE	tris acetic acid / ethylenediaminetetraacetic acid
TEV	tobacco etch virus protease
TOCSY	total correlation spectroscopy
TPR	tetratricopeptide repeat motif
Tris	tris(hydroxymethyl)aminomethane
UV	ultra-violet light
WD-40	short ~40 amino acid motifs, often terminating in Trp-Asp (W-D)
Y. lipolytica, Yl	*Yarrowia lipolytica*

1 Introduction

1.1 Peroxisomes

Peroxisomes are ubiquitious, eukaryotic cell organelles surrounded by a simple lipid-bilayer and varying in size, number and protein composition depending on cell type and species. Peroxisomes were named by de Duve and Baudhuin (1966) for the hydrogen peroxide which is accumulated during many of the metabolic processes inside peroxisomes and then degraded by the enzyme catalase. Beside the hydrogen peroxide respiration there are two other generally conserved functions of peroxisomes: β-oxidation of fatty acids and response to oxidative stress. A large variety of other metabolic processes have been described. This includes the glyoxylate cycle in fungal and plant glyoxysomes, photorespiration in plant leaf peroxisomes or methanol and amino oxidation in yeast. In mammals peroxisomes contribute to ether phospholipid and cholesterol biosynthesis, phytanic acid α-oxidation or xenobiotic detoxification (reviewed by Brown and Baker, 2003; Eckert and Erdmann, 2003; Purdue and Lazarow, 2001a). Although mammal mitochondria are capable of carrying out β-oxidation of fatty acids, very long chain fatty acids and other substrates inaccessible to the mitochondrial enzyme machinery are shortened by peroxisomal β-oxidation enzymes (reviewed by Clayton, 2001; reviewed by Wanders et al., 2001).

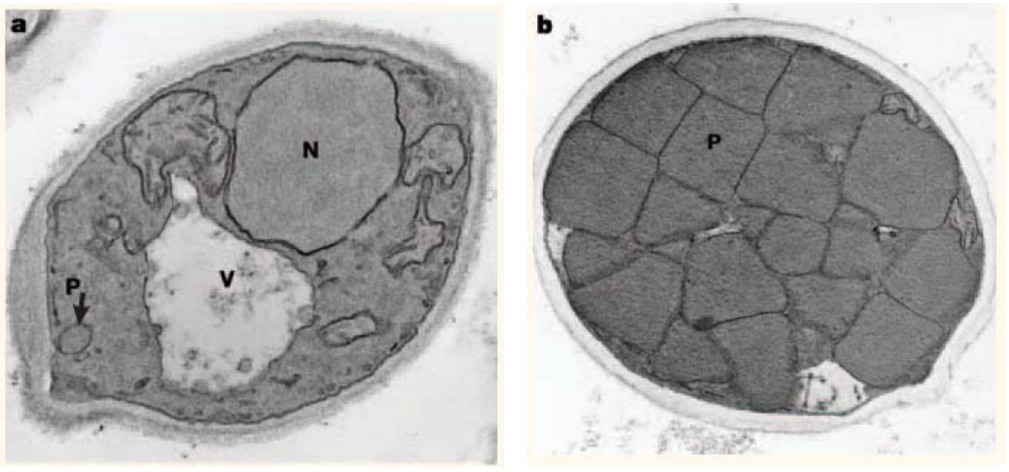

Fig1.1: Peroxisomes. Cells which were grown with glucose as carbon source contain a few small peroxisomes (**a**), whereas cells that were grown with methanol in the medium are filled with large peroxisomes which may take up more than 80% of the entire cell volume (**b**) (Erdmann and Schliebs, 2005)

1.2 Peroxisomal diseases

Several inherited diseases caused by impaired peroxisomal function have been identified so far. They can be categorized into two main classes; one is characterized by malfunction of a single peroxisomal enzyme, the other by defects in peroxisomal biogenesis. Examples for class one are Acyl CoA oxidase deficiency or X-linked adrenoleukodystrophy.
Class two can be divided into two subclasses. One subclass is characterized by loss of multiple peroxisomal functions normally caused by mutation of a single PEX gene. For example rhizomelic chondrodysplasia is caused by mutation of PEX7. The second subclass of peroxisomal biogenesis diseases is caused by mutations in multiple PEX genes und results in a general loss of peroxisomal function. These diseases, such as Zellwegers syndrome, neonatal adrenoleukodystrophy and infantile Refsum disease, differ in severity and patients survivability ranges from less than one year (Zellwegers syndrome) up to thirty years (infantile Refsum disease) (reviewed by Weller et al., 2003)

1.3 Identification of peroxins

Genetic complementation of yeast strains unable to grow on carbon sources that require functional peroxisomes for their metabolites, has led to the classification of the so called onu mutations (oleat non utilizers) which can be divided into two subgroups, the *fox* mutants (fatty acid oxidation) with defects in enzymes of the β-oxidation of fatty acids and the *pex* mutations (peroxisomal assembly) which are described by mislocalization of peroxisomal membrane or matrix proteins (Erdmann and Kunau, 1992; Erdmann et al., 1989). More recently, knock-out mouse models and RNA interference supplemented the complementation analysis and provided the tools for investigation of peroxisomal disorders in a disease context (Baumgart et al., 2003; Thieringer et al., 2003; Weller et al., 2003). So far 32 PEX genes and proteins derived of, called peroxins, were identified and categorized by localization and function (Table 1.1)

Table 1.1: Overview of peroxins identified to date

(adapted from Eckert and Erdmann, 2003; Wagner et al., 2005)

gene	identified in				proposed characteristics functions	localization	interacting peroxisomes
	yeasts	mammals	plants	Other			
PEX1	+	+	+	*Dm*	AAA-protein required for peroxisomal matrix import	mainly cytosolic	6
PEX2	+	+	+		RING zinc finger protein, matrix protein import, receptor recycling	iPMP*	10
PEX3	+	+	+		PMP import, membrane biogenesis	iPMP	19
PEX4	+	+	+		E2-ubiquitin conjugating enzyme	pPMP**	22
PEX5	+	+	+	*Dm, Cl, Ld, Tb*	TPR-protein, PTS1 receptor	mainly cytosolic	7, 8, 10, 12, 13, 14
PEX6	+	+	+	*Cl*	AAA-protein, required for matrix protein import	mainly cytosolic	1, 15/26
PEX7	+	+	+		WD-protein, PTS2 receptor	mainly cytosolic	5, 13, 14, 18, 20, 21
PEX8	+				matrix protein import	luminal	5, 20
PEX9	+				matrix protein import	iPMP	
PEX10	+	+	+		RING zinc finger protein, matrix protein import, receptor recycling	iPMP	2, 5, 12, 19
PEX11	+	+	+	*Cl, Tb*	peroxisome proliferation/ division	iPMP	19
PEX12	+	+	+	*Cl*	RING zinc finger protein, matrix protein import, receptor recycling	iPMP	5, 10, 19
PEX13	+	+	+	*Cl*	SH3-protein, matrix protein import, receptor docking	iPMP	5, 7, 14, 19
PEX14	+	+	+		matrix protein import, receptor docking	PMP	5, 7, 13, 17, 19
PEX15	+				membrane anchor, matrix protein import	iPMP	6
PEX16	+	+	+		PMP import	iPMP	19
PEX17	+		+		matrix protein import, receptor docking	pPMP	14, 19
PEX18	+				auxiliary protein, PTS2 import	mainly cytosolic	7
PEX19	+	+	+	*Cl*	farnesylated, peroxisomal biogenesis, PMP receptor	mainly cytosolic	3, 10, 12, 13, 14, 16, 17, 11a/b
PEX20	+				PTS2 matrix protein import	mainly cytosolic	
PEX21	+				auxiliary protein, PTS2 import	mainly cytosolic	7, 13, 14
PEX22	+				membrane anchor, matrix protein import	iPMP	4
PEX23	+				matrix protein import	iPMP	
PEX24	+				peroxisomal proliferation and abundance	iPMP	
PEX25	+				peroxisomal proliferation and abundance	pPMP	27
PEX26		+			membrane anchor, matrix protein import (human equivalent of Pex15p)	iPMP	6
PEX27	+				peroxisomal proliferation and abundance	pPMP	25
PEX28	+				peroxisomal proliferation and abundance	iPMP	
PEX29	+				peroxisomal proliferation and abundance	iPMP	
PEX30	+				peroxisomal proliferation and abundance	iPMP	28, 29,31, 32
PEX31	+				peroxisomal proliferation and abundance	iPMP	28, 29,30, 32
PEX32	+				peroxisomal proliferation and abundance	iPMP	28, 29,30, 31

*iPMP: integral peroxisomal membrane protein; **pPMP: peripheral peroxisomal membrane protein

Cl = Caenorhabditis. elegans; *Dm = Drosophila melanogaster*; *Tb = Trypanosoma brucei*

1.4 Peroxisomal Biogenesis and the role of Pex19p

Upon the first biological and biochemical characterization of peroxisomes two different models for peroxisomal biogenesis were proposed. While De Duve and Baudhin ((1966)) discussed the possibility of peroxisomes as autonomous organelles evolved from an endosymbiont, already 1964 Novikoff and Shin proposed the possibility of peroxisomes budding from the endoplasmatic reticulum. Lazarow and Fujiki (1985) described an ER-independed "growth and division" model, which excluded *de novo* synthesis and suggested peroxisomes proliferation exclusively by division of pre-existing ones. South and Gould (1999) proposed two overlapping pathways, one based on the division of mature peroxisomes mediated by Pex11p and the other on the conversion of pre-existing proto-peroxisomes by Pex16p. More recently, evidence supporting the ER as the origin of peroxisomes is rising (reviewed by Tabak et al., 2003; Titorenko and Rachubinski, 1998). Geuze at al. (2003) showed that the peroxisomal membrane proteins Pex13p and PMP70 could be found in subdomains of the ER continuous with peroxisomes. Hoepfner et al. (2005) demonstrated that the insertion of Pex3p into the ER and the recruitment of Pex19p lead to formation of peroxisomal membrane vesicles, giving rise to the assumption that peroxisomes receive their membrane exclusively from this organelle. In this new model (reviewed by Kunau, 2005), Pex3p and Pex19p, possibly under assistance of Pex11p and the dynamin-like protein Vps1p (Hoepfner et al., 2001), trigger the budding of a peroxisomal membrane from the ER. Peroxisomal membrane proteins (PMPs) are imported and, as soon as the translocation machinery is established, the peroxisome is filled with matrix proteins. Pex19p plays a major role in the import of PMPs and has been proposed as a cycling receptor for proteins carrying an mPTS (a targeting signal for peroxisomal membrane proteins) and/or, in complex with Pex3p, as a regulator for insertion and assembly of PMPs at the peroxisomal membrane. Apart from its function as receptor and regulator, Pex19p it has been described as a chaperone for newly synthesized PMPs in the cytosol (reviewed by Schliebs and Kunau, 2004).

1.5 Peroxisomal Protein Import

1.5.1 Targeting sequences

The import of cytosolic synthesized proteins into cell organelles requires the presence of special targeting sequences (Blobel and Dobberstein, 1975). Peroxins are synthesized at free ribosomes and posttranslationally imported into peroxisomes. During this process two peroxisomal targeting signals (PTS) play a crucial role. The vast majority of peroxisomal matrix proteins contain a PTS1, which consists of a C-terminal tripeptide with the consensus sequence (S/A/C)-(K/R/H)-L. The PTS2 sequence consists of an N-terminal nonapeptide with the consensus (R/K)(L/I/V)X5(H/Q)(L/A) (de Hoop and Ab, 1992) and is less common compared to PTS1. Furthermore proteins lacking a peroxisomal targeting sequence can be imported "piggyback" by PTS1 or PTS2 proteins (Glover et al., 1994; McNew and Goodman, 1994).

1.5.2 PTS-receptors and import models

The PTS sequences are recognized by two different proteins, the PTS1 receptor Pex5p and the PTS2 receptor Pex7p. The C-terminus of Pex5p consists of 7 tetratricopeptide repeats (TPR) and a C-terminal helix bundle which together form a ring like structure upon ligand binding(Gatto et al., 2000; Stanley et al., 2006). No structural data is available for the PTS2 receptor, but homology prediction characterizes Pex7p as a member of the family of WD40 proteins which adopt a β-propellar structure (Purdue et al., 1997; Rehling et al., 1996). While Pex5p is capable to direct its cargo to the peroxisomal membrane on its own, Pex7p requires the assistance of auxiliary proteins, such as Pex18p and Pex21p in *S.cerevisiae*, Pex20p in *Y. lipolytica* or a long isoform of Pex5p in mammals (Einwachter et al., 2001; Purdue et al., 1998; Schafer et al., 2004; Titorenko et al., 1998).

To explain the different localization of the receptors, which could be detected in the cytosol, at the peroxisomal membrane and in the peroxisomal lumen, several models have evolved during the years. All of them have four steps in common: cargo recognition in the cytosol by a PTS-receptor, docking to the peroxisomal membrane, dissociation of the receptor-cargo-complex and recycling of the receptor. (Fig. 1.5)

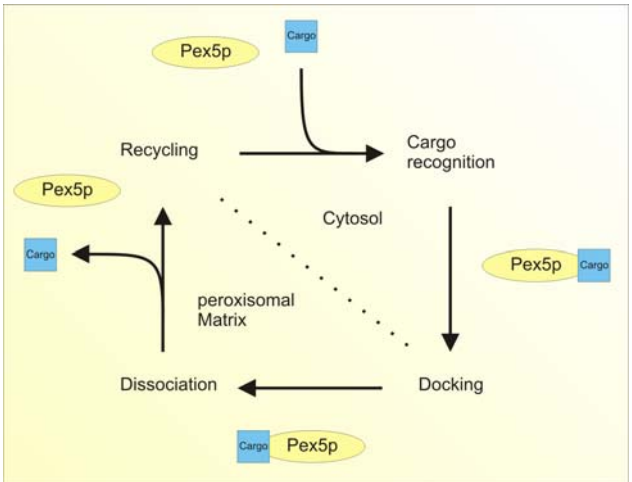

Fig 1.5: The four steps of PTS1 import. Cargo recognition, docking, dissociation and receptor recycling

A first approach to explain the processes involved in peroxisomal protein import was the "simple shuttle" model. The receptor transports the cargo to the membrane, releases the cargo to the translocation machinery and travels back to the cytosol (Marzioch et al., 1994). The original model was expanded to the "extended shuttle" theory, where the receptor together with the cargo is translocated over the membrane and enters the peroxisomal lumen (Rachubinski and Subramani, 1995). This hypothesis was supported by studies of Dammai et al. (2001), who could demonstrate that at least parts of the PTS1-receptor Pex5p are exposed to the peroxisomal matrix. The latest model of peroxisomal protein import is the "transient pore" model (Erdmann and Schliebs, 2005), which combines the ability of Pex5p to integrate into peroxisomal membranes (Oliveira et al., 2003) and its ubiquitination (Kiel et al., 2005; Kragt et al., 2005) with the existing shuttle models. It describes Pex5p as the key component of a transient pore that is characterized by a high flexibility in size, formation and disassembly.

1.5.3 Membrane bound components of the peroxisomal import machinery

In addition to the presence of PTS receptors, all models implicate the involvement of other components in the process of translocation through the peroxisomal membrane. The integral membrane protein Pex13p, Pex14p and, in yeast, the Pex14p-associated Pex17p (Huhse et al., 1998), were proposed as components of the docking complex (reviewed by Erdmann and Schliebs, 2005). Pex14p is essential for the import of peroxisomal matrix proteins and binds to the PTS-receptors Pex5p and Pex7p (Albertini et al., 1997). Pex14p deletion mutants exert defect in both import ways (Girzalsky et al., 1999). Pex13p also interacts with both PTS-receptors and with Pex14p (Elgersma et al., 1996; Erdmann and Blobel, 1996; Girzalsky et al., 1999) implicating a role in the docking process.

The RING (really interesting new gene) finger PMPs, Pex2p, Pex10p and Pex12p are widely thought to act downstream of receptor docking and are possibly involved in translocation of Pex5p or recycling of the PTS1 receptor via ubiquitination (reviewed by Erdmann and Schliebs, 2005; reviewed by Gould and Collins, 2002). Agne et al. (2003) have demonstrated that, in *S.cerevisiae* the docking proteins are linked with the RING finger complex within the peroxisomal matrix by the membrane associated protein Pex8p. So far, no Pex8p could be identified in mammals.

Epistasis analysis suggest a role of the peroxins Pex4p and Pex22p as well as Pex1p and Pex6p, downstream of the RING finger proteins (Collins et al., 2000). Pex4p, an E2 ubiquitin conjungating enzyme (Wiebel and Kunau, 1992), is anchored to the cytosolic site of the peroxisomal membrane via Pex22p. Together with the Pex2/10/12p complex - the RING finger motif is a common domain of E3 ubiquitin ligases (reviewed by Pickart, 2001). These proteins are thought to be involved in ubiquitination of Pex5p and receptor recycling (reviewed by Erdmann and Schliebs, 2005; reviewed by Purdue and Lazarow, 2001b). The peroxins Pex1p and Pex6p belong to the family of AAA-proteins (ATPase associated with various cellular activities) and interact physically as well as functionally. They are associated with the peroxisomal membrane via Pex15p in yeast or its orthologue Pex26p in mammals. The AAA complex has been proposed to play a role in an energy depending dislocation of the PTS1-receptor from the peroxisomal membrane (Erdmann and Schliebs, 2005; Gould and Collins, 2002).

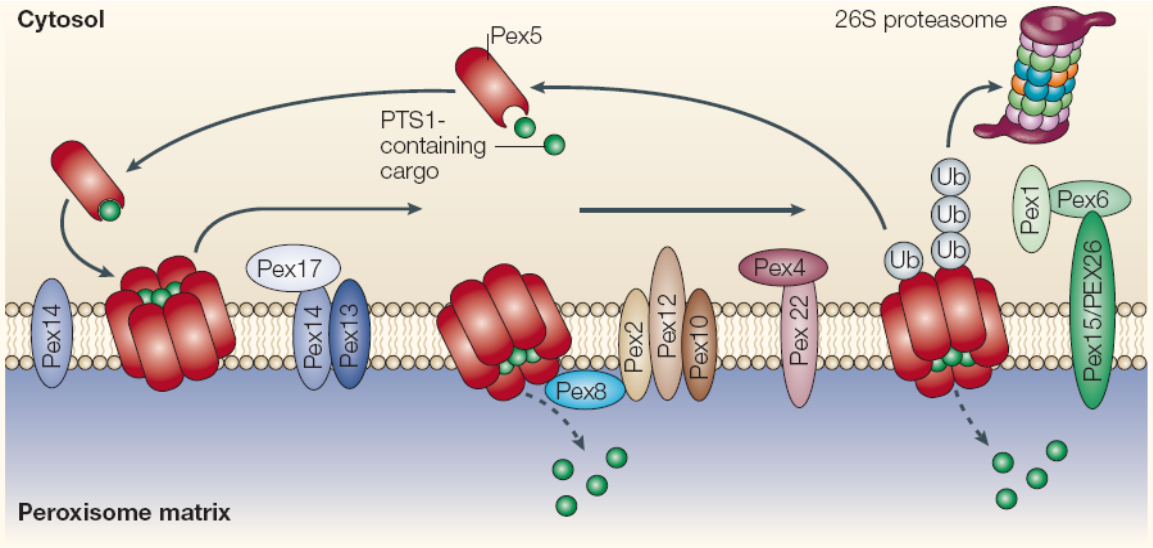

Fig. 1: The transient pore model (adopted from Erdmann & Schliebs, 2005)

Pex5p recognizes the PTS1 protein in the cytosol and transports the cargo to the peroxisomal membrane. It inserts into the peroxisomal membrane and becomes an integral part of the import machinery. The docking proteins Pex14 and Pex13p (and in yeast Pex17p) are possibly involved in tethering the receptor to the membrane and in assembly, stabilization and rearrangement of the translocon. Cargo release is suggested to be triggered by Pex8p which contains a PTS1 sequence. Recycling and disassembly is thought to be ATP depended and requires the AAA+ peroxins Pex1p and Pex6p which are anchored to the peroxisomal membrane by Pex15p (or the human orthologue Pex26p). The disassembly and recycling process could be regulated by ubiquitination, possibly carried out by Pex4p an E3 type conjugation enzyme and the RING finger peroxins Pex2p, Pex10p and Pex12p. In this case monoubiquitination would lead to receptor recycling, polyubiquitination to degradation.

1.6 The peroxin Pex14p and its ligands

Pex14p, as mentioned above, is thought to be part of the peroxisomal docking complex and one of the initial contact points for the PTS receptors. Depending on the organism it has been described to be an integral membrane protein or as membrane associated via a hydrophobic region (Albertini et al., 1997; Will et al., 1999). Pex14p contains at least one coiled-coil region, which allows the formation of homo-dimers (Oliveira et al., 2002). It has been suggested that in the hydrophobic domain of human Pex14p, two interaction motifs (AxxxA and GxxxG) together with the coiled-coil domain are responsible for homo-oligomerization of Pex14p (Itoh and Fujiki, 2006). The N-terminus of Pex14p is well conserved among species and interacts with the PTS1 receptor Pex5p, another component of the docking complex,

Pex13p, and with the multifunctional protein Pex19p (Albertini et al., 1997; Brocard et al., 1997; Sacksteder et al., 2000). The Pex14p-Pex5p interaction is mediated by a di-aromatic pentapeptide sequence motif (WxxxF/Y) in the N-terminal half of Pex5p (Schliebs et al., 1999). A second Pex5p binding site, independent of the WxxxF/Y motif, and a binding site for the PTS2-receptor Pex7p have been reported to be present at the C-terminus of *S.cerevisiae* Pex14p (Niederhoff et al., 2005; Williams et al., 2005).

Pex13p has been described as an integral membrane protein with two transmembrane domains and a cytosolic N- and C-terminus (Erdmann et al., 1996). The N-terminal half of Pex13p interacts with the PTS-receptors Pex5p and Pex7p, the C-terminal half contains a type three Src homology (SH3) domain and interacts with Pex14p (Fransen et al., 1998; Otera et al., 2002). An additional intraperoxisomal Pex14p-binding site has been reported in yeast (Schell-Steven et al., 2005). Douangamath et al. (2002) showed that the *Sc*Pex13p SH3 domain binds two distinct epitopes simultaneously. While the interaction with *Sc*Pex14p is mediated by a classical type two PxxP motif, *Sc*Pex5p binds *Sc*Pex13p via a non-classical WxxxF/Y motif, which displays no Pex14p binding (Williams et al., 2005). In humans, the homologous WxxxF/Y motif responsible for Pex13p interaction shows no Pex14p binding (Saidowsky et al., 2001). The interaction of *S.cerevisiae* Pex5p with Pex14p was reported to be mediated by an inverse WxxxF/Y (Williams et al., 2005). Human Pex5p contains five WxxxF/Y motifs (the long isoform of Pex5p contains an additional one) in its N-terminal half, which are able to bind Pex14p *in vitro* (Saidowsky et al., 2001). The reason for this multiplicity has not yet been fully explained. *In vivo* data about the stoichiometry of the mammalian Pex14p-Pex5p complex is contradictory, the described stoichiometries reach from 1 to 1(Itoh and Fujiki, 2006) to 5 to1 (Gouveia et al., 2000), and an exact quantitative determination still remains to be carried out..

Fransen et al (2005) were able to specify a region in the N-terminus of Pex19p that contains several aromatic residues. This non-classical WxxxF/Y motif interacts with the same conserved N-terminal domain present in Pex14p as Pex5p and Pex13p (Fransen et al., 2004). While Pex14p can bind Pex19p and Pex13p simultaneously, no complex of Pex14p, Pex5p and Pex19p has been reported (Itoh and Fujiki, 2006).

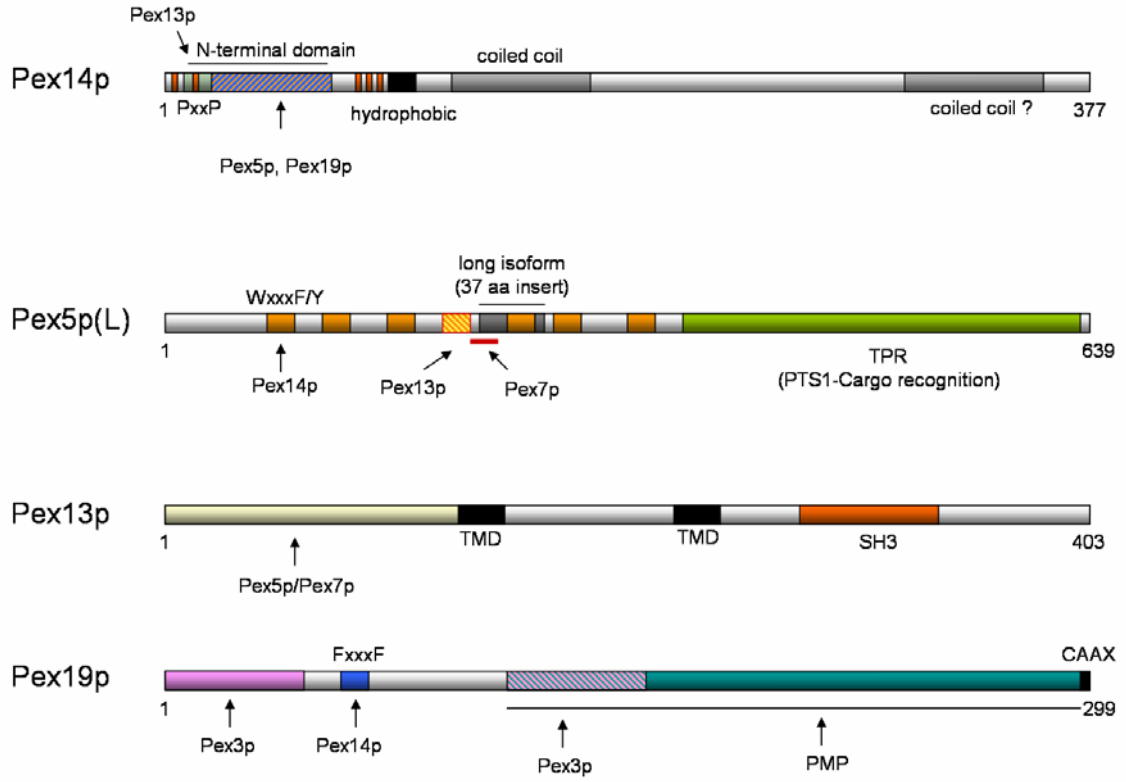

Fig 1.6: Domain composition of human Pex14p, Pex5p(L) and Pex19p. Pex14p contains a conserved N-terminal domain (aa 23-73), a hydrophobic region (aa 110-138) and a predicted coiled coil region (aa 157-197). Depending on the prediction algorithm an additional coiled-coil domain in the C-terminus is proposed. The N-terminal domain interacts with Pex13p, Pex5p and Pex19p. The N-terminus of Pex14p contains several non canonical PxxP motifs (aa 7-13, 21-27, 85-91, 86-92, 95-101). Pex5p(L) has seven WxxxF/Y motifs (W1 118-122; W2 140-144; W3 159-163; W4 184-188); W5 243-247; W6 257-261; W7 308-312), whereas W4 overlaps with the Pex13p binding site (aa 184-192) and does not interact with Pex14p. A stretch of 37 amino acids (aa 215-251) allows the long isoform of Pex5p to interact with Pex7p (aa 192-222). PTS1 cargo recognition is carried out by the C-terminal TPR domains (aa 335-589). Pex13p contains two transmembrane regions (aa 136-158 and aa 227-251) and a C-terminal SH3 domain. The N-terminus of Pex13p interacts with Pex5p and Pex7p. Pex19p shows two Pex3p binding sites, an N-terminal one (aa 1-51) and one overlapping with the interaction site of peroxisomal membrane proteins. Pex14p-Pex19p interaction is mediated by an aromate-rich motif (aa 66-77). A C-terminal CAAX-motif of Pex19p is responsible for farnesylation of the protein.

1.7 Objectives of this thesis

One of the major implications of proteins lies in their ability to interact with each other via specific binding. This directed association of peptide or protein molecules can be transient or permanent and is determined by the individual biochemical and biophysical properties of the interaction partners. To describe the mechanism of how proteins are able to discriminate among the multiplicity of possible interaction partners is certainly one of the major tasks in structural biology. The N-terminus of Pex14p constitutes the point of convergence of at least three different interaction partners and provides therefore an excellent target for studies of protein-protein interactions. The focus of this work laid on determination of a high resolution structure of N-terminal Pex14p and one of its ligand. Special attention was directed to the interaction of Pex14p with the PTS1 receptor Pex5p as well as the multifunctional protein Pex19p and the molecular details of interaction, i.e. how does the conserved WxxxF/Y of Pex5p mediate the binding? Is the binding of Pex19p and Pex5p competitive? Which protein is the stronger ligand? How does Pex19p bind Pex14p without a WxxxF/Y motif?

The initial approach to address these questions was X-ray crystallography. As a prerequisite to this method large scale protein purification and *in vitro* complex formation of N-Pex14p and its ligands needed to be established. However, when it became apparent that crystallization trails continued to fail, the method was changed to NMR spectroscopy. This provided the opportunity not only to determine the structure of complexed Pex14p but also allowed an estimation of the structural character of the free components and the structural changes induced upon ligand binding by secondary chemical shift analysis and NMR relaxation experiments. To investigate the competitive character of the Pex14p-Pex5p and –Pex19p interaction NMR titration experiments were carried out. The NMR data was supplement and quantified by isothermal titration calorimetry experiments

2 Materials and Methods

2.1 Materials

Chemicals were bought at the highest available purity from Sigma unless state otherwise. $^{15}NH_4Cl$, [U-13C]-glucose and D_2O were purchased from Spectral Isotopes. DNA oligonucleotide primers were purchased from MWG (Germany). Peptides were synthesized by Dr. Wolfgang Nastainczyk (Medizinische Biochemie und Molekularbiologie, Universität des Saarlandes)

2.1.1 Bacterial strains

Strain	Genotype
E. coli DH5α	F-, *lac*I-, *rec*A1, *end*A1, *hsd*R17, Δ(*lac*ZYA-*arg*F), U169, F80d*lac*ZΔM15, *sup*E44, *thi*-1, *gyr*A96, *rel*A1
E. coli BL21(DE3)PlysS	B, F-, dcm, ompT, hsdS(rB-mB-), gal, λ(DE3), pLysS Cam

2.1.2 Commonly used buffers and media

Antibiotics (1000x stock solutions)
Ampicilin 100mg/ml H2O
Kanamycin 50mg/ml H2O
Chloramphenicol 34mg/ml Ethanol

Coomassie staining solution
0.01% (w/v) Brilliant Blue R
10% acetic acid

Coomassie de-staining solution
10% acetic acid
20% Ethanol

DNA-Gel Sample buffer, 10ml
6ml Glycerol
60mM EDTA
9g Bromphenol blue
9g Xylene Cyanol FF

Luria-Bertani (LB) medium
10g tryptone
5g yeast extract
10g NaCl
(15g agar for plates)
ad 1 liter MilliQ H_2O

SDS-PAGE running buffer
0.1M Tris
0.1M Tricine
0.1% SDS

0.1M Sodium phosphate buffer pH 6.5
68.5% 0.1M NaH_2PO_4 solution
31.5% 0.1M Na_2HPO_4 solution

4M Sodium chloride
233.77g NaCl
ad 1 liter MilliQ H_2O

1M Tris/HCl
121.13g Tris base
ad 1 liter MilliHQ H_2O

SDS-PAGE Sample buffer
50mM Tris/HCl, pH 8.0
2% (w/v) SDS
10% (v/v) Glycerol
1% (v/v) b-ME
12.5mM EDTA
0.02% Bromphenol blue

TAE
40mM Tris-acetate
2mM EDTA

2.2 Methods

2.2.1 Plasmid construction

The following plasmids were kindly provided by our collaborators Wolfgang Schliebs and Marc Fransen

Table 3.1: Provided plasmids

Vector	Manufacturer	Insert	Provided by
pET9d	Novagen	Pex5p long full length	W. Schliebs
pET9d	Novagen	Pex5p aa 115-335	W. Schliebs
pET9d	Novagen	Pex5p aa 1-115	W. Schliebs
pGEX4T-3	Amersham	Pex14p full length	M. Fransen
pQE30	Quiagen	Pex13p full length	M. Fransen
pETM-30/11	EMBL, G.Stier	Pex19p aa 1-124	M. Fransen
pETM-30/11	EMBL, G.Stier	Pex19p aa 51-124	M. Fransen

Full length Pex14p (GenBank accession. No. AF045186), Pex13p (GenBank accession. No. AF048755) and Pex5pL (GenBank accession. No. Z66494) served as a template for the different constructs listed below (Table 2.2)

Table 2.2: Constructs created in this thesis

Insert
Pex14p aa 1-80W
Pex14p aa 1-78
Pex14p aa 16-78
Pex14p aa 16-80W
Pex14p aa 23-78
Pex14p aa 23-80W
Pex5p(L) aa 214-335
Pex13p aa 271-344
Pex5p aa 214-639
Pex5p aa 303-639

All constructs were cloned into a pETM-11 or pETM-30 vector via an *Nco*I/*Not*I site

All primers were designed for an annealing temperature of 65°C and with overhangs for the designated restriction enzymes. PCR reactions were performed according to the manufactures manual using KOD DNA Polymerase (Novagen, Germany)

PCR products, purified via the QIAquick PCR Purification Kit (Quiagen, Germany), and the desired vector were digested with *Nco*I and *Not*I in 50 µl reactions at 37°C overnight using Buffer No 3 (New England Biolabs, USA). The cleaved DNA was separated by agarose gel electrophoresis (between 0.8 and 1.5% agarose in TAE supplement with 25 µg ethidium bromide per 50 ml). The DNA bands were excised under UV light from the gel and isolated via the QIAquick Gel Extraction Kit (Quiagen, Germany).

Plasmid and insert were mixed in an approximate 1:5 ratio and incubated with 1 µl T4 DNA for 1 h at 16°C. The whole 10 µl reaction mix was used for transformation into DMSO competent DH5α *E.coli* cells and plated out on LB plates containing the respective antibiotic. Single colonies were picked and proliferated. Plasmid DNA was isolated using a Miniprep Kit (QIAprep Spin, Quiagen, Germany). All created constructs were analyzed by restriction enzyme digestion and sequenced by MWG (Germany)

Table 2.3: List of oligonucleotides used

Primer	**Sequence** (5' → 3')
14-1for	CATGCCATGGCGTCCTCGGAGCAG
14-80Wrev	ATAGTTTAGCGGCCGCTTACCACAAGGACGAAGGCTCATCG
14-16for	CATGCCCATGGCGACTCCAGGAAGTGAAAATGTG
14-78rev	ATAGTTTAGCGGCCGCTTTCCACCGAAATTCCT
14-23for	CATGCCCATGGCCTGAGAGCCGCTGATTGCCACGGC
13-271for	CATGCCATGGAGGATGACCATGTAGTTGC
13-344rev	TCCGAGCTCGCGGCCGTTAATTCCACCGTTTTCCTACCTTT
5-264for	CATGCCATGGAGGCCCACCCCTGGCT
5-639rev	TCCGAGCTCGCGGCCGTTACTGGGGCAGGCCAAACATAG
5-238for	CATGCCATGGCTCAGGCAGAACAGTG
5-267rev	TCCGAGCTCGCGGCCGTTAGATGTGTTTACTGGTCTTGT
5- 214for	CATGCCATGGTGTCTGAGTTCCTGAAATTCGTGCGGC
5- 335rev	TCCGAGCTCGCGGCCGCTAGTGATCACGCAAGGGGTTC

The first number specifies the peroxin, the second number the DNA base; for = forward/sense, rev = reverse/antisense

2.2.2 Expression and purification of His_6-tagged proteins

His6-tagged proteins were expressed in a BL21(DE3) pLysS E.coli strain. Cells were grown in LB medium containing the respective antibiotics at 37°C until OD600 of 0.6 was reached. The temperature was lowered to 30°C and the culture induced with 0.5 mM IPTG per liter for additional 3 hours. Cells were harvested by centrifugation, frozen and stored at -20°C.

For purification, pellets were resuspended in Lysis buffer supplemented with protease inhibitors (Complete Mini EDTA-free Tablets, Roche, Germany). Cell walls were disrupted via sonication (HD2200 generator, Bandelin Electronic, Germany). The cell extract was centrifuged at 45000xg (1h, 4°C, rotor SS34, Sorvall RC5B). The supernatant was applied to Ni-NTA Agarose. The resin was added to a disposable column (Quiagen, Germany), washed with 8 column volumes wash buffer and eluted with 3 column volumes elution buffer. Buffer

was exchange to cleavage buffer via a PD-10 desalting column (GE Healthcare, Europe). After overnight incubation with His_6 fused TEV-protease (ratio protein:protease 50:1) at room temperature a second Ni-NTA column removed uncleaved protein, the His_6 fusion tag and the protease. The flow through was concentrated and analyzed by SDS-PAGE using 10% Tris-glycine gels or 10-20% Tris-Tricine gels, followed by Coomassie staining.

Lysis buffer	Wash buffer
30mM Tris/HCl, pH 8	30mM Tris/HCl, pH 8
300mM NaCl	500mM NaCl
10mM Imidazol	25mM Imidazol
5mM, β-ME	5mM β-ME

Elution buffer	Cleavage buffer
30mM Tris/HCl, pH 8	30mM Tris/HCl, pH 8
150mM NaCl	150mM NaCl
400mM Imidazol	10mM Imidazol
5mM, β-ME	5mM, β-ME

To take account of the different biochemical properties the protocol was modified for the following proteins:

- Pex14p (aa 16-80W and aa 16-78)

The lysis and wash buffer contained 500mM NaCl. Buffer exchange and TEV cleavage was performed by overnight dialysis against cleavage buffer with the protease added to the eluat.

- Pex5p (all constructs)

The main culture was induced overnight with 0.5mM IPTG per liter at 22°C.
All purification steps were performed at 4°C with ice cold buffer. TEV cleavage was performed at room temperature for 5 hours.

2.2.3 Expression and Purification of isotopically labelled proteins

Isotopically labelled proteins were prepared by growing *E.coli* BL21(DE3) pLysS cells in minimal medium supplemented with either [U-13C]-Glucose and/or $^{15}NH_4Cl$ and the respective antibiotics at 37°C. After overnight induction with 0.5mM IPTG per liter culture at 25°C cells were harvested by centrifugation. Sample purification was conducted as described in 2.2.2. Proteins or protein complexes were exchanged into 50mM potassium phosphate with 100mM NaCl (pH 6.5) by gel filtration (paragraph 2.2.4)

M9 minimal medium	100x trace elements stock solution
6g Na_2HPO_4	5g EDTA, pH 7.5
3g KH_2PO_4	0.83g FeCl3*6H_2O
0.5g NaCl	84mg ZnCl2
0.5g ^{15}NH4Cl (Spectra Stable Isotopes)	13mg CuCl2*2H_2O
4g Glucose or 2g [U-^{13}C]-Glucose	10mg CoCl2*6H_2O
1ml 1M $MgSO_4$	13mg CuCl2*2H_2O
0.3ml 1M $CaCl_2$	10mg CoCl2*6H_2O
1mg Biotin	10mg H_3BO_3
1mg Thiamin	1.6mg $MnCl_2$*6H_2O
10ml 100x trace elements stock solution were dissolved in liter Milli-Q water and sterile filtered (0.22µm)	were dissolved in 1 liter Milli-Q water and sterile filtered (0.22µm)

2.2.4 Ion exchange and size-exclusion chromatography

Single proteins and complexes with equal ratios of the complex components were further purified by gelfiltration. Protein complexes were formed by mixing the single components in the desired stoichiometry followed by 15 min incubation on ice. Size-exclusion chromatography was performed on an Äkta Purifier or Äkta Explorer (GE Healthcare, Europe) at 4°C via a Superdex 200 or Superdex 75 column (GE Healthcare, Europe) in either Buffer A or B as running buffer

Buffer A (Crystallization Buffer)	Buffer B (ITC/NMR Buffer)
20mM BisTrisPropane, pH 7.5	50mM Potassium phosphate, pH 6.5
150mM NaCl	100mM NaCl
1 mM DTT	

Prior to gelfiltration, Pex5p constructs were purified by ion-exchange chromatography (HiTrap Q, GE Healthcare, Europe) using a salt gradient (50mM NaCl to 600mM NaCl, 25mM Tris/HCl pH 8, 5mM β-ME; gradient length 20 column volumns)

2.2.5 Determination of protein concentration

Protein samples were diluted 1:20 in 6M guanidinium hydrochloride buffered in 50mM potassium phosphate (pH 6.5). Absorption was measured at 280 nm and concentration was determined according to Beer-Lambert law

$$A_{280} = \varepsilon_{280} \cdot c \cdot l$$

the extinction coefficient ε_{280} was calculated by the program Protparam (www.expasy.org/tools/protparam.html), the path length l was 1cm

2.2.6 Dynamic light scattering

Measurements were conducted on a Dyna Pro 99 device (Wyatt Tech. Corp., USA). At least 20 data points of a 25 µl sample were recorded.

2.2.7 Crystallization strategies

Gelfiltrated N-terminal Pex14p constructs or binary and ternary complexes were diluted with MilliQ water to decrease buffer and salt concentration to 10mM BTP pH 7.5 and 75mM NaCl. N-Pex14p-peptide complexes were established by mixing protein and dissolved

peptides in the appropriate ratio. Proteins were concentrated to 10, 15, 20, 25 or 35 mg/ml and applied to the following sparse matrix crystallization screens.

Index Screen (Hampton Research, USA)
Crystal Screen I (Hampton Research, USA)
Crystal Screen II (Hampton Research, USA)
Ammonium sulphate Grid Screen (Hampton Research, USA)
PEG/Ion Screen(Hampton Research, USA)
Crystal Screen Lite (Hampton Research, USA)
Crystal Screen Cryo (Hampton Research, USA)
SaltRX (Hampton Research, USA)
Wizard I (Emerald BioStrucures, USA)
Wizard II (Emerald BioStrucures, USA)
Cryo I (Emerald BioStrucures, USA)
Cryo II (Emerald BioStrucures, USA)

Screens were set up by mixing 0.3 to1µl protein with reservoir solution in a 1:1 ratio on 96 well sitting drop plates with 120 µl reservoir solution or on 24 well hanging drop plates with 500µl reservoir solution. Screens were stored at 21°C and regularly inspected with a dissection microscope equipped with cross-polarizers. Promising conditions were tried to optimize by streak microseeding (Bergfors, 2003), additive screens (Cudney et al., 1994) and/or variations of pH and precipitant of the original condition. (McPherson, 1990)
The X-ray diffraction properties of crystalloids were tested under the supervision of Petri Kursula (EMBL-Hamburg, Germany) on EMBL beamline X13 of the DORIS III storage ring at the Deutsche Elektronen Synchrotron, Hamburg. X13 is a bending magnet beamline, equipped with a 165mm MAR charge-coupled device detector, operated with MARCCD version 0.9.7 software (MAR Research GmbH, Germany) and Oxford Cryosystems (Oxford, UK) cooling. A description of the current beamline set-up can be found at http://www.embl-hamburg.de/facilities/px_beamlines.html.

2.2.8 Exopeptidase assay

0.5 mg/ml Pex14p (aa 1-80W)-Pex5p (aa 214-335) complex was digested with 0.1 mg/ml Aminopeptdiase in 100mM MES buffer pH 6.5 or Carboxypeptidase in 100mM HEPES buffer pH 7.0 supplemented with 100mM NaCl at 20°C overnight. The samples were checked on a SDS-Gel and send to mass spectrometry (Dr. Jens Pfannstiel, Universität Heidelberg) for analysis.

2.2.9 Pull down assay

Proteins were expressed in separately expressed in *E.coli* and purified as described in paragraphs 2.2.2 and 2.2.4. with the exception that the His6-tag of the bait protein was not cleaved of. The bait was mixed in 20 mM BTP, pH 7.5 150 mM NaCl with an excess of untagged interaction partner and bound to Ni^{2+}-NTA beads by turning end over end at 4° for 0.5h. The beads were centrifuged and washed 5 times. Complexes were eluted either by cleavage with His_6-TEV protease or by boiling in SDS-sample buffer and analyzed by SDS-PAGE.

2.2.10 Isothermal titration microcalorimetry

ITC measurements were conducted on a MicroCal VP-ITC using Pex14p (aa 16-80) at 35 µM as a sample and Pex5p or Pex19p peptide at 300-500 µM as the titration ligand. The reference cell was filled with degassed Milli-Q water containing 1% sodium azide. Proteins and ligands were co-dialyzed against 50mM potassium phosphate buffer (pH 6.5) with 100mM NaCl. All experiments were conducted at 298K at a stirring speed of 300rpm. Per experiment, 18 subsequent injections of 10-12 µl were separated by 300s equilibration time. Ligand heats of dilution were subtracted and data was fitted using MicroCal Origin 7.0 with the standard model for a 1:1 stoichiometry complex based on the Wiseman isotherm (Turnbull and Daranas, 2003; Wiseman et al., 1989):

$$\frac{dQ}{d[X]_t} = \Delta H^o V_0 \left[\frac{1}{2} + \frac{1 - X_R - r}{2\sqrt{(1 + X_R + r)^2 - 4X_R}} \right] \quad (1)$$

with the standard enthalpy ΔH^o, the effective volume of the calorimeter cell V_0 and the total concentration of the ligand $[X]_t$. Equation 1 relates the stepwise change in heat of the system normalized with respect to moles of ligand added per injection ($dQ/d[X]_t$) to the absolute ratio of ligand to receptor concentration ($X_R = [X]_t / [M]_t$) at any point during the course of titration. $[M]_t$ is the total protein concentration and r is defined by

$$\frac{1}{r} = K_a [M]_t \quad (2)$$

where K_a is the association constant. Using the Helmholtz relationship

$$\Delta G = -RT \ln K_a = \Delta H - T\Delta S$$

where R is the gas constant (8.33 J/mol/K), T the temperature in Kelvin, the binding entropy ΔS and the Gibbs free energy of binding, ΔG was calculated. The dissociation constant K_d was calculated as the reciprocal of K_a (Leavitt and Freire, 2001)

2.2.11 NMR Spectroscopy

NMR spectra were acquired at 303K on a Bruker DRX500, DRX600 or DRX800 spectrometer with cryogenic probes unless otherwise stated. Spectra were processed with NMRPipe (Delaglio et al., 1995) and analyzed using NMRVIEW (Johnson, 1994)

2.2.11.1 Resonance assignments

Backbone and side chain chemical shifts of Pex14p (aa 16-80W) in complex with the Pex5p ligand were obtained using standard triple resonance experiments namely HNCA, CBCA(CO)NH, HNCACB, (H)CCONH-TOCSY, -TOCSY and HCCH-TOCSY (Sattler, 1999). Pex14p-Pex19p protein backbone and chemical shifts were transferred from the Pex14p-Pex5p complex and adapted. NOE restraints for NMR structure determination were

obtained from the following experiments (Table 3.4). All Pex14p-Pex19p complex spectra were recorded with a 2.5 fold excess of ligand.

Table 2.4: List of NOE experiments

Experiment	Mixing time Pex14p-Pex5p/Pex14p-Pex19p	Base frequency Pex14p-Pex5p/Pex14p-Pex19p
2D NOESY, D_2O	100/100;200 ms	800/800; 600 MHz
3D ^{15}N NOESY	120 ms	500/600 MHz
2D $^{12}C/^{14}N$-filtered NOESY , D_2O	120 ms	500/600 MHz
2D $^{12}C/^{14}N$-filtered NOESY , H_2O	120 ms	500/600 MHz
3D ^{13}C HMQC NOESY, D2O	120 ms	500 MHz
3D^{13}C-edited, $^{12}C/^{14}N$-filtered NOESY, D_2O	150 ms	500 MHz

2.2.11.2 Distance, torsion angle and orientational restraints

Intramolecular NOE restraints were obtained from 2D and 3D spectra. Intermolecular NOEs were derived from X-filtered 2D and 3D experiments and used as structural constraints for the calculation of the protein-peptide complex (Gemmecker, 1992). H^N-N RDCs were measured in a liquid crystalline medium (Otting et al., 2000). Protein backbone restraints were obtained from secondary chemical shifts and sequence homology by the programme TALOS (Cornilescu et al., 1999). Slow exchanging amide protons were identified from $^1H,^{15}N$-HSQC experiments after dissolving the lyophilized sample in ^2H_2O and included in structure calculations as hydrogen bond restraints.

2.2.11.3 Structure calculation and validation

The experimentally determined distance, dihedral and dipolar coupling restraints (Table 1) were applied in a simulated annealing protocol using ARIA1.2 (Linge et al., 2001). 100 structures were calculated in the final iteration of those the best 10 were refined in a shell of water molecules. Structural quality was analyzed and structural statistics were computed by ARIA1.2 and PROCHECK-NMR (Laskowski et al., 1996). Ring current shifts and r.m.s.

deviation of Pex14p-Pex5p and Pex14p-Pex19p complex structure were calculated by MOLMOL (Koradi et al., 1996). Protein-peptide interface area was calculated by NOC (http://noc.ibp.ac.cn/, according to (Richards, 1977)). 3-dimensional figures were prepared via PYMOL (DeLano, W.L.; http://www.pymol.org)

2.2.11.4 Chemical shift perturbation and secondary chemical shifts

Chemical shift changes of backbone amide groups (Δδ) were monitored in two-dimensional ^{1}H, ^{15}N-HSQC experiments and calculated with

$$\Delta\delta = \sqrt{\left(\Delta\delta^{1}H\right)^{2} + \left(\frac{1}{5}\Delta\delta^{15}N\right)^{2}}$$

where $\Delta\delta^{1}H$ and $\Delta\delta^{15}N$ are the changes of ^{1}H and ^{15}N chemical shift in ppm.

Secondary chemical shifts were calculated via NMRView, according to

$$\Delta\delta=\delta_{S\alpha}-\delta_{S\beta} = (\delta_{S\alpha}(obs)-\delta_{S\alpha}(rc))-(\delta_{S\beta}(obs)-\delta_{S\beta}(rc))$$

$\delta_{S\alpha}$ and $\delta_{S\beta}$ are the observed (obs) or random coil (rc) chemical alpha and beta shifts (i.e. C_α, C_β, H_α, H_β) (Wishart et al., 1995)

Ring current shifts were accounted for H_α secondary chemical shift calculation of bound peptides. An average ring current shift was determined for the ten lowest energy complex structures. Only ring current shifts larger than 0.3 ppm were considered for calculation of the avarage value. The determined average ring current shift was subtracted from the secondary chemical shift value.

3 Results

3.1 Constructs created in this thesis

The following human Pex14p and ligand constructs (Fig. 3.1) were created as described in Materials and Methods paragraph 2.2.1.

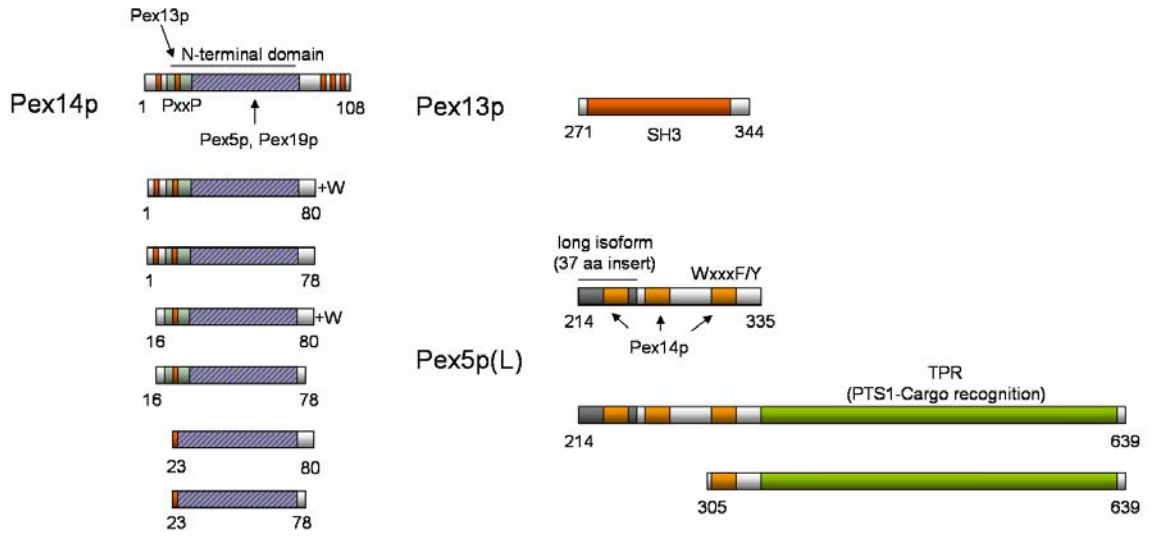

Fig. 3.1: Overview of Pex14p, Pex13p and Pex5p constructs for his work. For an overview of the complete domain composition see paragraph 1.6

The Pex14p (aa 1-108) constructs represents the N-terminal part of the protein up to its hydrophobic region. It contains 5 non canonical PxxP motifs, the conserved N-terminal domain and the reported binding sites for Pex13p, Pex5p and Pex19p. The construct was used for interaction studies with the SH3 domain of Pex13p (see paragraph 3.5)

Pex14p (aa 1-80W) was the initial N-terminal construct created in this work. The native protein fragment (Pex14p (aa 1-80)) contains no amino acid with an absorption maximum at 280 nm, thus the additional, C-terminal tryptophan facilitates quantification and purification

(especially size-exclusion chromatography). NMR studies revealed no effect of the tryptophan on the binding properties or ternary structure of the protein (see paragraph 3.6).
Additional N-terminal Pex14p constructs (Pex14p (aa 1-78); Pex14p (aa 16-80W); Pex14p (aa 16-78); Pex14p (aa 23-80W); Pex14p (aa 23-78) were designed according to the results of globularity prediction and exopeptidase assays (paragraph 3.2) and should facilitate crystallization (see paragraph 3.3).
To test the interaction of N-terminal Pex14p with different ligands (see paragraph 3.4 and 3.5), a construct containing the SH3 domain of Pex13p and three Pex5p constructs were cloned.

3.2 Domain boundaries of human N-Pex14p

Definition of domain boundaries of the N-terminal Pex14p as a target for structural studies was initially conducted by globular fold prediction. The program GLOBPLOT (Linding et al., 2003) predicts the very N-terminus of Pex14p as disordered. The chosen propensity (Russel-Linding) predicts the starting position of the structured N-terminal part for residue 23 (Fig. 3.2).

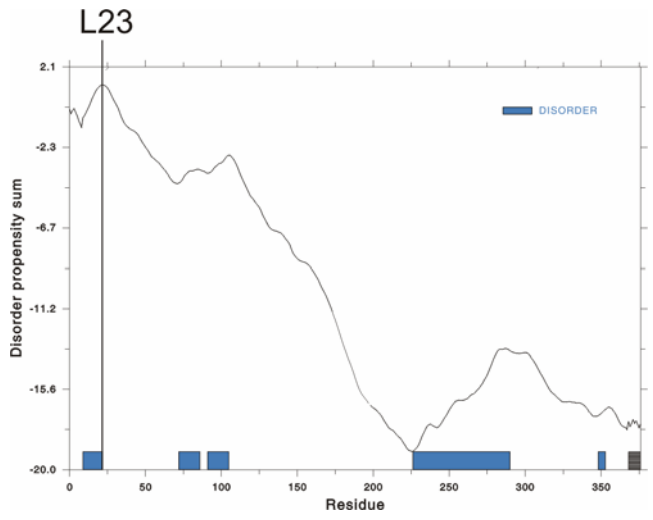

Fig. 3.2: Globularity prediction of *hs*Pex14p by Globplot (Linding et al., 2003). A downward trend indicates globularity, an upward trend disorder. The black line indicates the beginning of the structured N-terminal domain.

According to this prediction, two constructs Pex14p (aa 23-80W) and Pex14p (aa 23-78) were cloned. Although the expression was very well, the proteins were mainly insoluble and had a strong tendency to aggregate (data not shown).

To obtain a soluble and structured N-terminal domain fragment of Pex14p an exopeptidase assay was performed (Material and Methods 2.2.8). A complex of His_6-tev-Pex14p (aa 1-80W) and His_6-tev-Pex5p (aa 215-335) was incubated with aminopeptdiase M or carboxypeptidase Y at 20°C. The digested sample was flash frozen and sent to mass spectroscopy for analysis (see Appendix II 7.1).

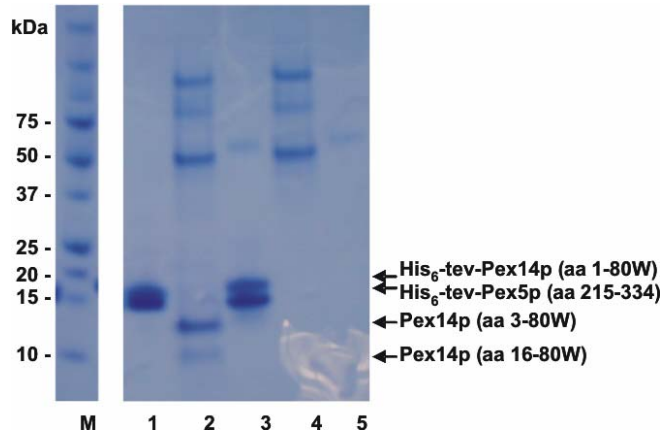

Fig. 3.3: Exopeptidase assay. A complex of His_6-tev-Pex14p (aa 1-80W) and His_6-tev-Pex5p (aa 215-335) was incubated with an N- and C-terminal exopeptidase. (1) protein complex alone, (2) protein complex plus aminopeptdiase M, (3) protein complex plus carboxypeptidase Y, (4) aminopeptdiase M alone, (5) carboxypeptidase Y alone.

Two different fragments, Pex14p (aa 3-80W) and Pex14p (aa 16-80W), could be identified in the N-terminal digestion. Interestingly no stable N-terminal Pex5p fragment was found, indicating a complete digestion of the protein. In the C-terminal sample His_6-tev-Pex14p (aa 1-78) and His_6-tev-Pex5p (aa 215-334) could be detected. According to these results three new constructs, Pex14p (aa 1-78), Pex14p (aa 16-80W) and Pex14p (aa 16-78), were cloned.

3.3 Expression, purification and crystallization of N-terminal Pex14p

Pex14p (aa 1-80W), Pex14p (aa 1-78), Pex14p (aa 16-80W) or Pex14p (aa 16-78) was expressed in *E.coli* and purified via Ni-affinity chromatography. The buffer was exchanged and the protein digested with His_6-TEV protease. The His_6-tag and the protease were removed

by a second Ni-affinity step. The flow through was collected, concentrated and further purified by gelfiltration. Fig. 3.4 (A) and (B) show exemplarily the purification of Pex14p (aa 16-80W).

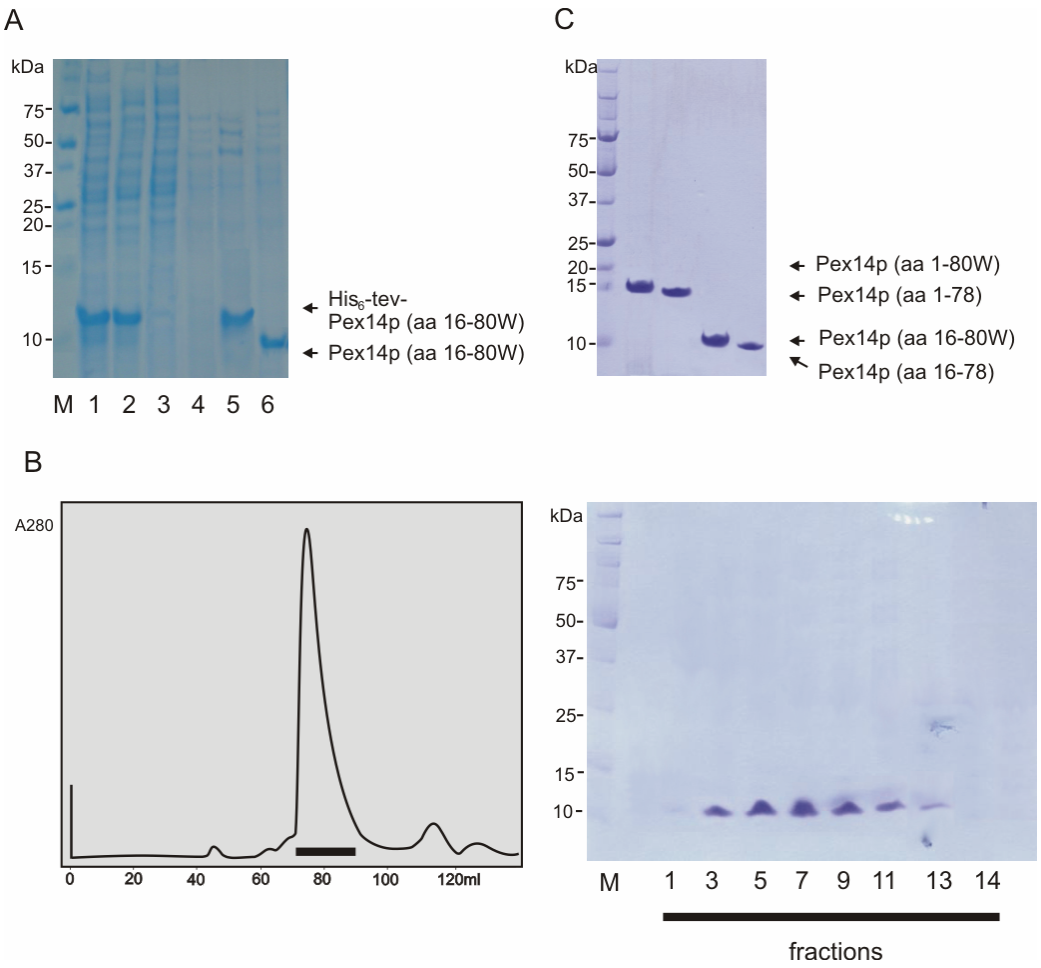

Fig. 3.4: (**A**) Purification of His6-tev-Pex14p (aa 16-80W). The protein was expressed in *E.coli* and purified by Ni-affinity chromatography. Total cell lysate (1), soluble (2) and unbound fractions (3), wash (4), elution (5) and the flow through after TEV cleavage (6) of the affinity column were separated by SDS-PAGE and analyzed by Coomassie staining. (**B**) Cleaved Pex14p (aa 16-80W) was subjected to size exclusion chromatography using a Superdex 75 column. The protein elutes as single peak. Fractions containing the purified protein were pooled, concentrated and used for crystallization trials or NMR studies. (**C**) Purity of N-terminal Pex14p constructs after gelfiltration.

The protein containing fractions were pooled and concentrated to 10, 15 25 or 35mg. Monodispersity was checked by dynamic light scattering, only samples with values higher than 75% were used for crystallization. The proteins alone (Fig 3.4 (C)) or in complex with Pex5p peptide were applied to sparse matrix crystallization screens (Material and Method,

paragraph 2.2.7). Table 3.1 shows the different protein concentration and the protein/peptide ratio.

Table 3.1: Overview of the N-Pex14p-Peptide complexes used for crystallization

N-Pex14p	Protein : peptide ratio	
	Pex5p (aa 114-126)	Pex5p (116-124)
Pex14p (aa 1-80W), 10 and 15 mg/ml	1:0, 1:1, 1:1.5, 1:2	1:1.5
Pex14p (aa 1-80W), 25 mg/ml	1:0, 1:1	
Pex14p (aa 1-80W), 35 mg/ml	1:0	
Pex14p (aa 1-78), 10 and 20 mg/ml	1:0, 1:1	
Pex14p (aa 16-80W), 10 and 15 mg/ml	1:0, 1:1.5	1:1, 1:1.5, 1:2
Pex14p (aa 16-80W), 20 mg/ml		1:0, 1:1
Pex14p (aa 16-78), 10 and 15 mg/ml		1:0, 1:1

Micro-crystals and "spherulites" were mainly found in conditions containing 0.5-2M ammonium sulphate, pH 5.5-7.5 or 15-25% PEG 3350, pH 5.5-8.0. Crystalloids were tested on EMBL beamline X13 of the DORIS III storage ring at the Deutsche Elektronen Synchrotron, Hamburg. So far, no diffraction pattern could be obtained.

3.4 *In vitro* complex formation and crystallization of N-terminal Pex14p and ligands

N-Pex14p and the different ligand constructs were expressed separately in *E.coli*, purified and complexed *in vitro* (see paragraph 2.2.2 and 2.2.4). In addition to the constructs cloned in this thesis (see paragraph 3.1) constructs provided by our collaborators, i.e. Pex5p (aa 1-335), Pex5p (aa 115-335), Pex5p(L) and Pex19p (aa 1-124) (see Material and Methods 2.2.1) were used for *in vitro* complex formation and crystallization trials.

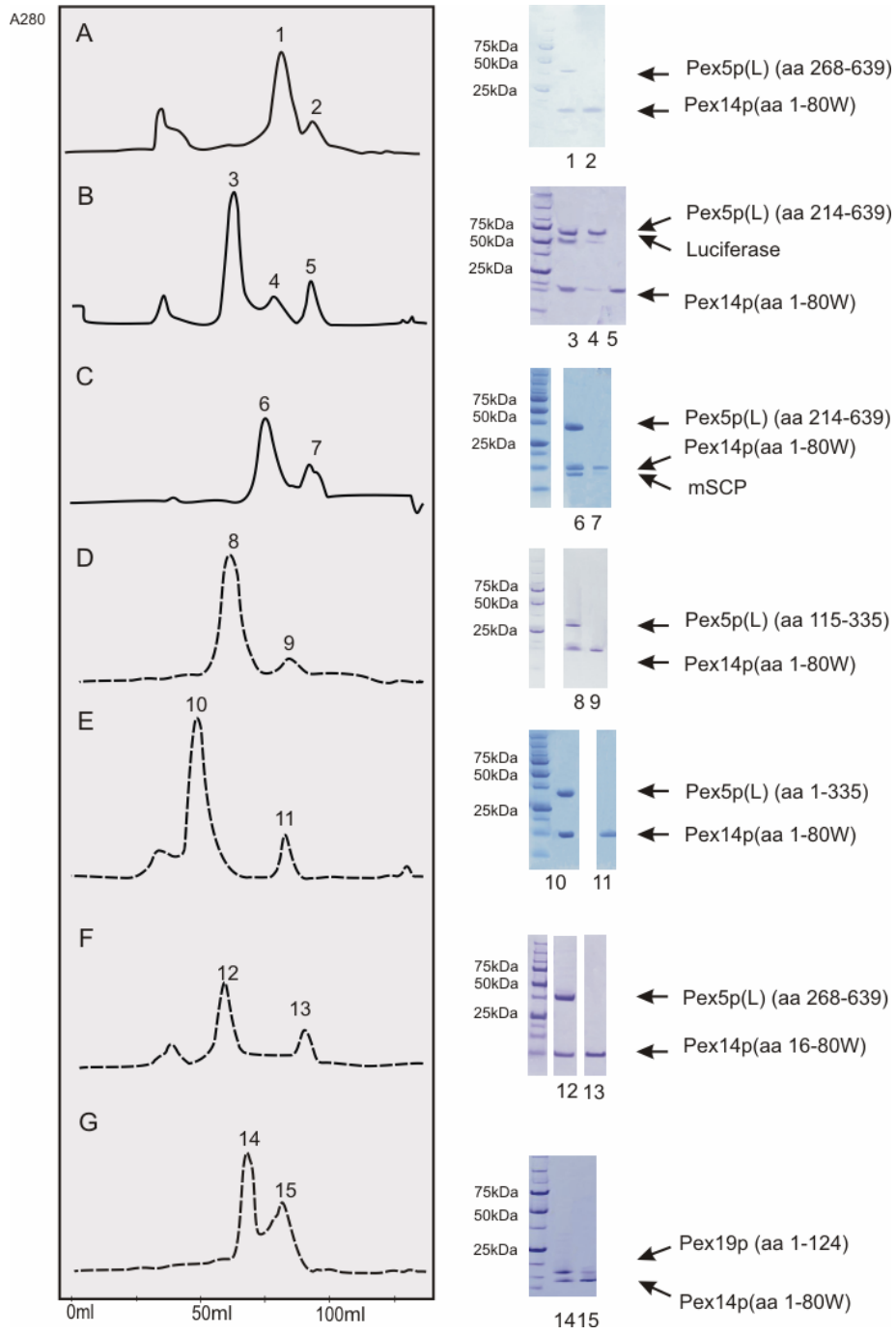

Fig. 3.5: Gelfiltration of N-terminal Pex14p complexes were carried out on a Superdex 200 or Superdex 75 (dashed line) column

All constructs showed an *in vitro* interaction with N-terminal Pex14p as demonstrated by size-exclusion chromatography. (Fig. 3.5). Beside the dimeric Pex14p-Pex5p or Pex14p-Pex19p complex, complexes of N-terminal Pex14p, C-terminal Pex5p and the Pex5p-Cargo proteins mSCP2 or Luciferase could be established. Luciferase, a synonym for the enzyme luciferin 4-monooxygenase from north-american firefly, contains a PTS1 signal and is

commercially available (Sigma). Although such a complex is artificial, luciferase, introduced to mammalian cells, is targeted to peroxisomes (Keller et al., 1987).

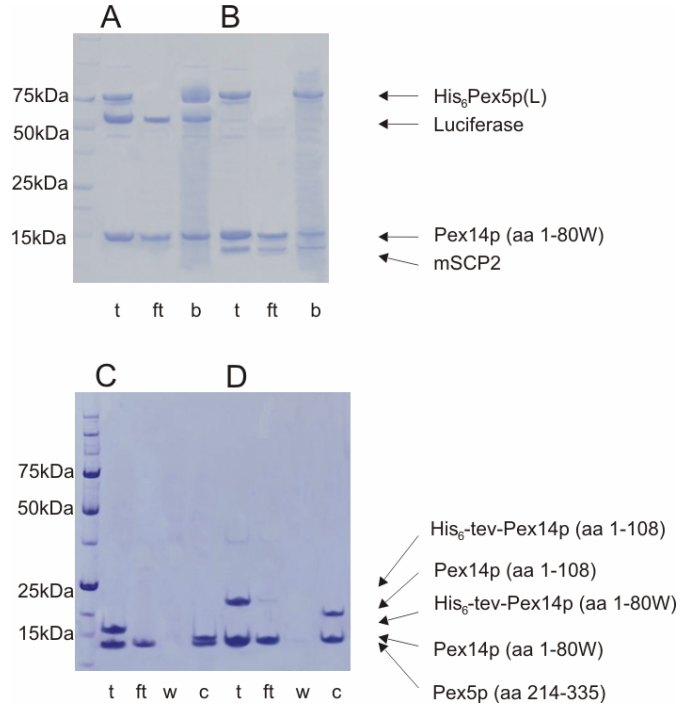

Fig. 3.6: Pull down assays of purified recombinant His_6Pex5p(L), Luciferase and Pex14p (aa 1-80W) (**A**), His_6Pex5p(L), mSCP2 and Pex14p (aa 1-80W) (**B**), Pex5p (aa 214-335) and His_6-tev-Pex14p (aa 1-80W) (**C**) and His6-tev-Pex14p (1-108) and Pex5p (aa 214-335). Proteins were mixed and incubated with Ni-NTA beads. Samples of proteins in total (**t**), flow through (**ft**) wash (**w**), after TEV cleavage (**c**) or Ni-NTA beads (**b**) were separated by SDS-PAGE and analyzed by Coomassie staining.

The *in vitro* interaction of N-terminal Pex14p with Pex5p (aa 214-335) as well as the formation of a ternary complex of N-terminal Pex14p, Pex5p(L) and mSCP2 could be confirmed by a pull down assay (Fig. 3.6).

All complexes were applied to sparse matrix crystallization screens (Material and Methods 2.2.7). So far, no crystals could be obtained.

3.5 In vitro interaction tests of the Pex13p-SH3 domain and N-terminal Pex14p constructs

Human Pex13p has been described to interact with N-terminal Pex14p (Fransen et al., 2004; Itoh et al., 2006). In order to investigate if this interaction is mediated by the SH3 domain and non canonical PxxP motifs in Pex14p, different Pex14p constructs were tested for their ability to bind the SH3 domain of Pex13p

Recombinant and purified Pex13p (aa 271-344) and His_6-tev-Pex14p (aa 1-80W) or His_6-tev-Pex14p (aa 1-108) were mixed in an 1:1 ratio and incubated with Ni-NTA beads. The N-terminal his-tagged Pex14p constructs served as bait and were checked for their ability to pull down Pex13p. While both constructs were able to bind Pex5p (aa 214-335) in vitro (Fig. 3.5), no interaction with the SH3 domain of Pex13p was observed (Fig. 3.7).

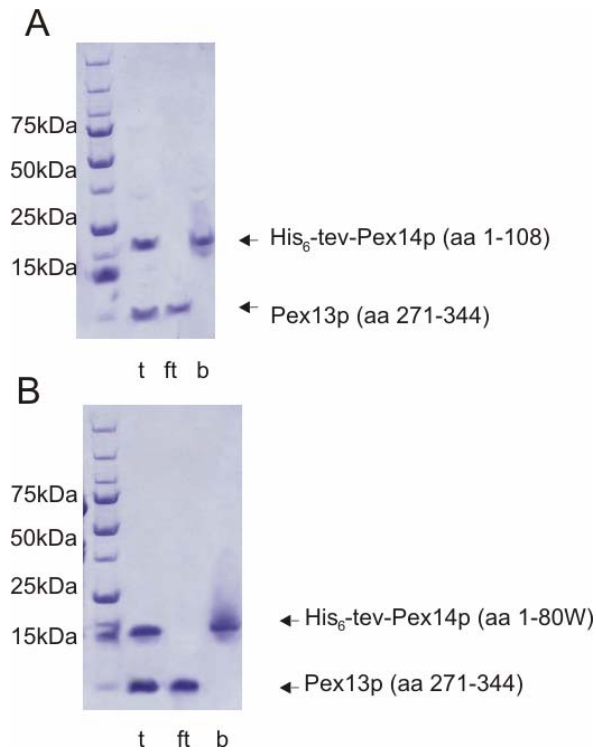

Fig. 3.7: Pull down assays of purified recombinant Pex13p (aa 271-344) and His_6-tev-Pex14p (aa 1-80W) (**A**) or His_6-tev-Pex14p (aa 1-108) (**B**). Proteins were mixed and incubated with Ni-NTA beads. Samples of proteins in total (**t**), flow through (**ft**) and Ni-NTA beads (**b**) were separated by SDS-PAGE and analyzed by Coomassie staining.

Additionally, $^{1}H^{15}N$ HSQC spectra of Pex14p (aa 16-78) alone and after addition of a 2 fold excess of Pex13p (SH3) were recorded and superimposed. No chemical shift perturbation of N-terminal Pex14p could be observed (Fig. 3.8), leading to the conclusion that the Pex13p construct used is either not functional or the SH3 domain alone is not sufficient to bind Pex14p.

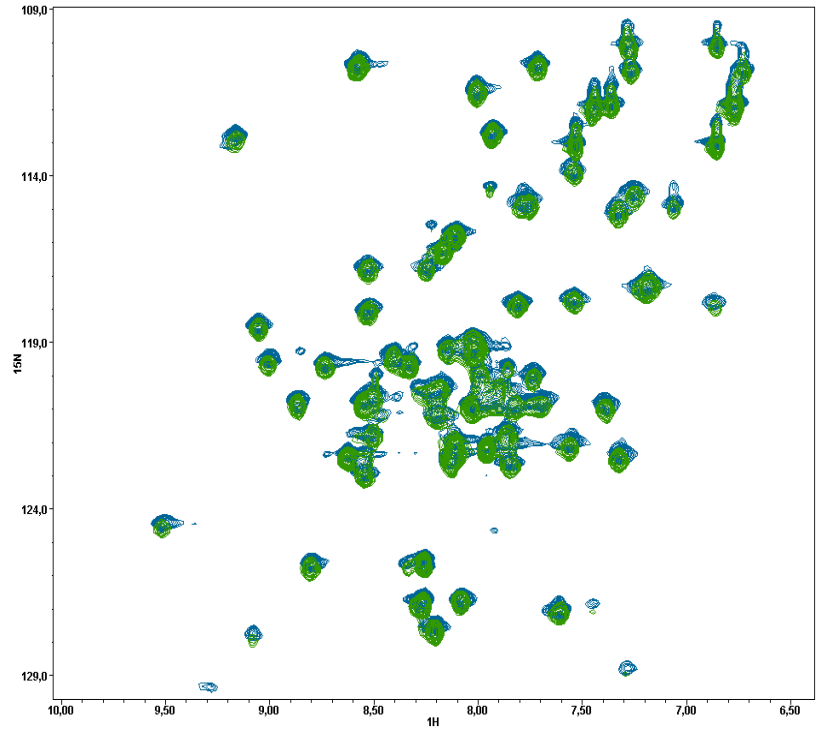

Fig. 3.8: Overlay of the $^{1}H^{15}N$ HSQC of 0.8mM Pex14p (aa 16-78) alone (blue) and after addition of a 2 fold excess of Pex13p (aa 271-344) (green). Spectra were recorded at 500 MHz and 303K. Experimental time was 20 minutes.

3.6 Comparison of the $^{1}H^{15}N$-HSQC spectra of Pex14p (aa 16-78) and Pex14p (aa 16-80W)

In order to investigate the influence of the additional tryptophane W81 on the binding properties of Pex14p or on the tertiary structure of the protein, $^{1}H^{15}N$-HSQC spectra of Pex14p (aa 16-78) and (aa16-80W) were recorded and superimposed (Fig. 3.9). Both spectra are identical except for the additional residues. No peaks are shifted proving that the proteins are folded equally.

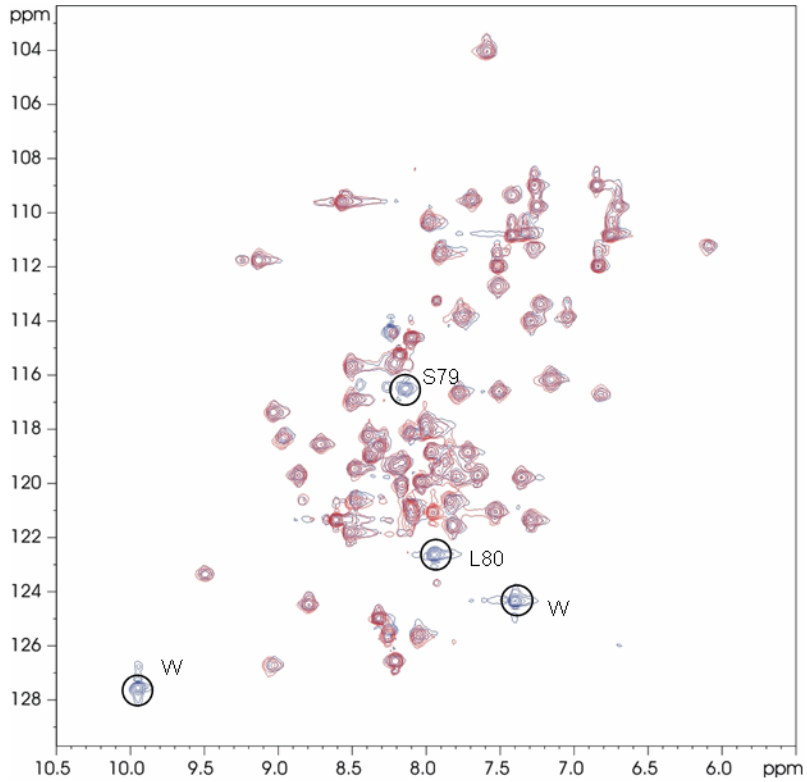

Fig. 39:
Overlay of the $^{1}H^{15}N$-HSQC of Pex14p (aa 16-78) (red) and Pex14p (aa 16-80W) (blue). Except of the additional residues the spectra are identical. Spectra were recorded at 500 MHz for 20 minutes.

3.7 Structural studies of N-terminal Pex14p by NMR

3.7.1 Backbone assignment of free and peptide bound N-Pex14p

Backbone resonance assignments of free and complexed Pex14p (aa 16-80W) were obtained using standard triple resonance experiments (Material and Methods, paragraph 2.2.11.1). While the backbone of the protein in complex with the Pex5p peptide (aa 116-124) and Pex19p (aa 66- 77) could be assigned completely, 6 residues were missing for free N-Pex14p (39, 41, 45, 55, 57, 70). Comparison of the secondary chemical shifts of free and bound Pex14p (aa 16-80W) show a three helical bundle in both cases. While in complex the linker between α1 and α2 appears to be helical, it seems more flexible in the free protein (Fig. 3.10).

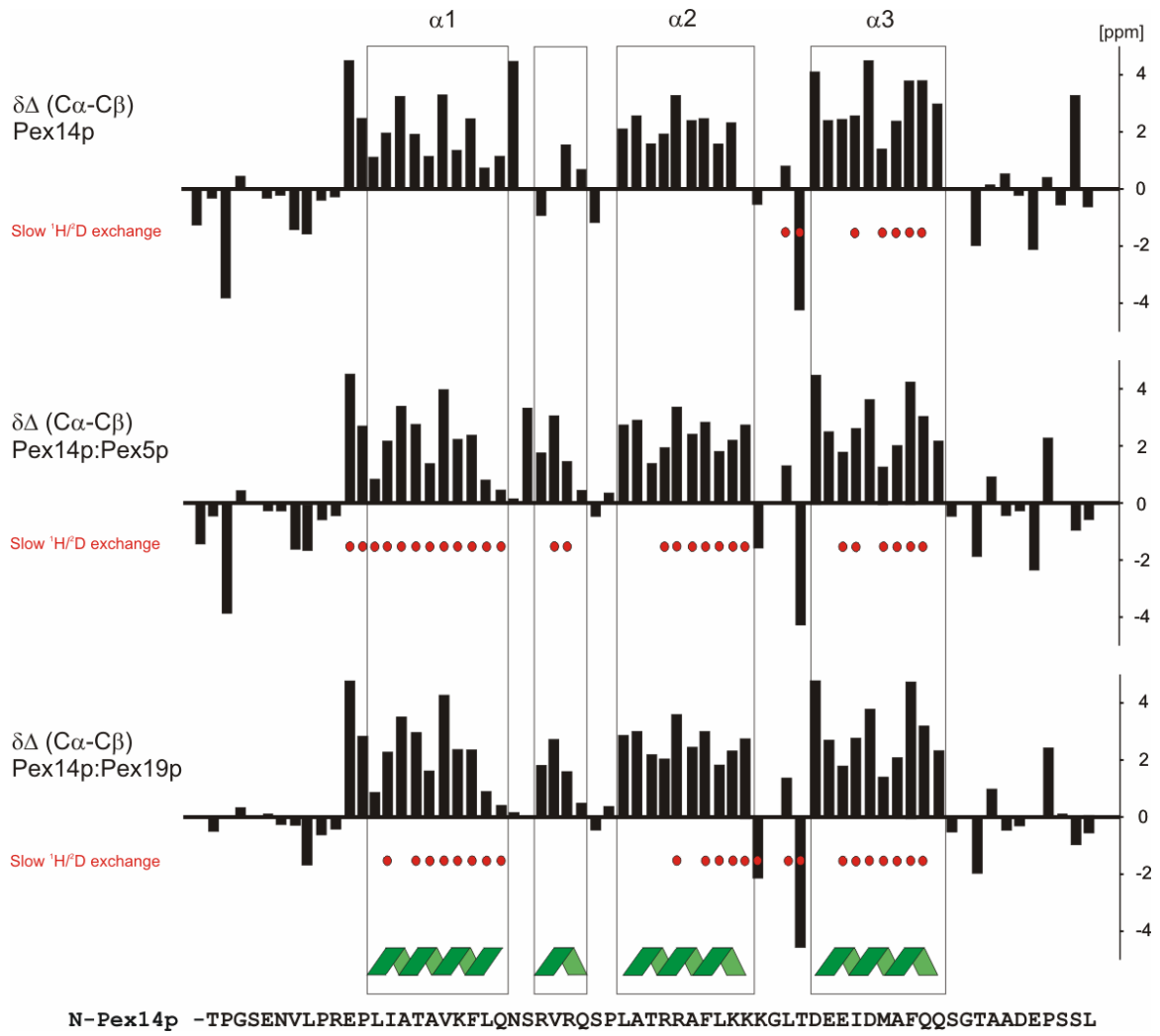

Fig. 3.10: Secondary chemical shifts (Δδ(Cα-Cβ)) are indicated as black bars. Solvent protected amide protons are displayed by red circles. Secondary structure elements are shown above the sequence.

Compared to free Pex14p, where only the scaffold helix α3 is solvent protected, complexed Pex14p shows slowly exchanging amide protons at helix α1 and α2. Depending on the ligand, the helical linker between helix α1 and α2 (Pex14p-Pex5p), or the loop region between helix α2 and α3 (Pex14p-Pex19p) is also protected.

3.7.2 Secondary structure of free and Pex14p-bound peptides

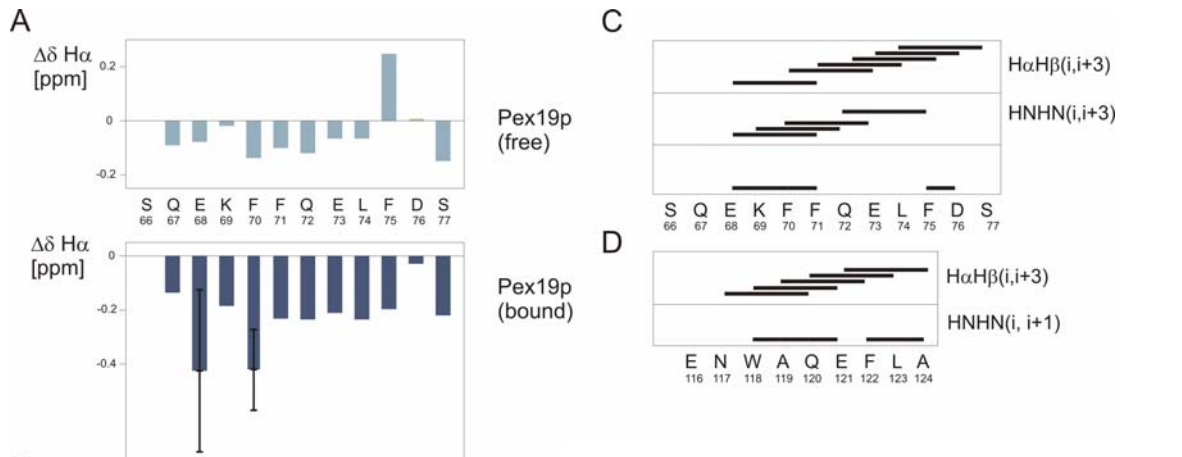

Fig. 3.11: H_α secondary chemical shift for the residues 66-77 of the Pex19p peptide (**A**) and residues 116-124 of the Pex5p (**B**). Free and bound Pex19p are shown in light and dark blue, free and bound Pex5p in light and dark red. Ring current effects on the residues E68, F70 and for Pex19p and the residues N117 and W118 of the Pex5p peptide were accounted for calculation. Error bars are shown in black.
Secondary structure defining NOEs of Pex19p (**C**) and Pex5p peptides (**D**) bound to Pex14p.

Homonuclear TOCSY and NOESY experiments were used to characterize free Pex5p and Pex19p peptides while heteronuclear $^{12}C/^{14}N$ -filtered TOCSY and NOESY experiments were recorded for the bound form (see paragraph 2.2.11). The helical conformation of the bound peptides could be confirmed by H_α secondary chemical shifts and helical (i,i+3) NOE connectivities. The comparison of the free peptide versus Pex14p-bound indicates a reduced α-helical content in the free Pex19p peptide suggesting induced folding upon binding. In contrast the secondary chemical shifts of the free Pex5p peptide indicate already a mainly helical conformation. The average ring current shifts were determined from the ten lowest energy complex structures by the program MOLMOL and the shifts of residues Gln117, Trp118 of Pex5p and Glu68, Phe70 of Pex19p were corrected accordingly for secondary chemical shift calculation (see paragraph 2.2.11.4).

3.7.3 Relaxation Experiments

^{15}N relaxation data including T1, T2 and ^{15}N heteronuclear NOE were recorded at 500 MHz for free and Pex5p bound N-terminal Pex14p. The first and last 7 amino acids of Pex14p (aa 16-80W) show low ^{15}N heteronuclear NOE values (below 0.5) and therefore high flexibility. Residues 24 to 73 are more rigid and constitute the structured part of the domain.

In comparison to the average behavior of the molecule, some differences in the relaxation parameters are apparent in the bound form of Pex14p versus the free protein. The linking regions between the helical elements of bound Pex14p have lower values than the average T1. In contrast very little variation in T1 was observed across the entire free protein. Comparison of bound and unbound Pex14p shows a 2 fold decrease of T2 upon binding of the Pex5p peptide. The correlation time decreases from 8.2ns at 303K for free N-terminal Pex14p to 4.2ns for the bound form. The linear relation between correlation time and molecular weight suggests that an N-terminal Pex14p dimer gets disrupted upon the addition of Pex5p peptide ligand. Fig. 3.12 provides an overview of relaxation data of free and bound N-terminal Pex14p. Although a biological relevance of this dimerization can not be excluded, it is very likely that it results from the high concentration of the NMR sample.

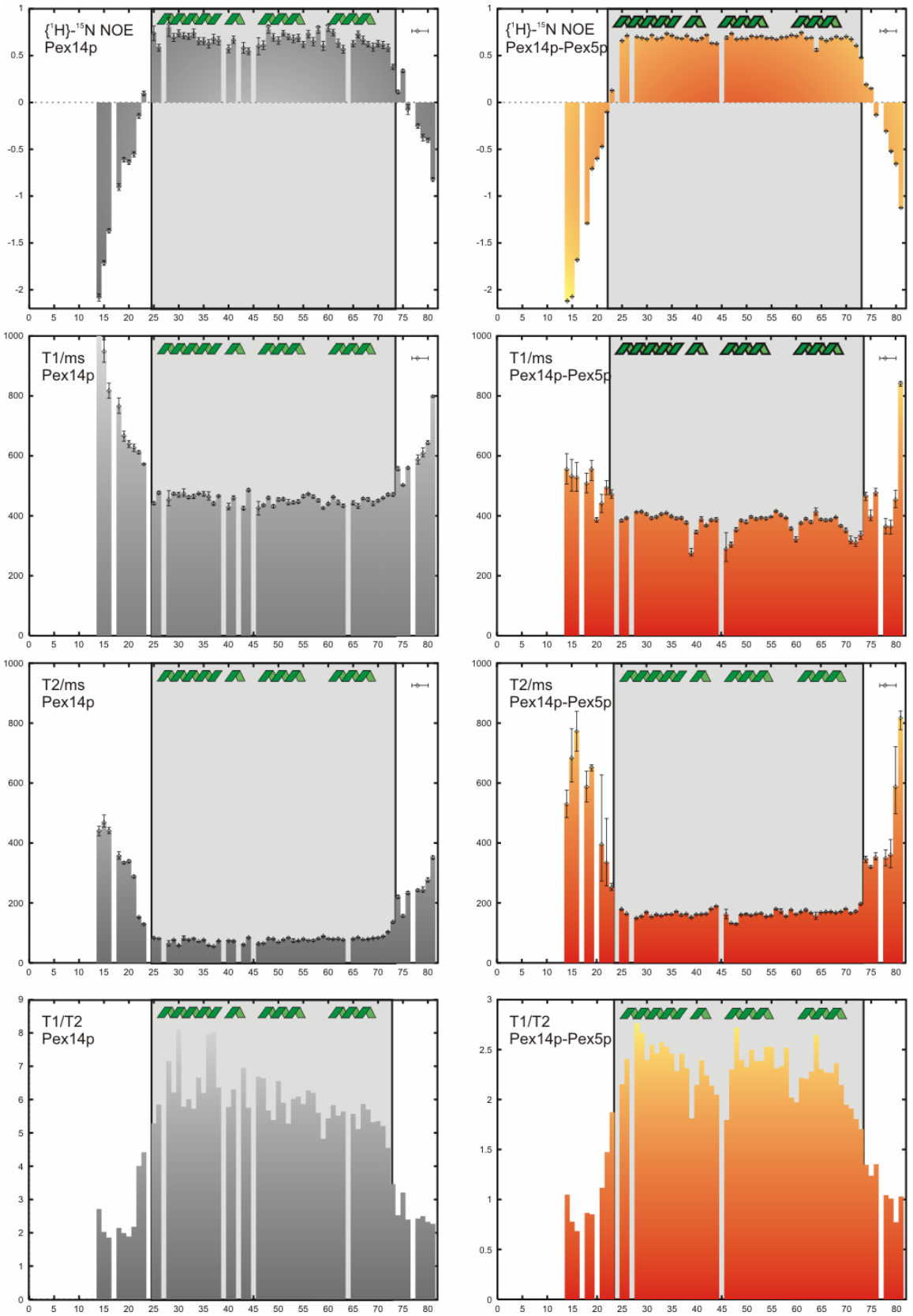

Fig. 3.12: Overview of free and bound N-terminal Pex14p relaxation data.

3.7.4 Structure of N-Pex14p in complex with a Pex5p and a Pex19p ligand

An almost complete assignment of Pex14p (aa 16-80W) in complex with a Pex5p peptide (aa 116-124) was obtained following the iterative step procedure as described in Materials and Methods 2.2.11. The 3-dimensional structure was calculated by a simulated annealing protocol using the program ARIA1.2 (Linge et al., 2001) based on the experimentally determined distance, dihedral and dipolar coupling.

The NMR spectra of the Pex14-Pex19p complexes were strongly dependent on the protein-ligand ratio. Therefore, and due to stability reasons all spectra were recorded on a single sample with a 2.5 fold excess of Pex19p ligand. This includes the filtered spectra, which were used to assign and derive restraints for the bound peptide. The degree of saturation is 36% for the peptide (F_{LB}) and 89% for the protein (F_{PB}), calculated

$F_{LB} = [PL]/[L]_0$ and $F_{PB} = [PL]/[P]_0$

with the starting concentration of the protein $[P]_0$ and the ligand $[L]_0$. The complex concentration [PL] was determined by:

$$[PL] = ½ (K_d + [P]_0 + [L]_0) - (¼ (K_d + [P]_0 + [L]_0)^2 - [L]_0 [P]_0)^{½}$$

with the dissociation constant K_d (= 9.23 µM, see Table 3.3). The Pex14p-Pex19p complex is in the fast binding regime on the chemical shift time scale and shows a spectrum representing the weighted average of the free and bound ligand signals. Nevertheless, deriving distance restraints from the filtered NOESY spectra should not introduce notable errors since the free Pex19p exists mainly in a random coil conformation and the NOESY spectrum of the free peptide is virtually void of cross-peaks (see Appendix II 7.2). Therefore, it is safe to assume that the sequential and long-range NOEs in the X-filtered NOESY experiments correspond to the bound form of Pex19p.

Table 3.2 and 3.3 provide an overview of the structural statistics of Pex14p (aa 16-80W) in complex with a Pex5p or Pex19p ligand. A total number of 1030 intraresidual restraints and 85 interresidual restraints for the Pex14p-Pex5p complex, as well as 904 and 127 for the Pex14p-Pex19p complex, were employed in the structure calculation. Structure quality and precision are satisfactory for the final ensemble including no distance or torsion angle violation higher than 0.5 A and 5°, respectively and is confirmed by superimposition of the low energy structures (Fig. 3.13 (A) and (B))

Table 3.2: Structural statistics of the Pex14p (aa 16-80W) and Pex5p (aa 116-124) complex.

	<SA> [1]	<SA>$_{water-ref}$
Number of NOE derived distance restraints		
All (unambiguous/ambiguous)	1115 / 3	
Sequential (|i-j| = 1)	199 / 0	
Medium range (1< |i-j| ≤ 4)	107 / 0	
Long range (|i-j| > 4)	149 / 0	
Intraresidual	575 / 0	
Hydrogen bonds	2* 19	
Pex14p intramolecular(unambiguous/ambiguous)	925 / 1	
Pex5p intramolecular(unambiguous/ambiguous)	105 / 0	
Intermolecular(unambiguous/ambiguous)	85 / 2	
R.m.s. deviation (Å) from experimental distance restraints [2]		
R.m.s.d. (unambiguous)	0.01 ± 0.001	0.02 ± 0.001
Hydrogen bonds (2* 19)	0.024 ± 0.003	0.029 ± 0.005
R.m.s. deviation (°) from experimental torsion restraints [3]		
R.m.s.d. (52 ϕ/ψ)	0.32 ± 0.04	0.29 ± 0.05
Q-factor for experimental residual dipolar coupling restraints [4]		
$^1D_{HN}$ (42)	0.13 ± 0.01	0.19 ± 0.01
Coordinate Precision (Å) [5]		
N, C^{α}, C'	0.36 ± 0.06	0.46 ± 0.06
All heavy atoms	0.86 ± 0.09	0.95 ± 0.1
Structural quality [6]		
Bad contacts	1 ± 0.9	0 ± 0
Ramachandran plot		
% in most favored region	91.3 ± 2.1	94.4 ± 3.6
% in additionally allowed region	8.4 ± 1.9	4.9 ± 2.2

[1]<SA> is an ensemble of 10 lowest-energy solution structures (out of 100 calculated) of the Pex14p/Pex5p complex before water-refinement. The CNS E_{repel} function was used to simulate van der Waals interactions with an energy constant of 25.0 kcal mol^{-1} Å^{-4} using "PROLSQ" van der Waals radii (Linge et al., 2003); r.m.s. deviations for bond lengths, bond angles and improper dihedral angles are 0.00206 ± 0.00008 Å, 0.41 ± 0.01° and 0.468 ± 0.015°. 1 kcal = 4.18 kJ.
[2]Distance restraints were employed with a soft square-well potential using an energy constant of 50 kcal mol^{-1} Å^2. For hydrogen bonds, distance restraints with bounds of 1.8-2.3 Å (H-O), and 2.8-3.3 Å (N-O) were derived for slow exchanging amide protons. No distance restraint was violated by more than 0.3 Å in the <SA> structures.

(see next page)

Table 3.3: Structural statistics of the Pex14p (aa 16-80W) and Pex19p (aa 66-77) complex.

	<SA> [1]	<SA>$_{water-ref}$
Number of NOE derived distance restraints		
All (unambiguous/ambiguous)	1015 / 15	
Sequential (|i-j| = 1)	111 / 8	
Medium range (1< |i-j| ≤ 4)	151 / 2	
Long range (|i-j| > 4)	175 / 2	
Intraresidual	467 / 2	
Hydrogen bonds	2* 20	
Pex14p intramolecular(unambiguous/ambiguous)	777 / 13	
Pex5p intramolecular(unambiguous/ambiguous)	127 / 1	
Intermolecular(unambiguous/ambiguous)	111 / 1	
R.m.s. deviation (Å) from experimental distance restraints [2]		
R.m.s.d. (unambiguous)	0.014 ± 0.001	0.023 ± 0.001
Hydrogen bonds (2* 19)	0.026 ± 0.002	0.034 ± 0.005
R.m.s. deviation (°) from experimental torsion restraints [3]		
R.m.s.d. (52 ϕ/ψ)	0.27 ± 0.06	0.40 ± 0.08
Coordinate Precision (Å)		
N, C^{α}, C'	0.51 ± 0.11	0.55 ± 0.07
All heavy atoms	1.106 ± 0.10	1.07 ± 0.08
Structural quality [6]		
Bad contacts	1.2 ± 0.6	0 ± 0
Ramachandran plot		
% in most favored region	86.9 ± 1.9	91.7 ± 2.0
% in additionally allowed region	13.1 ± 1.9	7.8 ± 2.1

[3]Dihedral angle restraints derived from TALOS (Cornilescu et al., 1999) were applied to φ, ψ backbone angles using energy constants of 200 kcal mol^{-1} rad^{-2}. No dihedral angle restraint was violated by more than 5.0°.
[4]Quality factor for the RDC refinement (Cornilescu et al., 1999). Residual dipolar couplings were applied with a final energy constant of 0.05 kcal mol^{-1} Hz^{-2} for an alignment tensor with an axial component of 19 Hz and a rhombicity of 0.37.
[5]Coordinate precision is given as the Cartesian coordinate r.m.s. deviation of the 10 lowest-energy structures in the NMR ensemble (residues 24-73 of Pex14p, 117-124 of the Pex5p peptide and 67-77 of the Pex19p peptide) with respect to their mean structure.
[6]Structural quality of the NMR ensemble before and after water refinement was analyzed using PROCHECK-NMR (Laskowski et al., 1996).

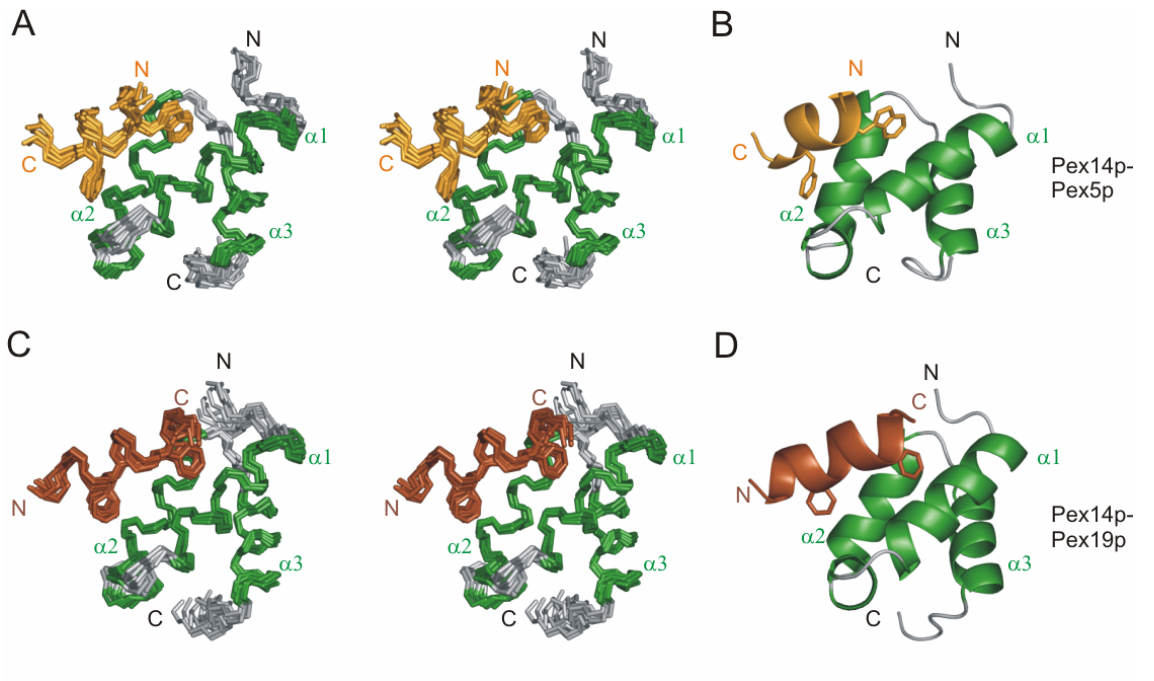

Fig. 3.13: Structure of the N-terminal Pex14p domain in complex with a Pex5p or Pex19p peptide

(**A**) Stereo view of the backbone atoms of the N-terminus of Pex14p (residues 19-76) in complex with the residues 116-124 of Pex5p. An NMR ensemble of the 10 lowest-energy structures (out of 100 calculated) is shown. The helices α1, α2, α3 and the helical linker between α1 and α2 of the protein are colored in green. The peptide is shown in gold. The side chains of Trp103 and Phe106 are highlighted.

(**B**) Ribbon diagram of the lowest energy structure in (A). The residues Trp103 and Phe106 of the peptide are shown as sticks representation.

(**C**) best-fit superposition of the backbone atoms of Pex14p (aa 19-76) in complex with Pex19p (aa 66-77). The ensemble shows 10 low-energy structures (out of 100 calculated). The peptide is shown in brown, the aromates Phe71and Phe75 of the Pex19p peptide are highlighted.

(**D**) Ribbon presentation of the lowest energy structure in (C). The residues Phe71 and Phe75 of Pex19p are displayed as sticks.

The complex consists of three α-helices and a helical linker between helix α1 and α2. This linking region shows typical features of a 3_{10} helix, such as a (i,i+3) hydrogen bond of the backbone carbon and amide atom of the residues 40 and 41 and Φ/Ψ angles of -93° ± 9/-28° ± 11, -60° ± 5/-35° ± 6, -58° ± 3/-29° ± 9 and -108° ± 11/-6° ± 23 for the residues R40, V41, R42 and N43 of Pex14p (calculated by MOLMOL as the average value of the 10 lowest energy structures of the Pex14p-Pex5p complex).

Helix α1 and α2 of N-Pex14p are aligned in an anti-parallel orientation (Fig. 3.13). Helix α3 forms a stabilizing scaffold in a transverse arrangement from the tip of helix α2 to the bottom

of helix α1 and does not contribute to the binding. The bound Pex5p or Pex19p peptide forms an amphipathic α-helix whereas Pex19p is oriented in the opposite direction compared to Pex5p. No evidence was found that Pex19p can bind in both orientation and all observed intermolecular NOEs can be accounted for the inverse interaction. Fig 3.14 shows a cut out of a $^{1}H^{1}H$-NOESY spectra. Intermolecular NOEs between the peptide residues Phe70, Phe71 of Pex19p and V41 of Pex14p as well as Phe75 and T31 demonstrate clearly the inverse orientation. The large distance of about 10Å between these residues makes the assignment unambiguous.

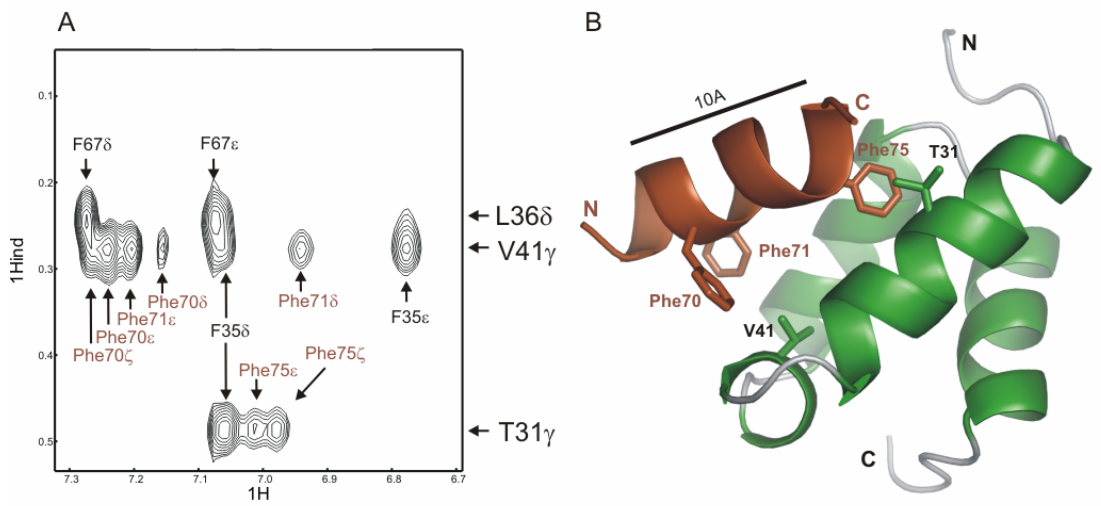

Fig 3.14: (**A**) Part of a $^{1}H,^{1}H$-NOESY (600 MHz, 200ms mixing time, 303K) depicting NOEs between Pex14p (black) and Pex19p (brown). The peptide residue Phe70 and Phe71 show NOEs to residue V41 of Pex14p. Residue Phe75 of Pex19p interacts with residue T31 of the protein (**B**) Ribbon diagram of N-terminal Pex14p in complex with Pex19p. The residues Phe70, Phe71 and Phe75 of Pex19p and V41 and T31 of the protein are shown as sticks. The black bar indicates a

The protein-peptide binding interface is 390A^2 for Pex14p-Pex5p and 460A^2 for Pex14p-Pex19p large (calculated according to (Richards, 1977), via the program NOC) and is mainly stabilized by hydrophobic interactions. The N-Pex14p interaction surface is built up by residues from helices α1 and α2, as well as the linking elements between α1-α2 and α2-α3, respectively. It forms two hydrophobic pockets, separated by two aromatic residues (F35 and F52), which are flanked by basic amino acids; leading to a positive charged protein surface. One of these basic residues, K56 of Pex14p, is highly conserved (Fig. 3.16).

Intermolecular NOEs from Pex14p residues L28, T31, F35, N38, R40, V41, S44, T48, R49, F52, L53, K56, L58 to residues Trp118, A119, F122 and Leu123 of Pex5p were used as distance restraints to calculate a structural ensemble of the N-Pex14p-Pex5p complex. The amino acids Phe70, Phe71, Leu74, Phe75, Asp76 and Ser77 of Pex19p interact with similar residues, but while additional NOEs to the residues K34 and P44 could be identified, the ones to R49 and L53 were missing for the Pex14p-Pex19p complex (Fig 3.15). Compared to the helix of the Pex5p peptide, which is centered between helix α1 and α2 of the protein, the hydrophobic side chains of the Pex19p peptide are oriented to a larger extent towards helix α1 of Pex14p (Fig.3.15 (A) and (B)).

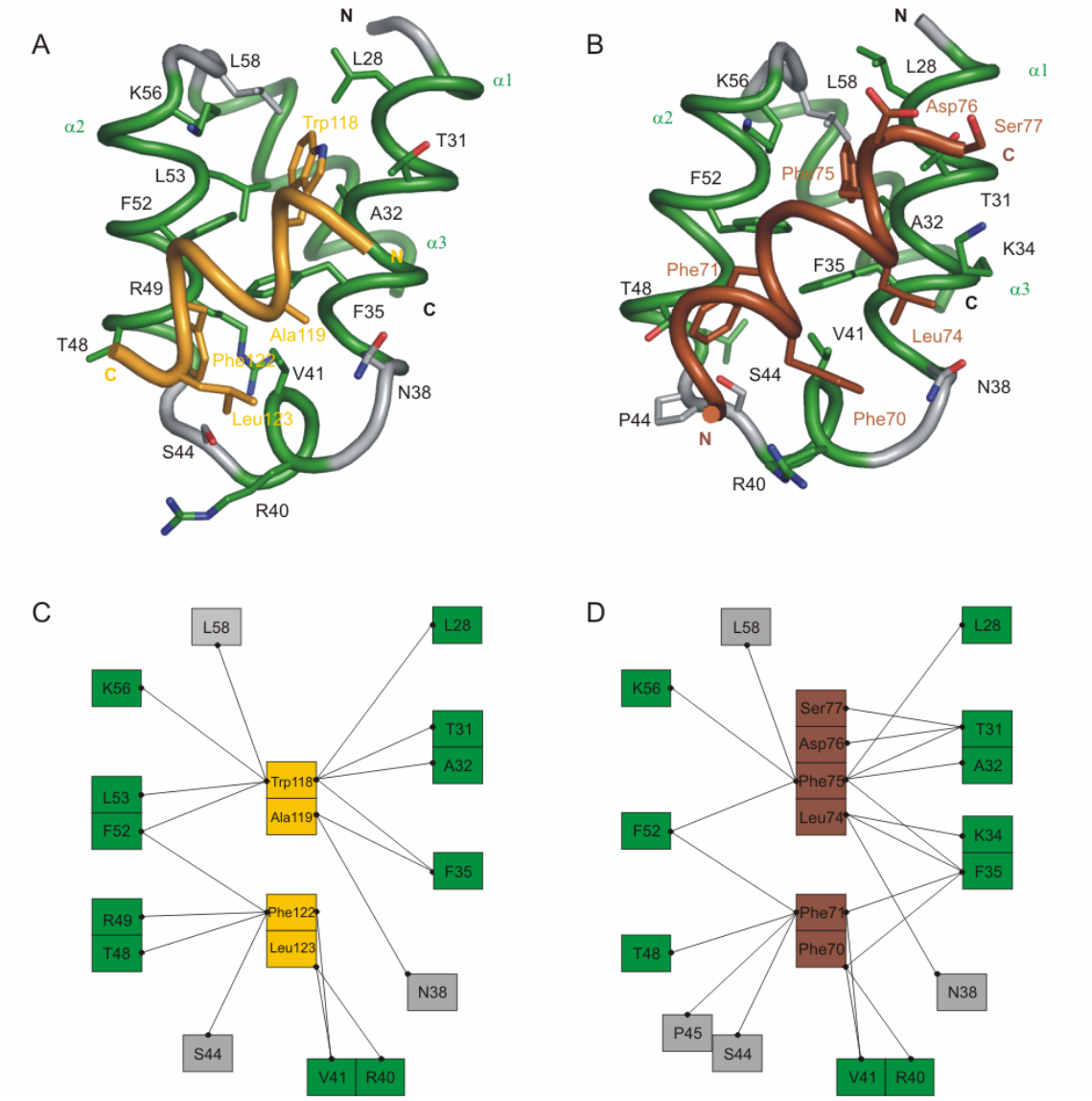

Fig. 3.15: (**A**) and (**B**) Worm and stick model of the molecular recognition interface of Pex14p and Pex5p (**A**) and Pex14p and Pex19p (**B**). The protein is shown in grey, the peptide in gold or brown. Helical elements of Pex14p are green. Positive and negative charged residues are colored in blue and red, respectively. Protein residues contributing to intermolecular NOEs are labeled.
(**C**) and (**D**) schematic overview of the intermolecular NOEs between Pex14p and its ligand. Residues of Pex14p in loops are shown in grey, helical residues in green. The peptide residues are colored gold (Pex5p) and brown (Pex19p).

The aromatic residues of the ligand, Trp118 and Phe122 of Pex5p or Phe71 and Phe75 of Pex19p insert directly into the Pex14p binding pockets (Fig. 3.16A and C). While the Pex14p-Pex19p binding is only mediated by hydrophobic interactions, residue Glu116 of Pex5p forms a salt-bridge to the conserved protein residue K56. Structural calculations of the Pex19p

ligand suggest an intrahelical salt bridge. All 10 lowest energy structures calculated by ARIA show an orientation of Glu73 towards Lys69 of Pex19p. In 4 of the 10 lowest energy structures the distance between the residues is close enough to form a salt bridge. In comparison to Pex5p the Pex19p peptide is shifted half a helix turn "upwards" (Fig. 3.16).

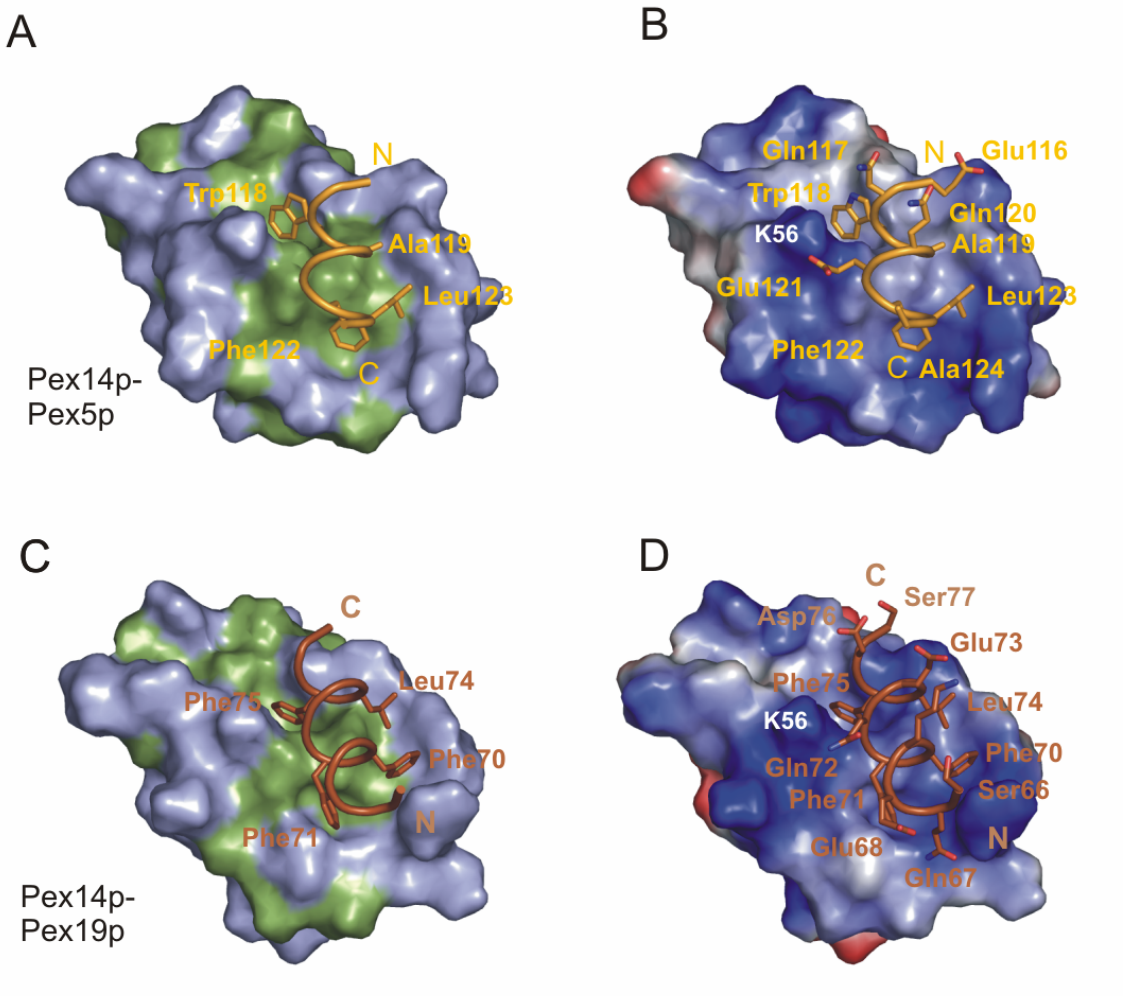

Fig. 3.15: Surface representation of the N-terminus of Pex14p and a stick representation for Pex5p (aa 116-124) (gold) or Pex19p (aa 66-77) (brown). The conserved K56 of Pex14p is indicate in white (**A** and **C**) Hydrophobic residues are colored green, hydrophilic light blue. Hydrophobic peptide residues are shown as sticks. (**B** and **D**) Electrostatic charge distribution, positive charges are indicated by blue colors, negative charges are shown in red.

3.7.5 Comparison of the Pex5p and Pex19p ligand interaction

The orientation of the 3 helix bundle of N-Pex14p in complex with Pex5p is identical to the Pex14p-Pex19p complex. The backbone atoms within the helical regions of the protein superimpose with an r.m.s deviation of 0.9 Å, reflecting the differences between the two structures, especially in the interaction interface. Compared to the Pex14p-Pex5p interaction the helix α2 of Pex14p in complex with Pex19p is slightly shifted, allowing a tighter packing towards the aromatic peptide residue Phe75. The superimposition of the two peptide sidechains shows a strong similarity between the key residues of both peptides (Fig. 3.17).

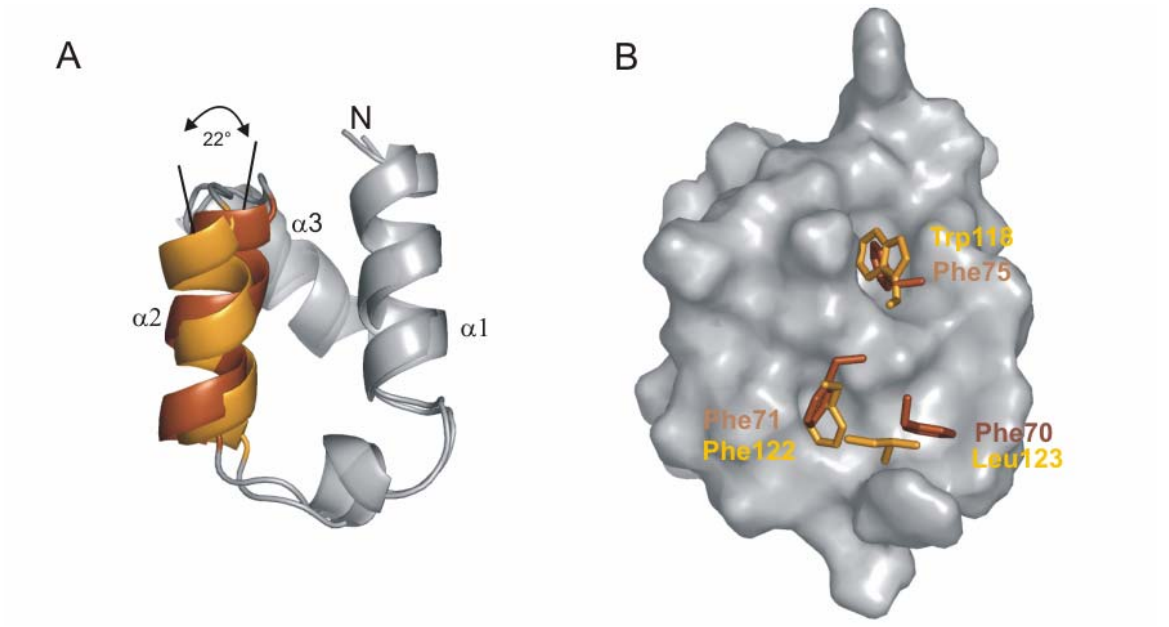

Fig. 3.17: Superimposition of N-Pex14p complexes. The Pex14p-Pex5p complex is displayed in gold, the Pex14p-Pex19p complex in brown. (A) Ribbon diagram of Pex14p-Pex5p and Pex14p-Pex19p. Helix α2 angles are indicated by black bars. (B) Surface representation of N-Pex14p. Peptide residues inserting into the binding pockets are shown as sticks

The Trp118 of Pex5p and the Phe75 of Pex19p occupy the "upper" binding pocket in the same vertical orientation. Both residues can be accounted as the key anchor residues of the interaction with a ΔASA of 173Å^2 and 158Å^2, respectively. Phe71 (Pex19p) and Phe122 (Pex5p) share a similar position in the "lower" binding pocket, whereas the Pex5p residue is oriented more towards the aromatic residues F35 and F52 of the protein and inserts deeper into the binding pocket (ΔASA 118Å^2 compared to 94Å^2) In contrast to Phe70 of Pex19p,

which is embedded laterally in the "lower" binding pocket, the Leu123 of Pex5p is only attached peripherally (ΔASA 87Å^2 for Phe70 compared to 25Å^2 for Leu123). Sums of all key residues show a comparable change in accessible surface area (Table 3.2).

Table 3.2: ΔASA of key residues

	ΔASA		ΔASA
5-Trp118	173 Å^2	19-Phe75	158 Å^2
5-Phe122	118 Å^2	19-Phe71	94 Å^2
5-Leu123	25 Å^2	19-Phe70	87 Å^2
Σ	316 Å^2		339 Å^2

3.8 Competitive binding of Pex19p and Pex5p

3.8.1 NMR titration experiments

To investigate the binding properties of Pex19p and Pex5p ligand competitive NMR titration experiments were performed. First Pex14p (aa 16-80) was titrated up to the point of saturation with Pex5p and Pex19p peptide alone. The change of chemical shifts was monitored via a 2-dimensional $^1H^{15}N$-HSQC. Mapping of perturbed backbone amide signals upon Pex5p or Pex19 addition onto the surface of N-Pex14p reveal a well overlapping binding groove between helices α1 and α2 and the connecting linker l1 (Fig. 3.18C). While the peaks of the N-Pex14p-Pex19p were in fast exchange on the chemical shift time scale, the resonances of the N-Pex14p-Pex5p complex are in slow exchange, suggesting a tighter binding of the Pex5p ligand. In a third experiment N-Pex14p was first titrated with Pex19p peptide and then cross-titrated with the Pex5p ligand. The chemical shift perturbation was monitored again and compared with the single titration experiments (Fig. 3.18C). The endpoints of the cross-titration (Fig. 3.18B) are identical with the single titration (Fig. 3.18A), suggesting that Pex19p ligand is quantitatively replaced by the stronger binding Pex5p peptide.

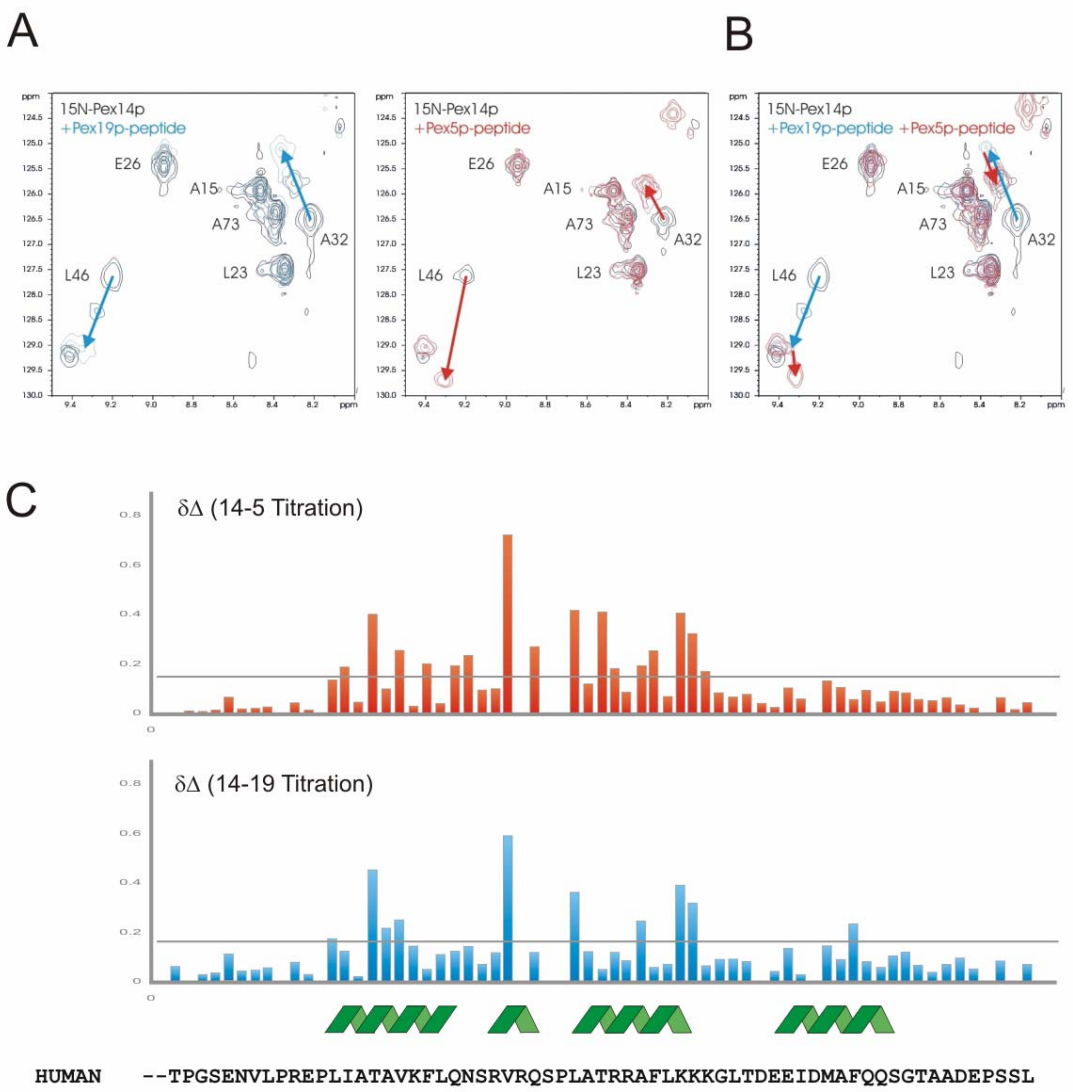

Fig. 3.18: Competitive NMR titration of N-terminal Pex14p with a Pex19p and Pex5p peptide (**A**) $^{1}H,^{15}N$ correlation spectra of ^{15}N-labeled recombinant N-terminal Pex14p (aa 16-80W) in free form (black) and in complex with Pex19p peptide (aa 61-77) (blue) and Pex5p (red) (aa 116-124). (**B**) Free 15N-labeled recombinant Pex14p (aa 16-80W) (black) was titrated with Pex19p peptide (aa 61-77) (blue) to the point of saturation. The complex was cross-titrated with Pex5p peptide (aa 116-124) (red). (**C**) NMR chemical shift changes ($\Delta\delta=(\delta_{15N}^{2}+\delta_{1H}^{2})^{1/2}$) of Pex14p (aa 16-80W) in the presence of saturated concentrations of the Pex5p (red) and the Pex19p (blue) ligand. Secondary structure elements are indicated at the top of the sequence.

3.8.2 Isothermal titration calorimetry

To verify and to quantify the NMR titration data ITC experiments were performed. As expected both ligands form a 1:1 complex with N-terminal Pex14p.

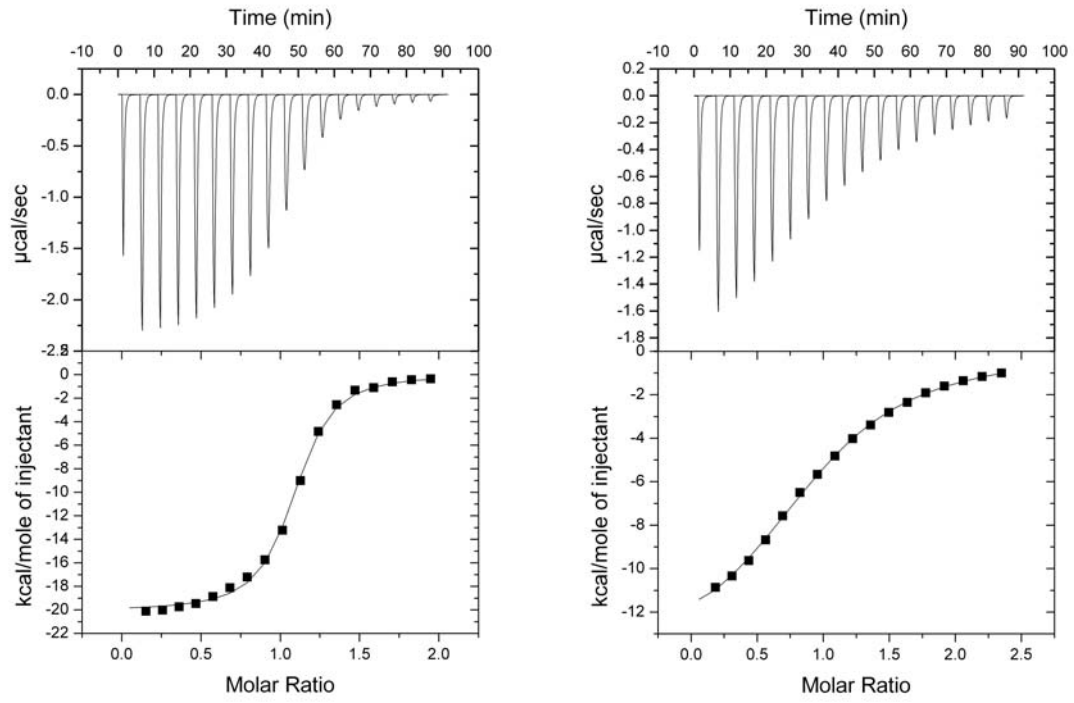

Fig. 3.19: ITC of N-Pex14p with a Pex5p or a Pex19p ligand
Representative raw ITC data (top) and integrated data fits (bottom) are shown for Pex14p (aa 16-80W) with Pex5p (aa 116-124) (left) and Pex14p (aa 16-80W) with Pex19p (aa 61-77) (right). All experiments were conducted at 25°C in 50mM potassium phosphate buffer pH 6.5 supplemented with 100mM NaCl. Ligand dilution controls were substracted.

The binding of the Pex5p peptide is about 20 times stronger than the Pex19p-Pex14p interaction (with a K_d of 0.45µM compared to 9.13µM). Both reactions are enthalpy driven. The free energy of the Pex14p-Pex5p interaction is about 20% higher than the energy of the Pex14p-Pex19p interaction (36.2kJ/mol to 28.8kJ/mol). Entropy values of both interactions are in the same range of -0.16 kJ/molK (Pex14p-Pex5p) and -0.1 kJ/molK (Pex14p-Pex19p). Table 3.3 shows a summary of the binding data.

Table 3.3: Summary of the binding thermodynamic parameters of the N-Pex14p-ligand interactions

Reaction	N	K_a x10^5 (M^{-1})	K_d (μM)	ΔH (kJ mol^{-1})	ΔS (J mol^{-1} K^{-1})	ΔG (kJ mol^{-1})
Pex14p (aa 16-80W) – Pex5p (aa 116-124)	1.02 ± 0.03	22.2 ± 0.78	0.45 ± 0.02	-83.4 ± 1.02	-159.5 ± 3.6	-36.2 ± 0.88
Pex14p (aa 16-80W) – Pex19p (aa 61-77)	1 ± 0.07	1.14 ± 0.29	9.13 ± 2.26	-59.5 ± 0.65	-103 ± 3.6	-28.8 ± 0.63

Fig. 3.20 shows a qualitative ITC experiment. Addition of Pex5p to an N-Pex14p-Pex19p complex leads to a heat release, whereas addition of Pex19p to an N-Pex14p-Pex5p complex does not cause further release of free energy.

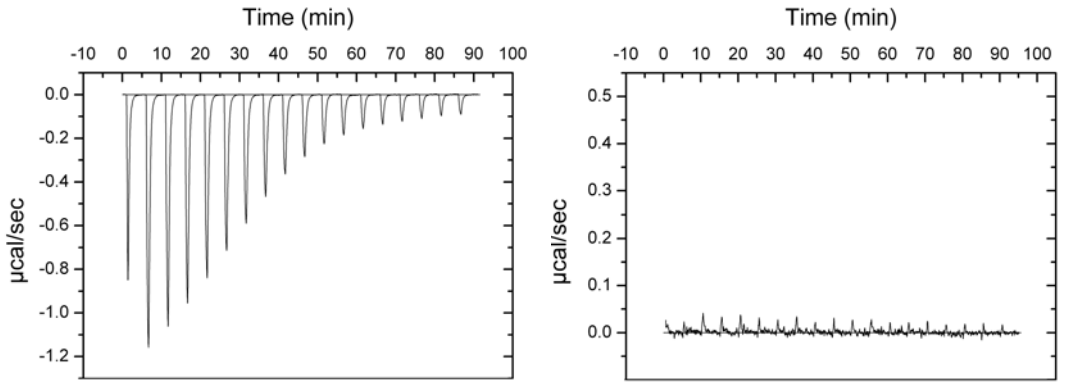

Fig. 3.20: Qualitative ITC experiment

Raw ITC data of the titration of a Pex14p (aa 16-80W)-Pex19p (aa 61-77) complex with Pex5p (aa 116-124) (left) and a Pex14p (aa 16-80W)-Pex5p (aa 116-124) with Pex19p (aa 61-77) (right). Both experiments were conducted in 50mM potassium phosphate buffer pH 6.5 supplemented with 100mM NaCl at 25°C. Ligand dilution controls were substracted

4 Discussion

The principles of peroxisomal protein import are well conserved among the species. Four stages can be distinguished: cargo recognition, docking to the peroxisomal membrane, cargo release and receptor recycling (overview by Erdmann and Schliebs, 2005). Pex14p is a central component of the docking complex and interacts with the PTS receptors Pex5p and Pex7p (Brocard et al., 1997; Rehling et al., 1996), as well as with several other membrane bound peroxins. Human Pex14p comprises different functional domains, i.e. a highly conserved N-terminal region, a hydrophobic segment, and a coiled coil domain. The N-terminus of Pex14p interacts with the PTS1 receptor Pex5p, Pex13p, a member of the peroxisomal docking complex (Albertini et al., 1997) and the multifunctional protein Pex19p (Fransen et al., 2004). This work presents functional und structural studies of the N-terminus of human Pex14p in complex Pex5p and Pex19p and provides insight into the molecular details of the early steps of peroxisomal protein import.

4.1 Definition of domain borders of N-terminal Pex14p

So far the only two biophysical techniques that allow structural studies at atomic resolution are X-ray crystallography and NMR spectroscopy. A starting point for both methods is the availability of a well structured and soluble protein target. Although several studies defined domain borders N-terminal of human Pex14p (Fransen et al., 2004; Itoh and Fujiki, 2006; Saidowsky et al., 2001), these were characterized rather on functional than structural aspects and are mainly based on the ability of N-Pex14p truncation constructs to bind to a ligand. An exopeptidase assay performed for the present study defined a globular N-terminal domain of Pex14p reaching from residue 16 to 78. NMR relaxation experiments revealed a slightly shorter structured region comprising amino acids 24 to 73. The residues preceding and following this domain, displayed a high flexibility, an observation that possibly provides an

explanation for the failure to obtain crystals of N-terminal Pex14p-constructs with more than these 50 residues. On the other hand protein constructs comprising only the structured part of the N-terminal domain turned out to be insoluble. Protein insolubility is often a result of misfolding (Dobson and Karplus, 1999), thus the insolubility of these constructs could possibly indicate protein misfolding and implicate the requirement of these flexible residues for structural stabilization of the domain.

4.2 Large scale *in vitro* complex formation of N-terminal Pex14p and different ligands

During the last years several studies of mammalian Pex14p and its ligands were published (Fransen et al., 2002; Fransen et al., 2001; Itoh and Fujiki, 2006; Otera et al., 2002; Reguenga et al., 2001; Saidowsky et al., 2001; Will et al., 1999). Most of the interaction studies were carried out by using recombinant or endogenous proteins in pull down assays. On the basis of these publications and as a prerequisite for crystallization trials, we established extensive, large scale *in vitro* complex formation between N-terminal Pex14p constructs and different N- and C-terminal Pex5p constructs or N-terminal Pex19p. Although all complexes were soluble and showed high purity, crystallization failed. Interestingly, we were able to show interaction between N-terminal Pex14p and Pex5p (aa 268-639), a construct, whose WxxxF/Y motif has been reported to show no or very low *in vitro* interaction with N-terminal Pex14p (Otera et al., 2002; Saidowsky et al., 2001). This discrepancy may be due to various causes, such as different experimental conditions, higher sample concentrations or a stabilizing influence of the structured TPR domain.

4.3 N-terminal Pex14p does not interact with the SH3 domain of Pex13p *in vitro*

The interaction of a classical PxxP II motif of N-*Sc*Pex14p with the SH3 domain of *Sc*Pex13p has been clearly demonstrated on a molecular level (Douangamath et al., 2002). However, there seem to be differences between yeast and higher eukaryotes. Mammalian Pex14p lacks a classical PxxP II motif, but has several non canonical PxxP motifs in its N-terminus. Recent studies locate the Pex13p binding site at the conserved N-terminal domain of Pex14p

(Fransen et al., 2004; Otera et al., 2002), even narrowing down the respective region to a few residues containing a PxxP motif (Itoh and Fujiki, 2006). The same studies suggested an influence of the Pex13p-Pex14p interaction on the binding behavior of Pex14p to Pex5p and to Pex19p. To specify these influences we investigated the interaction of N-Pex14p and the SH3 domain of Pex13p. Surprisingly, *in vitro* binding assays revealed no interaction between the two domains. These results could be confirmed by NMR experiments since fingerprint spectra of N-terminal Pex14p show no chemical shift perturbation upon addition of Pex13p-SH3 and thus no interaction. A major difference between the studies mentioned above and ours lies in the different length of Pex13p constructs used. While the interaction data described in these publications was based on Pex13p constructs comprising the whole C-terminus of Pex13p, the construct used in this study contained only the SH3 domain. Although it can not be excluded that the recombinant SH3 construct used was misfolded and not functional, it might also be possible that the SH3 domain of human Pex13p alone is not sufficient to bind N-terminal Pex14p. Nevertheless, current data is limited and further experiments will be required to investigate this phenomenon.

4.4 Three dimensional fold of N-terminal Pex14p

The N-terminal Pex14p domain consists of a 3-helical bundle. Helices α1 and α2 are aligned in an antiparallel orientation and together with the linker regions between helix α1/α2 and α2/α3, form a groove which buries hydrophobic ligands. Helix α3 provides a stabilizing scaffold and does not contribute to the binding. The interaction interface overlaps well with the conserved signature sequence $AX_2FLX_7SPX_6FLKXKGL/V$ present in all Pex14p proteins described previously (Madrid and Jardim, 2005). The linking element between helix α1 and α2 is flexible in free Pex14p and adapts helical conformation upon ligand binding. Depending on the ligand, helix α2 is slightly shifted. This displacement causes an enlargement of the "upper" and narrowing of the "lower" binding pocket on Pex5p binding. The structural arrangements upon ligand binding can be accounted as an induced fit mechanism (Jorgensen, 1991; Koshland, 1958) providing optimal interactions resulting in a tightly packed interface. In addition to hydrophobic interactions the Pex5p binding is stabilized by an additional salt-bridge. While the Pex5p ligand is centered between the two interface helices, Pex19p is oriented towards helix α1. This leads to a larger protein-peptide interface and potentially

stronger hydrophobic interactions between Pex14p and Pex19p. This is consistent with previous findings that an N-terminal Pex14p construct with a truncated helix α1 is still able to bind Pex5p but not Pex19p (Itoh and Fujiki, 2006).

4.5 Pex19p and Pex5p compete for the same Pex14p binding site

Previous studies have shown that Pex19p and Pex5p bind to the same N-terminal domain of Pex14p (Fransen et al., 2004; Itoh and Fujiki, 2006). Although these studies indicated that this binding might be competitive and Pex5p was likely the stronger interaction partner, no details were known. In order to investigate and quantify the binding properties of the Pex14p ligands Pex5p and Pex19p we carried out NMR and ITC experiments. Cross titration showed that the Pex5p peptide can quantitatively replace Pex14p-bound Pex19p, while Pex19p is not able to substitute bound Pex5p. The collected ITC data characterize the Pex5p-Pex14p binding about 20 times stronger than Pex19p-Pex14p interaction. Interestingly, dissociation constants received for the Pex14p-Pex5p complex are about one magnitude higher than reported previously (Saidowsky et al., 2001). An explanation for this discrepancy could lie in the different experimental approach (Surface plasmon resonance spectroscopy and fluorescence titration analysis compared to isothermal titration calorimetry) or in the different length of measured peptides (see paragraph 4.7).

The NMR fingerprint spectra of the titration of N-terminal Pex14p with a Pex5p and a Pex19p peptide, respectively, reveal an identical binding groove. These results support our three-dimensional models of both the Pex14p-Pex19p and Pex14p–Pex5p complex and contrasts recent suggestions that competition could occurs via induction of structural changes, rather than by direct competition for binding sites (Fransen et al., 2004). The lower affinity of Pex19p suggests a more intermediate character of the Pex14p-Pex19p interaction while the stronger binding of Pex5p to Pex14p would suit its role in the early steps of peroxisomal protein import (see paragraph 4.9).

4.6 Molecular details of ligand recognition

Protein interactions involve the specific complementary recognition of two molecules to form a stable complex. Thereby recognition depends mainly on a few critical residues at the binding interface, which are often conserved. The association processes is driven by different favouring factors like hydrophobic and electrostatic interactions and shape complementarity (Bogan and Thorn, 1998; Jones and Thornton, 1996; Valdar and Thornton, 2001).

Our studies revealed that Pex19p and Pex5p bind to Pex14p in a similar manner, although Pex19p lacks a classical WxxxF/Y motif (Fransen et al., 2005). Both peptides form an amphipathic helix which allows their aromatic residues to insert into the Pex14p binding pockets, forming the main anchors of interaction. The aromatic residues of the conserved WxxxF/Y motif are deeply buried into two binding pockets at the Pex14p interaction interface. The interaction is stabilized by a salt-bridge between the conserved K56 of Pex14p and Glu121 of Pex5p. Compared to Pex5p, Pex19p binds in a reverse orientation and is shifted towards the "upper" binding pocket, in which a C-terminal phenylalanine mimics the tryptophan of Pex5p. The Pex14p-Pex19p complex lacks an intermolecular salt bridge but the Pex19p ligand is stabilized by a potential intrahelical salt bridge between Lys69 and Glu73. Intrahelical (i,i+4) salt bridges contribute to helix stability by a value of up to -0.5 kcal/mol (Lyu et al., 1992). The change in accessible surface area of the residues in both complexes is similar (paragraph 3.7.5). The Pex14p-Pex19p interaction has an even larger overall interaction surface, which leads to potentially stronger hydrophobic interactions, a main driving force in the stabilization of protein associations (Chothia and Janin, 1975; Dill, 1990). Nevertheless, Pex5p binds stronger to Pex14p than Pex19p. One possible explanation may be found in the formation of the intermolecular salt bridge between Pex5p and Pex14p. Although the energy contribution of solvent exposed salt bridges to free binding energy is rather low (-0.16-1 kcal/mol) (Brown et al., 1978; Louie et al., 1988), they lead to a decrease in the off rate of complex association. Thereby the salt-bridge serves as a "latch", which stabilizes the interaction by locking down forming complexes to their final position. (Kimura et al., 2001). Another reason for the higher binding affinity of Pex5p might be the different prefold of free ligands. The term prefold is used herein to describe the conformity in structural arrangement of the free and bound ligand. Secondary chemical shift analysis reveals a helical conformation for free Pex5p peptide. Although free Pex19p displays a helical tendency, the structural rearrangements upon binding appear to be larger compared to Pex5p. Structural rearrangements come along with a loss of translational and rotational freedom of amino acids

and oppose the association of proteins. A prefolded interaction motif leads to a faster recognition, an increase of the on rate of complex formation and therefore to higher binding affinities (Camacho et al., 2000; Kimura et al., 2001; Rajamani et al., 2004).

4.7 Pex14p binds helical ligands in different orientations

Although it has been reported that Pex14p is able to bind an inverse WxxxF/Y motifs in *S.cerevisae*, the reverse orientation of the FxxxF Pex19p peptide was unexpected, but can be explained on a molecular level. Regular orientation of Pex19p offers two alternatives how the aromatic side chains of Phe70, Phe71 and Phe75 can insert into the Pex14p binding pockets: one would lead to a complete mismatch of the amphipathic helix (Fig. 4.2A-3 and 4.2B-3), the other to a sterically unfavorable alignment of key residues by switched positions of the medium-size hydrophobic residue Leu74 and the bulky anchor residue Phe71. (Fig. 4.2A/B-2 and 4.2A/B-4). The salt bridge formation possible to form between K56 of Pex14p and Glu73 of Pex19p is either not sufficient to stabilize this orientation or may even have the opposite effect by removing a favorable intrahelical salt bridge between Lys69 and Glu73. Regular orientation would further lead to unfavorable contacts of hydrophilic Pex19p residues to the surface of Pex14p (Fig 4.2B-3 and -4). In contrast, a C-terminal elongation of the observed inverse Pex19p and N-terminal elongation of the Pex5p helix show a perfect match between hydrophobic ligand residues and protein surface (Fig 4.2B-1 and -2). The additional contact surface probably enhances both binding affinity and complex stability. This is consistent with studies showing that longer amphipathic peptides elicit higher affinity to the N-terminus of Pex14p (Choe et al., 2003).

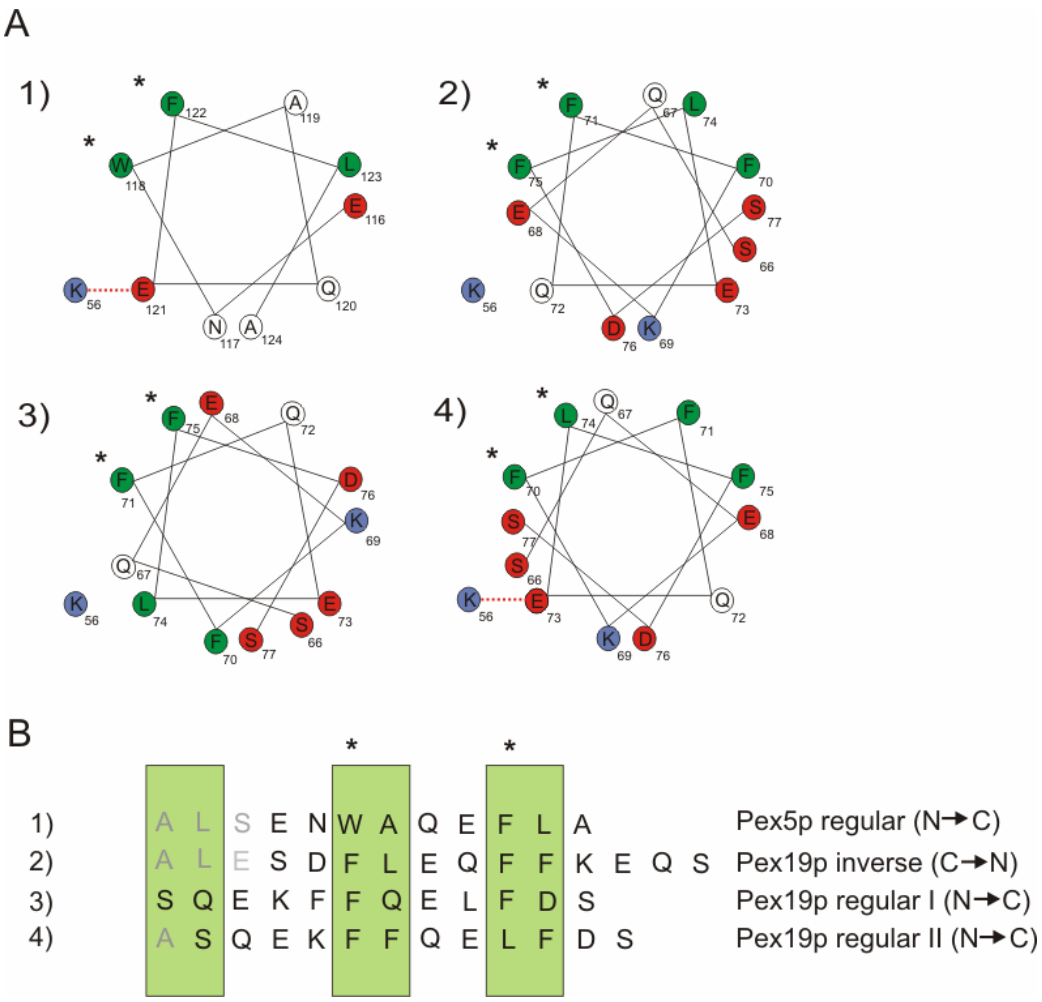

Fig. 4.2: (**A**) Helical wheel representation (Schiffer and Edmundson, 1967) of the Pex5p (aa 116-124) peptide (**1**), the inverse orientation (**2**) and the regular orientation I (**3**) and II (**4**) of Pex19p (aa 66-77) in complex with Pex14p. Basic residues are coloured in blue, acidic ones in red and hydrophobic ones in green. Small or neutral residues were left blank. Residues inserting into the binding pockets are marked by an asterisk. Salt bridge formation to K56 of Pex14p is indicated by dashed lines. (**B**) Alignment of Pex5p and Pex19p peptide in different orientations. Gray letters display the elongated ligand sequence, black letters the peptide sequence used in this study. Residues facing the Pex14p protein surface are indicated in light green.

The ability to bind to helical peptides in either direction is a feature that Pex14p shares only with calmodulin, Sin3 corepressor PAH2 domain and SH3 domains (Hoeflich and Ikura, 2002; Kuriyan and Cowburn, 1997; Swanson et al., 2004) (Fig. 4.2).

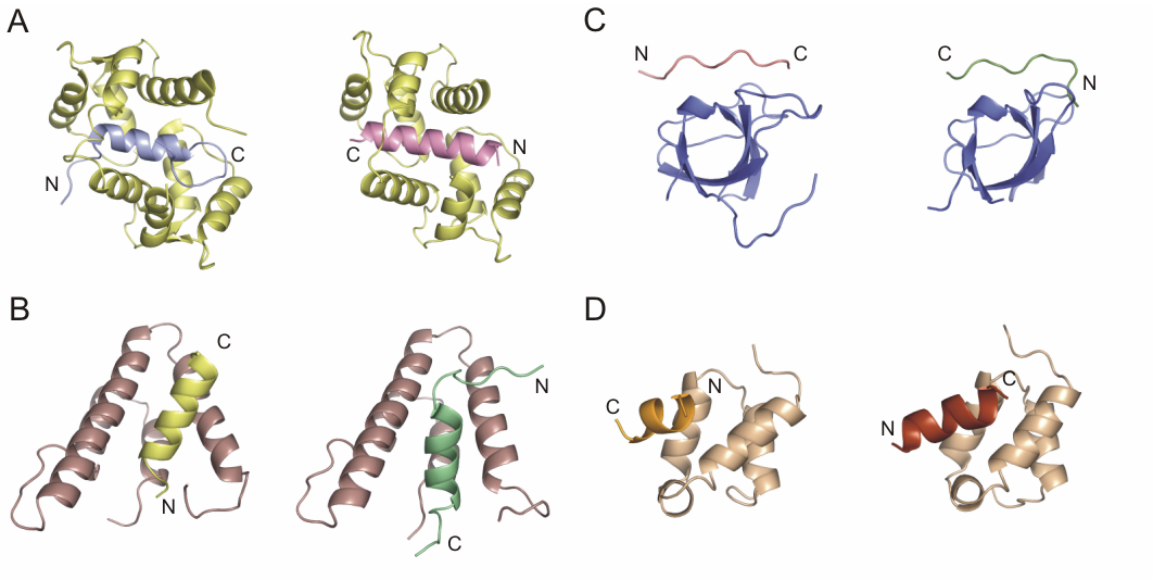

Fig. 4.2: Examples of modular domains with different ligand orientations:
(**A**)Ribbon diagramm of the CaM-CaMKK (left) and CaMKII complex (right). (**B**) PH2 domain of the Sin3 corepressor in complex with Mad1 SID (left) and HBP1 SID (right). (**C**) *Sc*Pex13p SH3 in complex with the PPII motif of *Sc*Pex14p (left) c-CRK SH3 domain in complex with a PPI ligand (right). (**D**) N-terminal domain of hsPex14p in complex with the first WxxxF/Y motif of hsPex5p and the FxxxF motif of *hs*Pex19p.

The former two domains interact with short amphipathic helices, the later with polyproline helices. Ligand orientation of SH3 domains and calmodulin is determined by ionic interactions between positively charged residues in the peptide and their counterpart on the protein surface. The PAH2 domain of Sin3 recognizes a patch of conserved hydrophobic residues whose alignment also determines the orientation of the ligand. N-Pex14p appears to combine both features. As mentioned above, ligand orientation is mainly determined by the alignment of the WxxxF/Y motif in the protein sequence. In case of a pseudo-symmetrical motif like the FxxxF of Pex19p the ligand orientation is determinant by residues flanking the aromatic core motif. Thereby, sterical arrangement of large hydrophobic residues and ionic interactions between a conserved lysine and its counterpart in the ligand sequence serve as selection criteria. The inverse binding of the Pex19p ligand gives rise to the question if such a feature has evolved accidentally, or has a biological function to fulfill.

4.8 The N-terminus of Pex14p, a new modular domain?

Protein-protein interactions are widely spread and probably involved in every biological process. Despite the large variety of interactions coupled with the differences in interfacial size and nature, two general classes of interactions can be discriminated. The domain-domain interaction is characterized by complexation of prefolded structural units, while domain-peptide interactions comprise the binding of a structured component to a short, often unstructured, recognition motif (Wodak and Janin, 2002). The latter one is often divided into sub classes according to popular modules repeatedly found in homologous and modified forms. Such modules are compact, stable units with a typical three-dimensional structure, which can fold and function independently of the rest of the protein. The functions of modular domains are variable, but a large group is specialized in recognition of regular motifs and/or folds (Liddington, 2004). This study reveals that N-Pex14p displays characteristics of a new modular protein structure. The modular domain comprises about 50 residues and is conserved among the species. Its molecular scaffold consists of a three-helical bundle, recognizes a diaromatic motif and is the target of at least two different ligands, i.e. Pex5p and Pex19p, in mammals. The main function of the N-terminus of Pex14p certainly lies in the peroxisomal protein import. Nevertheless an involvement of the N-terminal part of Pex14p in peroxisomal degradation (Bellu et al., 2001) and a possible role as a corepressor of the transcriptional regulation factor NF-E2 has been reported (Gavva et al., 2002).

4.9 Role of the Pex14p-Pex5p and Pex14p-Pex19p interaction

It is generally accepted that Pex14p is a key component of the docking complex and plays a crucial role in the early steps of peroxisomal protein import. Nonetheless, the exact function of Pex14p is still unclear. While some studies propose it as the initial docking site of Pex5p, others suggest an involvement in formation and stabilization of a putative Pex5p import channel. A key argument for all proposed models is the localization of the N-terminal domain, which has been investigated by immunofluorescence and protease protection assays and has been reported to be cytosolic, luminal and/or embedded into the peroxisomal membrane (reviewed by Azevedo and Schliebs, 2006). Our structural data shows large clusters of hydrophilic residues on the domain surface, making a complete embedment into the peroxisomal membrane very unfavourable. However, the hydrophobic interaction interface of

N-terminal Pex14p is surrounded by an accumulation of positively charged residues, which could provide a perfect counterpart for the carboxyl headgroup of membrane lipids. This direct attachment to the peroxisomal membrane could occur on either site of the peroxisomal membrane and would probably sufficient to protect the N-terminus of Pex14p from proteases or antibodies. On the other hand, such a limited accessibility would also affect the recognition of a ligand, i.e. Pex5p. The problem would most likely be overcome, if Pex5p approximates the N-terminal domain from the membrane site. In such a model, Pex14p could stabilize, or anchor, membrane inserting Pex5p on the luminal site of the peroxisomal membrane (Fig. 4.3).

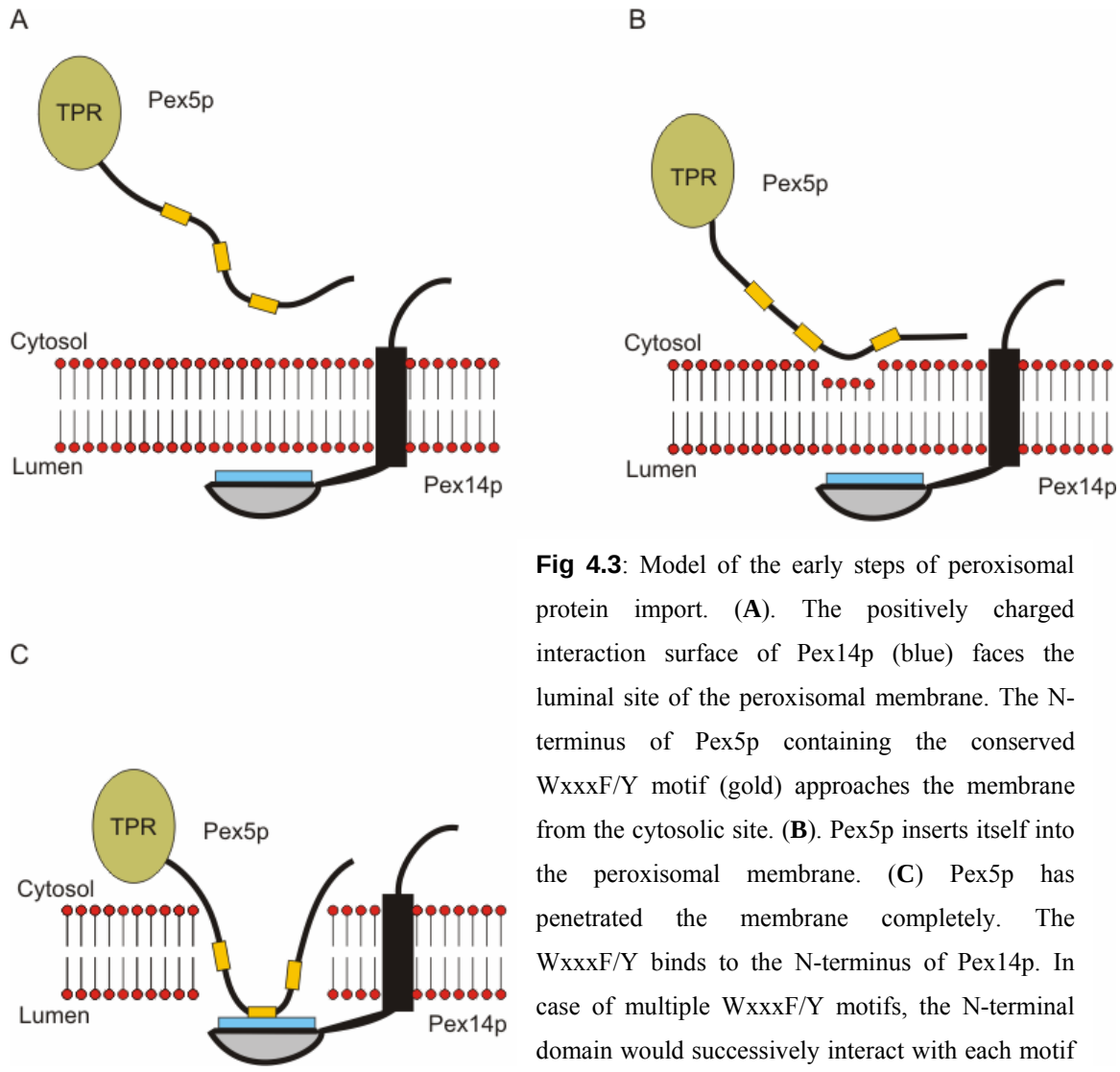

Fig 4.3: Model of the early steps of peroxisomal protein import. (**A**). The positively charged interaction surface of Pex14p (blue) faces the luminal site of the peroxisomal membrane. The N-terminus of Pex5p containing the conserved WxxxF/Y motif (gold) approaches the membrane from the cytosolic site. (**B**). Pex5p inserts itself into the peroxisomal membrane. (**C**) Pex5p has penetrated the membrane completely. The WxxxF/Y binds to the N-terminus of Pex14p. In case of multiple WxxxF/Y motifs, the N-terminal domain would successively interact with each motif until the one with the highest binding affinity is reached.

Although the membrane insertion of Pex5p takes place independently of other proteins, as proposed before (Erdmann and Schliebs, 2005), the model implicates the requirement of other factors on the cytosolic site of the membrane which direct the Pex5p over the luminal position of the N-terminal domain of Pex14p. Studies in yeast have recently revealed a second Pex5p binding site in the C-terminal part of Pex14p (Niederhoff et al., 2005), providing a good candidate for such factor. Alternatively, Pex13p which interacts with both Pex14p and Pex5p (Erdmann and Blobel, 1996; Fransen et al., 2002) could fulfil this role. Azevedo and Schliebs (2006) suggested that the Pex14p-Pex5p interaction represents the minimum free energy state of Pex5p and that subsequent steps require energy. Our results show that the free energy of the Pex14p-Pex5p interaction (36 kJ) is in the same range as free energy provided by phosphorylation. Studies in *H.polymorpha* and *P.pastoris* revealed that at least parts of the Pex14p population are phosphorylated (Johnson et al., 2001; Komori et al., 1999). Interestingly, phosphorylation site prediction of the N-terminal domain shows a conserved motif in the helical linker between helix α1 and α2. It is tempting to speculate that phosphorylation in this region could lead to the disruption of the Pex14p-Pex5p interaction, allowing the release of Pex5p and/or the transfer to downstream interaction partners.

Pex19p has been proposed as multifunctional protein. It has been assigned a role as receptor for PMPs, as chaperon or, in a more general way, as crucial factor in peroxisomal biogenesis (reviewed by Schliebs and Kunau, 2004). Rottensteiner et al. (Rottensteiner et al., 2004) defined a classical mPTS consisting of a transmembrane domain and an amphipathic helix of basic and hydrophobic residues. Although Pex14p lacks a typical Pex19p binding site, it is possible that its N-terminal interaction serves as an unusual recognition motif for Pex19p and holds therefore responsible for its targeting to the peroxisomal membrane. On the other hand previous studies have shown that Pex14p is mislocalized in Pex13p defective cells, indicating that the Pex14p-Pex19p interaction on its own is not sufficient to direct Pex14p to peroxisomal membrane (Fransen et al., 2004; Itoh and Fujiki, 2006). Studies in *S.cerevisiae* have shown that the N-terminus of Pex14p significantly contributes to the insertion of the protein into the peroxisomal membrane (Niederhoff et al., 2005). This could lead to the conclusion that the Pex19p interaction facilitates, perhaps with help of Pex13p, the correct orientation of Pex14p into, rather than its targeting to the peroxisomal membrane. Secondary chemical shifts and relaxation experiments suggest a higher flexibility of free Pex14p, indicating a better accessibility to proteases. Furthermore, we could observe a more rigid structure of N-terminal Pex14p upon ligand binding, giving rise to an alternative role of

Pex19p, in which the protein might serve as a protective “cap” for Pex14p until it is replaced by Pex5p.

4.10 Short summary and further perspectives

The complex structure of N-terminal Pex14p with Pex5p provides details about molecular recognition during the first steps of peroxisomal import. We were able to demonstrate that the binding of amphipathic ligands to Pex14p is flexible in target recognition, leading to a broader spectrum of possible ligands, but selective enough to discriminate between these ligands. As demonstrated on the analysis of the regular orientation of Pex19p, these results can help to explain and probably to predict further possible N-terminal Pex14p interaction motifs. Based on the characteristic properties of the N-terminal domain we introduced a model for the role of the Pex14p-Pex5p interaction. Further investigation are needed, especially the confirmation of the luminal localizaton of the N-terminal domain. A further major goal will be the transfer of our results into an *in vivo* model system, answering questions such as if Pex19p and Pex5p, two key proteins at different stages of the peroxisomal life cycle, converge at Pex14p or interact successively. Another interesting point to be specified is the question if the inverse Pex14p-Pex19p binding is biological relevant or has evolved accidentally. Furthermore, investigation of the Pex13p-Pex14p interaction and the determination and quantification of the minimal Pex14p binding site in Pex13p will be needed. Finally, we introduced the conserved the N-terminal domain as a new modular protein structure.

5 References

Agne, B., Meindl, N. M., Niederhoff, K., Einwachter, H., Rehling, P., Sickmann, A., Meyer, H. E., Girzalsky, W., and Kunau, W. H. (2003). Pex8p: an intraperoxisomal organizer of the peroxisomal import machinery. Mol Cell *11*, 635-646.

Albertini, M., Rehling, P., Erdmann, R., Girzalsky, W., Kiel, J. A., Veenhuis, M., and Kunau, W. H. (1997). Pex14p, a peroxisomal membrane protein binding both receptors of the two PTS-dependent import pathways. Cell *89*, 83-92.

Azevedo, J. E., and Schliebs, W. (2006). Pex14p, more than just a docking protein. Biochim Biophys Acta.

Baumgart, E., Fahimi, H. D., Steininger, H., and Grabenbauer, M. (2003). A review of morphological techniques for detection of peroxisomal (and mitochondrial) proteins and their corresponding mRNAs during ontogenesis in mice: application to the PEX5-knockout mouse with Zellweger syndrome. Microsc Res Tech *61*, 121-138.

Bax, A. (2003). Weak alignment offers new NMR opportunities to study protein structure and dynamics. Protein Sci *12*, 1-16.

Bellu, A. R., Komori, M., van der Klei, I. J., Kiel, J. A., and Veenhuis, M. (2001). Peroxisome biogenesis and selective degradation converge at Pex14p. J Biol Chem *276*, 44570-44574.

Bergfors, T. (2003). Seeds to crystals. J Struct Biol *142*, 66-76.

Blobel, G., and Dobberstein, B. (1975). Transfer of proteins across membranes. I. Presence of proteolytically processed and unprocessed nascent immunoglobulin light chains on membrane-bound ribosomes of murine myeloma. J Cell Biol *67*, 835-851.

Bogan, A. A., and Thorn, K. S. (1998). Anatomy of hot spots in protein interfaces. J Mol Biol *280*, 1-9.

Brocard, C., Lametschwandtner, G., Koudelka, R., and Hartig, A. (1997). Pex14p is a member of the protein linkage map of Pex5p. Embo J *16*, 5491-5500.

Brown, L. A., and Baker, A. (2003). Peroxisome biogenesis and the role of protein import. J Cell Mol Med *7*, 388-400.

Brown, L. R., De Marco, A., Richarz, R., Wagner, G., and Wuthrich, K. (1978). The influence of a single salt bridge on static and dynamic features of the globular solution conformation of the basic pancreatic trypsin inhibitor. 1H and 13C nuclear-magnetic-resonance studies of the native and the transaminated inhibitor. Eur J Biochem *88*, 87-95.

Camacho, C. J., Kimura, S. R., DeLisi, C., and Vajda, S. (2000). Kinetics of desolvation-mediated protein-protein binding. Biophys J *78*, 1094-1105.

Choe, J., Moyersoen, J., Roach, C., Carter, T. L., Fan, E., Michels, P. A., and Hol, W. G. (2003). Analysis of the sequence motifs responsible for the interactions of peroxins 14 and 5, which are involved in glycosome biogenesis in Trypanosoma brucei. Biochemistry *42*, 10915-10922.

Chothia, C., and Janin, J. (1975). Principles of protein-protein recognition. Nature *256*, 705-708.

Clayton, P. T. (2001). Clinical consequences of defects in peroxisomal beta-oxidation. Biochem Soc Trans *29*, 298-305.

Collins, C. S., Kalish, J. E., Morrell, J. C., McCaffery, J. M., and Gould, S. J. (2000). The peroxisome biogenesis factors pex4p, pex22p, pex1p, and pex6p act in the terminal steps of peroxisomal matrix protein import. Mol Cell Biol *20*, 7516-7526.

Cornilescu, G., Delaglio, F., and Bax, A. (1999). Protein backbone angle restraints from searching a database for chemical shift and sequence homology. J Biomol NMR *13*, 289-302.

Cudney, R., Patel, S., Weisgraber, K., Newhouse, Y., and McPherson, A. (1994). Screening and optimization strategies for macromolecular crystal growth. Acta Crystallogr D Biol

Dammai, V., and Subramani, S. (2001). The human peroxisomal targeting signal receptor, Pex5p, is translocated into the peroxisomal matrix and recycled to the cytosol. Cell *105*, 187-196.

De Duve, C., and Baudhuin, P. (1966). Peroxisomes (microbodies and related particles). Physiol Rev *46*, 323-357.
de Hoop, M. J., and Ab, G. (1992). Import of proteins into peroxisomes and other microbodies. Biochem J *286 (Pt 3)*, 657-669.

Delaglio, F., Grzesiek, S., Vuister, G. W., Zhu, G., Pfeifer, J., and Bax, A. (1995). NMRPipe: a multidimensional spectral processing system based on UNIX pipes. J Biomol NMR *6*, 277-293.

Dill, K. A. (1990). Dominant forces in protein folding. Biochemistry *29*, 7133-7155.

Dobson, C. M., and Karplus, M. (1999). The fundamentals of protein folding: bringing together theory and experiment. Curr Opin Struct Biol *9*, 92-101.

Douangamath, A., Filipp, F. V., Klein, A. T., Barnett, P., Zou, P., Voorn-Brouwer, T., Vega, M. C., Mayans, O. M., Sattler, M., Distel, B., and Wilmanns, M. (2002). Topography for independent binding of alpha-helical and PPII-helical ligands to a peroxisomal SH3 domain. Mol Cell *10*, 1007-1017.

Eckert, J. H., and Erdmann, R. (2003). Peroxisome biogenesis. Rev Physiol Biochem Pharmacol *147*, 75-121.

Einwachter, H., Sowinski, S., Kunau, W. H., and Schliebs, W. (2001). Yarrowia lipolytica Pex20p, Saccharomyces cerevisiae Pex18p/Pex21p and mammalian Pex5pL fulfil a common function in the early steps of the peroxisomal PTS2 import pathway. EMBO Rep *2*, 1035-1039.

Elgersma, Y., Kwast, L., Klein, A., Voorn-Brouwer, T., van den Berg, M., Metzig, B., America, T., Tabak, H. F., and Distel, B. (1996). The SH3 domain of the Saccharomyces cerevisiae peroxisomal membrane protein Pex13p functions as a docking site for Pex5p, a mobile receptor for the import PTS1-containing proteins. J Cell Biol *135*, 97-109.

Erdmann, R., and Blobel, G. (1996). Identification of Pex13p a peroxisomal membrane receptor for the PTS1 recognition factor. J Cell Biol *135*, 111-121.

Erdmann, R., and Kunau, W. H. (1992). A genetic approach to the biogenesis of peroxisomes in the yeast Saccharomyces cerevisiae. Cell Biochem Funct *10*, 167-174.

Erdmann, R., and Schliebs, W. (2005). Peroxisomal matrix protein import: the transient pore model. Nat Rev Mol Cell Biol *6*, 738-742.

Erdmann, R., Veenhuis, M., Mertens, D., and Kunau, W. H. (1989). Isolation of peroxisome-deficient mutants of Saccharomyces cerevisiae. Proc Natl Acad Sci U S A *86*, 5419-5423.

Fransen, M., Brees, C., Ghys, K., Amery, L., Mannaerts, G. P., Ladant, D., and Van Veldhoven, P. P. (2002). Analysis of mammalian peroxin interactions using a non-transcription-based bacterial two-hybrid assay. Mol Cell Proteomics *1*, 243-252.

Fransen, M., Terlecky, S. R., and Subramani, S. (1998). Identification of a human PTS1 receptor docking protein directly required for peroxisomal protein import. Proc Natl Acad Sci U S A *95*, 8087-8092.

Fransen, M., Vastiau, I., Brees, C., Brys, V., Mannaerts, G. P., and Van Veldhoven, P. P. (2004). Potential role for Pex19p in assembly of PTS-receptor docking complexes. J Biol Chem *279*, 12615-12624.

Fransen, M., Vastiau, I., Brees, C., Brys, V., Mannaerts, G. P., and Van Veldhoven, P. P. (2005). Analysis of human Pex19p's domain structure by pentapeptide scanning mutagenesis. J Mol Biol *346*, 1275-1286.

Fransen, M., Wylin, T., Brees, C., Mannaerts, G. P., and Van Veldhoven, P. P. (2001). Human pex19p binds peroxisomal integral membrane proteins at regions distinct from their sorting sequences. Mol Cell Biol *21*, 4413-4424.

Gatto, G. J., Jr., Geisbrecht, B. V., Gould, S. J., and Berg, J. M. (2000). A proposed model for the PEX5-peroxisomal targeting signal-1 recognition complex. Proteins *38*, 241-246.

Gavva, N. R., Wen, S. C., Daftari, P., Moniwa, M., Yang, W. M., Yang-Feng, L. P., Seto, E., Davie, J. R., and Shen, C. K. (2002). NAPP2, a peroxisomal membrane protein, is also a transcriptional corepressor. Genomics *79*, 423-431.

Gemmecker, G., Olejniczak, E.T., Fesik (1992). J Magn Reson *96*, 199.

Geuze, H. J., Murk, J. L., Stroobants, A. K., Griffith, J. M., Kleijmeer, M. J., Koster, A. J., Verkleij, A. J., Distel, B., and Tabak, H. F. (2003). Involvement of the endoplasmic reticulum in peroxisome formation. Mol Biol Cell *14*, 2900-2907.

Girzalsky, W., Rehling, P., Stein, K., Kipper, J., Blank, L., Kunau, W. H., and Erdmann, R. (1999). Involvement of Pex13p in Pex14p localization and peroxisomal targeting signal 2-dependent protein import into peroxisomes. J Cell Biol *144*, 1151-1162.

Glover, J. R., Andrews, D. W., Subramani, S., and Rachubinski, R. A. (1994). Mutagenesis of the amino targeting signal of Saccharomyces cerevisiae 3-ketoacyl-CoA thiolase reveals conserved amino acids required for import into peroxisomes in vivo. J Biol Chem *269*, 7558-7563.

Gould, S. J., and Collins, C. S. (2002). Opinion: peroxisomal-protein import: is it really that complex? Nat Rev Mol Cell Biol *3*, 382-389.

Gouveia, A. M., Reguenga, C., Oliveira, M. E., Sa-Miranda, C., and Azevedo, J. E. (2000). Characterization of peroxisomal Pex5p from rat liver. Pex5p in the Pex5p-Pex14p membrane complex is a transmembrane protein. J Biol Chem *275*, 32444-32451.

Hoeflich, K. P., and Ikura, M. (2002). Calmodulin in action: diversity in target recognition and activation mechanisms. Cell *108*, 739-742.

Hoepfner, D., Schildknegt, D., Braakman, I., Philippsen, P., and Tabak, H. F. (2005). Contribution of the endoplasmic reticulum to peroxisome formation. Cell *122*, 85-95.

Hoepfner, D., van den Berg, M., Philippsen, P., Tabak, H. F., and Hettema, E. H. (2001). A role for Vps1p, actin, and the Myo2p motor in peroxisome abundance and inheritance in Saccharomyces cerevisiae. J Cell Biol *155*, 979-990.

Huhse, B., Rehling, P., Albertini, M., Blank, L., Meller, K., and Kunau, W. H. (1998). Pex17p of Saccharomyces cerevisiae is a novel peroxin and component of the peroxisomal protein translocation machinery. J Cell Biol *140*, 49-60.

Huyghues-Despointes, B. M., Pace, C. N., Englander, S. W., and Scholtz, J. M. (2001). Measuring the conformational stability of a protein by hydrogen exchange. Methods Mol Biol *168*, 69-92.

Itoh, R., and Fujiki, Y. (2006). Functional domains and dynamic assembly of the peroxin pex14p, the entry site of matrix proteins. J Biol Chem *281*, 10196-10205.

Johnson, B. A., Blevins, R. A. (1994). NMRView: a computer program for the visualization and analysis of NMR data. J Biomol NMR *4*, 603-614.

Johnson, M. A., Snyder, W. B., Cereghino, J. L., Veenhuis, M., Subramani, S., and Cregg, J. M. (2001). Pichia pastoris Pex14p, a phosphorylated peroxisomal membrane protein, is part of a PTS-receptor docking complex and interacts with many peroxins. Yeast *18*, 621-641.

Jones, S., and Thornton, J. M. (1996). Principles of protein-protein interactions. Proc Natl Acad Sci U S A *93*, 13-20.

Jorgensen, W. L. (1991). Rusting of the lock and key model for protein-ligand binding. Science *254*, 954-955.

Karplus, M. (1959). J Phys Chem *30*, 11-15.

Kay, L. E. (1998). Protein dynamics from NMR. Biochem Cell Biol *76*, 145-152.

Keller, G. A., Gould, S., Deluca, M., and Subramani, S. (1987). Firefly luciferase is targeted to peroxisomes in mammalian cells. Proc Natl Acad Sci U S A *84*, 3264-3268.

Kiel, J. A., Emmrich, K., Meyer, H. E., and Kunau, W. H. (2005). Ubiquitination of the peroxisomal targeting signal type 1 receptor, Pex5p, suggests the presence of a quality control mechanism during peroxisomal matrix protein import. J Biol Chem *280*, 1921-1930.

Kimura, S. R., Brower, R. C., Vajda, S., and Camacho, C. J. (2001). Dynamical view of the positions of key side chains in protein-protein recognition. Biophys J *80*, 635-642.

Komori, M., Kiel, J. A., and Veenhuis, M. (1999). The peroxisomal membrane protein Pex14p of Hansenula polymorpha is phosphorylated in vivo. FEBS Lett *457*, 397-399.

Koradi, R., Billeter, M., and Wuthrich, K. (1996). MOLMOL: a program for display and analysis of macromolecular structures. J Mol Graph *14*, 51-55, 29-32.

Koshland, D. E. (1958). Application of a Theory of Enzyme Specificity to Protein Synthesis. Proc Natl Acad Sci U S A *44*, 98-104.

Kragt, A., Voorn-Brouwer, T., van den Berg, M., and Distel, B. (2005). Endoplasmic reticulum-directed Pex3p routes to peroxisomes and restores peroxisome formation in a Saccharomyces cerevisiae pex3Delta strain. J Biol Chem *280*, 34350-34357.

Kunau, W. H. (2005). Peroxisome biogenesis: end of the debate. Curr Biol *15*, R774-776.

Kuriyan, J., and Cowburn, D. (1997). Modular peptide recognition domains in eukaryotic signaling. Annu Rev Biophys Biomol Struct *26*, 259-288.

Laskowski, R. A., Rullmannn, J. A., MacArthur, M. W., Kaptein, R., and Thornton, J. M. (1996). AQUA and PROCHECK-NMR: programs for checking the quality of protein structures solved by NMR. J Biomol NMR *8*, 477-486.

Lazarow, P. B., and Fujiki, Y. (1985). Biogenesis of peroxisomes. Annu Rev Cell Biol *1*, 489-530.

Leavitt, S., and Freire, E. (2001). Direct measurement of protein binding energetics by isothermal titration calorimetry. Curr Opin Struct Biol *11*, 560-566.

Liddington, R. (2004). Structural Basis of Protein–Protein Interactions. Methods in Molecular Biology *261*.

Linding, R., Russell, R. B., Neduva, V., and Gibson, T. J. (2003). GlobPlot: Exploring protein sequences for globularity and disorder. Nucleic Acids Res *31*, 3701-3708.

Linge, J. P., O'Donoghue, S. I., and Nilges, M. (2001). Automated assignment of ambiguous nuclear overhauser effects with ARIA. Methods Enzymol *339*, 71-90.

Linge, J. P., Williams, M. A., Spronk, C. A., Bonvin, A. M., and Nilges, M. (2003). Refinement of protein structures in explicit solvent. Proteins *50*, 496-506.

Louie, G., Tran, T., Englander, J. J., and Englander, S. W. (1988). Allosteric energy at the hemoglobin beta chain C terminus studied by hydrogen exchange. J Mol Biol *201*, 755-764.

Lyu, P. C., Gans, P. J., and Kallenbach, N. R. (1992). Energetic contribution of solvent-exposed ion pairs to alpha-helix structure. J Mol Biol *223*, 343-350.

Madrid, K. P., and Jardim, A. (2005). Peroxin 5-peroxin 14 association in the protozoan Leishmania donovani involves a novel protein-protein interaction motif. Biochem J *391*, 105-114.

Marzioch, M., Erdmann, R., Veenhuis, M., and Kunau, W. H. (1994). PAS7 encodes a novel yeast member of the WD-40 protein family essential for import of 3-oxoacyl-CoA thiolase, a PTS2-containing protein, into peroxisomes. Embo J *13*, 4908-4918.

McNew, J. A., and Goodman, J. M. (1994). An oligomeric protein is imported into peroxisomes in vivo. J Cell Biol *127*, 1245-1257.

McPherson, A. (1990). Current approaches to macromolecular crystallization. Eur J Biochem *189*, 1-23.

Niederhoff, K., Meindl-Beinker, N. M., Kerssen, D., Perband, U., Schafer, A., Schliebs, W., and Kunau, W. H. (2005). Yeast Pex14p possesses two functionally distinct Pex5p and one Pex7p binding sites. J Biol Chem *280*, 35571-35578.

Oliveira, M. E., Gouveia, A. M., Pinto, R. A., Sa-Miranda, C., and Azevedo, J. E. (2003). The energetics of Pex5p-mediated peroxisomal protein import. J Biol Chem *278*, 39483-39488.

Oliveira, M. E., Reguenga, C., Gouveia, A. M., Guimaraes, C. P., Schliebs, W., Kunau, W. H., Silva, M. T., Sa-Miranda, C., and Azevedo, J. E. (2002). Mammalian Pex14p: membrane topology and characterisation of the Pex14p-Pex14p interaction. Biochim Biophys Acta *1567*, 13-22.

Otera, H., Setoguchi, K., Hamasaki, M., Kumashiro, T., Shimizu, N., and Fujiki, Y. (2002). Peroxisomal targeting signal receptor Pex5p interacts with cargoes and import machinery components in a spatiotemporally differentiated manner: conserved Pex5p WXXXF/Y motifs are critical for matrix protein import. Mol Cell Biol *22*, 1639-1655.

Otting, G., Ruckert, M., Levitt, M. H., and Moshref, A. (2000). NMR experiments for the sign determination of homonuclear scalar and residual dipolar couplings. J Biomol NMR *16*, 343-346.

Pickart, C. M. (2001). Mechanisms underlying ubiquitination. Annu Rev Biochem *70*, 503-533.

Purdue, P. E., and Lazarow, P. B. (2001a). Peroxisome biogenesis. Annu Rev Cell Dev Biol *17*, 701-752.

Purdue, P. E., and Lazarow, P. B. (2001b). Pex18p is constitutively degraded during peroxisome biogenesis. J Biol Chem *276*, 47684-47689.

Purdue, P. E., Yang, X., and Lazarow, P. B. (1998). Pex18p and Pex21p, a novel pair of related peroxins essential for peroxisomal targeting by the PTS2 pathway. J Cell Biol *143*, 1859-1869.

Purdue, P. E., Zhang, J. W., Skoneczny, M., and Lazarow, P. B. (1997). Rhizomelic chondrodysplasia punctata is caused by deficiency of human PEX7, a homologue of the yeast PTS2 receptor. Nat Genet *15*, 381-384.

Rachubinski, R. A., and Subramani, S. (1995). How proteins penetrate peroxisomes. Cell *83*, 525-528.

Rajamani, D., Thiel, S., Vajda, S., and Camacho, C. J. (2004). Anchor residues in protein-protein interactions. Proc Natl Acad Sci U S A *101*, 11287-11292.

Reguenga, C., Oliveira, M. E., Gouveia, A. M., Sa-Miranda, C., and Azevedo, J. E. (2001). Characterization of the mammalian peroxisomal import machinery: Pex2p, Pex5p, Pex12p, and Pex14p are subunits of the same protein assembly. J Biol Chem *276*, 29935-29942.

Rehling, P., Marzioch, M., Niesen, F., Wittke, E., Veenhuis, M., and Kunau, W. H. (1996). The import receptor for the peroxisomal targeting signal 2 (PTS2) in Saccharomyces cerevisiae is encoded by the PAS7 gene. Embo J *15*, 2901-2913.

Richards, F. M. (1977). Areas, volumes, packing and protein structure. Annu Rev Biophys Bioeng *6*, 151-176.

Rottensteiner, H., Kramer, A., Lorenzen, S., Stein, K., Landgraf, C., Volkmer-Engert, R., and Erdmann, R. (2004). Peroxisomal membrane proteins contain common Pex19p-binding sites that are an integral part of their targeting signals. Mol Biol Cell *15*, 3406-3417.

Sacksteder, K. A., Jones, J. M., South, S. T., Li, X., Liu, Y., and Gould, S. J. (2000). PEX19 binds multiple peroxisomal membrane proteins, is predominantly cytoplasmic, and is required for peroxisome membrane synthesis. J Cell Biol *148*, 931-944.

Saidowsky, J., Dodt, G., Kirchberg, K., Wegner, A., Nastainczyk, W., Kunau, W. H., and Schliebs, W. (2001). The di-aromatic pentapeptide repeats of the human peroxisome import receptor PEX5 are separate high affinity binding sites for the peroxisomal membrane protein PEX14. J Biol Chem *276*, 34524-34529.

Sattler, M., Schleucher, J., Griesinger, C. (1999). Heteronuclear multidimensional NMR experiments for thestructure determination of proteins in solution employing pulsed field gradients. Progress in Nuclear Magnetic Resonance Spectroscopy *34*, 93–158.

Schafer, A., Kerssen, D., Veenhuis, M., Kunau, W. H., and Schliebs, W. (2004). Functional similarity between the peroxisomal PTS2 receptor binding protein Pex18p and the N-terminal half of the PTS1 receptor Pex5p. Mol Cell Biol *24*, 8895-8906.

Schell-Steven, A., Stein, K., Amoros, M., Landgraf, C., Volkmer-Engert, R., Rottensteiner, H., and Erdmann, R. (2005). Identification of a novel, intraperoxisomal pex14-binding site in pex13: association of pex13 with the docking complex is essential for peroxisomal matrix protein import. Mol Cell Biol *25*, 3007-3018.

Schiffer, M., and Edmundson, A. B. (1967). Use of helical wheels to represent the structures of proteins and to identify segments with helical potential. Biophys J *7*, 121-135.

Schliebs, W., and Kunau, W. H. (2004). Peroxisome membrane biogenesis: the stage is set. Curr Biol *14*, R397-399.

Schliebs, W., Saidowsky, J., Agianian, B., Dodt, G., Herberg, F. W., and Kunau, W. H. (1999). Recombinant human peroxisomal targeting signal receptor PEX5. Structural basis for interaction of PEX5 with PEX14. J Biol Chem *274*, 5666-5673.

South, S. T., and Gould, S. J. (1999). Peroxisome synthesis in the absence of preexisting peroxisomes. J Cell Biol *144*, 255-266.

Stanley, W. A., Filipp, F. V., Kursula, P., Schueller, N., Erdmann, R., Schliebs, W., Sattler, M., and Wilmanns, M. (2006). Recognition of a Functional Peroxisome Type 1 Target by the Dynamic Import Receptor Pex5p. Molecular Cell *24*.

Swanson, K. A., Knoepfler, P. S., Huang, K., Kang, R. S., Cowley, S. M., Laherty, C. D., Eisenman, R. N., and Radhakrishnan, I. (2004). HBP1 and Mad1 repressors bind the Sin3 corepressor PAH2 domain with opposite helical orientations. Nat Struct Mol Biol *11*, 738-746.

Tabak, H. F., Murk, J. L., Braakman, I., and Geuze, H. J. (2003). Peroxisomes start their life in the endoplasmic reticulum. Traffic *4*, 512-518.

Thieringer, H., Moellers, B., Dodt, G., Kunau, W. H., and Driscoll, M. (2003). Modeling human peroxisome biogenesis disorders in the nematode Caenorhabditis elegans. J Cell Sci *116*, 1797-1804.

Titorenko, V. I., and Rachubinski, R. A. (1998). The endoplasmic reticulum plays an essential role in peroxisome biogenesis. Trends Biochem Sci *23*, 231-233.

Titorenko, V. I., Smith, J. J., Szilard, R. K., and Rachubinski, R. A. (1998). Pex20p of the yeast Yarrowia lipolytica is required for the oligomerization of thiolase in the cytosol and for its targeting to the peroxisome. J Cell Biol *142*, 403-420.

Tjandra, N., and Bax, A. (1997). Measurement of dipolar contributions to 1JCH splittings from magnetic-field dependence of J modulation in two-dimensional NMR spectra. J Magn Reson *124*, 512-515.

Turnbull, W. B., and Daranas, A. H. (2003). On the value of c: can low affinity systems be studied by isothermal titration calorimetry? J Am Chem Soc *125*, 14859-14866.

Valdar, W. S., and Thornton, J. M. (2001). Protein-protein interfaces: analysis of amino acid conservation in homodimers. Proteins *42*, 108-124.

Wanders, R. J., Vreken, P., Ferdinandusse, S., Jansen, G. A., Waterham, H. R., van Roermund, C. W., and Van Grunsven, E. G. (2001). Peroxisomal fatty acid alpha- and beta-oxidation in humans: enzymology, peroxisomal metabolite transporters and peroxisomal diseases. Biochem Soc Trans *29*, 250-267.

Weller, S., Gould, S. J., and Valle, D. (2003). Peroxisome biogenesis disorders. Annu Rev Genomics Hum Genet *4*, 165-211.

Wiebel, F. F., and Kunau, W. H. (1992). The Pas2 protein essential for peroxisome biogenesis is related to ubiquitin-conjugating enzymes. Nature *359*, 73-76.

Will, G. K., Soukupova, M., Hong, X., Erdmann, K. S., Kiel, J. A., Dodt, G., Kunau, W. H., and Erdmann, R. (1999). Identification and characterization of the human orthologue of yeast Pex14p. Mol Cell Biol *19*, 2265-2277.

Williams, C., van den Berg, M., and Distel, B. (2005). Saccharomyces cerevisiae Pex14p contains two independent Pex5p binding sites, which are both essential for PTS1 protein import. FEBS Lett *579*, 3416-3420.

Wiseman, T., Williston, S., Brandts, J. F., and Lin, L. N. (1989). Rapid measurement of binding constants and heats of binding using a new titration calorimeter. Anal Biochem *179*, 131-137.

Wishart, D. S., Bigam, C. G., Holm, A., Hodges, R. S., and Sykes, B. D. (1995). 1H, 13C and 15N random coil NMR chemical shifts of the common amino acids. I. Investigations of nearest-neighbor effects. J Biomol NMR *5*, 67-81.

Wodak, S. J., and Janin, J. (2002). Structural basis of macromolecular recognition. Adv Protein Chem *61*, 9-73.

Wüthrich, K. (1986). NMR of proteins and nucleic acids Wiley-Interscience.

Zuiderweg, E. R. (2002). Mapping protein-protein interactions in solution by NMR spectroscopy. Biochemistry *41*, 1-7.

6 Appendix I - NMR spectroscopy

Besides the application of NMR in medicine, chemistry, it is also commonly used in structural biology. So far X-ray crystallography and NMR spectroscopy are the only techniques that allow an insight in the structure of proteins at an atomic resolution (Wüthrich, 1986). Although the practical application of NMR spectroscopy is restricted to smaller molecules and the process of structure determination is still not automated to an extent comparable to X-crystallography, the method provides a number of advantages. In addition to the 3-dimensional structure which provides the basis for further functional analysis, NMR gives an insight in the dynamic processes (reviewed by Kay, 1998) of molecules in solution and the study of molecular interactions(Zuiderweg, 2002).

6.1 Basic principles of NMR

NMR spectroscopy is based on an intrinsic quantum mechanic feature of nuclei known as spin, which is determined by a nuclear spin quantum number I. A nucleus with a non-zero spin interacts with an external magnetic field, resulting in a splitting of its energy levels. The number of levels is defined by the magnetic quantum number m and can adopt numbers of integer steps from –I to +I (Zeeman levels). The most commonly used nuclei in NMR (e.g. ^{1}H, ^{15}N and ^{13}C) have a spin number of ½ and split in two possible energy levels, i.e. parallel (m= + ½) and antiparallel (m= - ½). In addition, nuclei with a spin possess a proportionally linked nuclear magnetic moment which aligns with the magnetic field. The energy levels of a nucleus in a magnetic field are described by

$$E = -\mu_z B_0 = -\gamma\ I_z B_0 = -\gamma\ m\hbar B_0$$

where μ_z and I_z are the z-component of the magnetic moment μ and spin I along the external magnetic field and γ the gyromagnetic ratio. Transitions between energy stages can be stimulated by external radiation of a certain frequency called Larmor frequency which is identical to with the frequency of precession of the magnetic moment around the main axis of the static magnetic field. The Larmor frequency depends on the gyromagnetic ratio and the strength of the external magnetic field.

At equilibrium the different energy stages are populated unequally whereby the difference is given by the Boltzmann distribution. Lower energy levels are slightly more preferred than higher ones leading to a bulk magnetization of the sample parallel to the static magnetic field. This macroscopic magnetization is called longitudinal magnetization and characterized by the strength of the magnetic field, the number of involved spins and the temperature. In a simple NMR experiment the equilibrium longitudinal magnetization $M_{z,eq}$ is disturbed by an external electromagnetic pulse. If the magnetic field of this pulse is applied vertically to the static field transverse magnetization $M_{x,y}$ can be introduced. A pulse that leads to a complete transformation of longitudinal to transverse magnetization is called 90° pulse.

6.2 Chemical shift

The deflection of the static magnetic field by the surrounding electronic environment of a nucleus leads to a slightly different Larmor precession. This effect is called chemical shift δ and represents one of the basic parameters of NMR-spectroscopy. It determines the dispersion of signals in a NMR spectrum. The chemical shift is measured in ppm (parts per million) to a reference frequency and is defined by

$$\delta = \frac{\omega_{signal} - \omega_{reference}}{\omega_{reference}}$$

The chemical shift can be exploited for polypeptide backbone angle prediction (Φ and Ψ) leading to an improvement in the quality of protein structures (Cornilescu et al., 1999).

6.2.1 Scalar coupling experiments

Spins close to each other exert an influence on each other's magnetic field. This effect can be observed by NMR spectroscopy and it provides information about the chemical environment of the nucleus. Interactions mediated through chemical bonds are called scalar or J couplings.

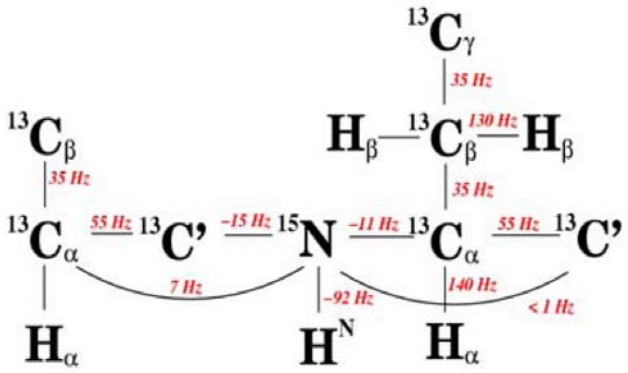

Fig 6.1: Typical values for one- and two bond scalar couplings (^{1}J and ^{2}J) in polypeptides. Numbers in red are given in Hertz (Hz) and shown at top of the bond

The scalar coupling allows the transfer of magnetization between nuclei coupling with each other as long as the distance is not greater than three bond lengths. Beside the nuclear Overhauser effect (NOE) scalar coupling is one of the most important mechanisms exploited in NMR spectroscopy.

6.3 Dipolar coupling experiments

Dipolar couplings mediate spin interactions through space and depend on the internuclear distance between two spins and its orientation to a static magnetic field. NOE and relaxation are phenomena derived from dipolar couplings.

6.3.1 NOESY experiments

NMR protein structure determination derives mainly from proton-proton distance restraints calculated from the intensities of NOE signals. The nuclear Overhauser effect is a result of spin-spin cross relaxation and depends on the distance between two dipolar coupled spins. The relation between signal intensity I and the distance between two nuclei i and j is approximately

$$I(NOE_{ij}) \propto \frac{1}{r_{ij}^6}$$

The distances are defined by mathematical integration of the NOE signal. Alternatively a qualitative estimation of its intensity is feasible but requires a reference. To avoid signal

overlap three dimensional 13C and 15N-edited NOESY experiments are performed. For structural analysis of complexes between a labelled protein and an unlabelled ligand, edited-filtered NOESY experiments are applied. This allows either to select or to suppress the evolution of magnetization of protons bound to a hetero-nucleus.

6.3.2 Relaxation and protein dynamics

After the disturbance by an external radio pulse the system of spins aims to return to equilibrium. Equilibrium is reached when the longitudinal magnetization is restored to a certain value (determined by the population of energy levels predicted by the Boltzman distribution) and transverse magnetization is zero. The first process is called longitudinal or spin-lattice, the second transverse or spin-spin relaxation. Longitudinal relaxation occurs via transition of spins from higher to lower energy levels or vice versa until the equilibrium population is reached. The time constant of this process is T_1. Transverse relaxation is the loss of phase coherence of spins and results in the vanishing of transverse magnetization. Both phenomena are induced by random, time-dependent interactions, mainly dipolar interactions and chemical shift anisotropy, caused by the thermal motion of the molecule, i.e. random tumbling of molecules or molecular flexibility. A measure for the speed of the tumbling of a molecule is τ_c the rotational correlation time. It describes the time that it takes for the molecule to reorient, which is much shorter for small molecules compared to large molecules such as proteins. For small molecules, with a fast tumbling rate T_1 is equal to T_2. For proteins, with larger correlation times, T_2 is smaller than T_1 (Fig. 6.2).

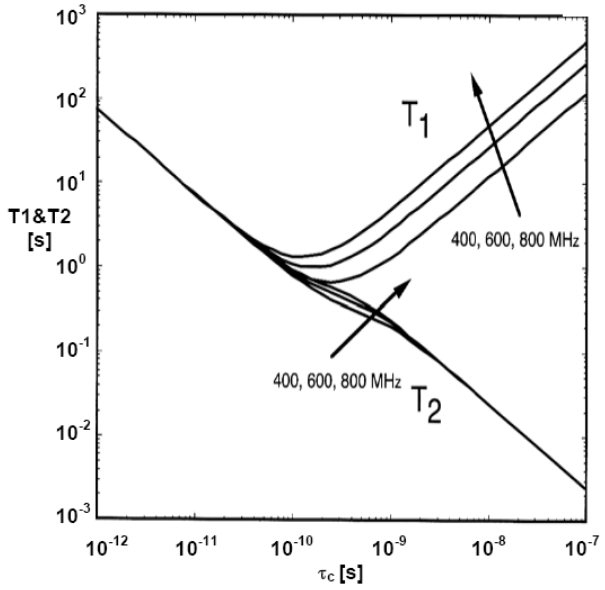

Fig. 6.2: Logarithmic plots of T1 and T2 times. Curves are given for proton resonance frequencies of 400, 600 and 800 MHz

For larger molecules T_2 is inversely proportional to τ_c which itself is proportional to the molecular weight. Thus T_2 relaxation times provide a tool to estimate the molecular weight of proteins in solution. Another application of relaxation times is the characterization of the dynamic properties of a molecule. For proteins relaxation rates are usually determined for the backbone amide nitrogens. Residues with ratios of T_1/T_2 significantly different from the average indicate different dynamic properties und show regions of high flexibility or structured regions, respectively.

6.4 NMR structure determination

NMR structure determination involves information obtained from various experiments. Although the main sources for structural restraints are short proton-proton distances derived from NOESY (Nuclear Overhauser and Exchange Spectroscopy) experiments, additional information, e.g. dihedral angles, residual dipolar couplings or solvent exchange, help to complement the final structure.

Table 6.1: NMR observables for structure determination.

Observable	Information
Chemical shifts (1H, 13C, 15N, 31P)	Assignments, secondary structure
J-couplings (through bond) 3J(HN, Ha),	Dihedral angles
NOE (through space)	Interatomic distances (< 5A)
Residual dipolar couplings (1H-15N)	Bond projection angles
Solvent exchange (HN)	Hydrogen bonds

6.4.1 Backbone and Side chain assignments

Assignments of proteins are in general carried out on uniformly and isotopically labelled protein samples. To obtain a suitable sample, protein expression is carried out by bacteria in minimal media containing 15N and/or 13C isotopes as the only nitrogen and/or carbon source. The protons of an isotopically labelled sample are correlated with the resonances of heteronuclei, providing the advantage of clearer spectra and less overlap of signals.

The sequence specific assignment of the protein backbone is done under application of triple resonance experiments, correlating the C_α and/or C_β atoms with the amide nitrogen and proton of either the same residue *i* and/or the previous residue *i*-1 in the polypeptide chain. Double labelled protein samples are a prerequisite for these experiments. The magnetization is transferred directly via the covalent peptide bond leading to a high sensitivity.

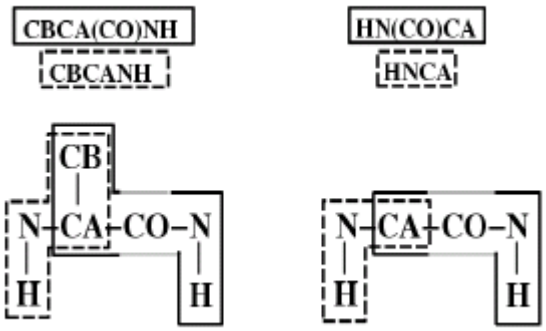

Fig. 6.3: Overview of NMR backbone experiments. Correlated spin system are boxed in the same manner as the associated experiment.

Usually, a set of four different experiments is recorded: the HNCA-, HN(CO)CA-, CBCANH and CBCA(CO)NH). HNCA and CBCANH experiments reveal the chemical shifts of the intraresidual carbon atom and the previous one. Experiments involving a transfer of magnetization over the backbone carbonyl carbon (CO) do not allow the intraresidual magnetization between H^N and C_α. Thus, only observation of sequential cross peaks is possible. Comparison of peaks can be used for a complete "walk" over the protein sequence (or at least until a proline is reached) allowing the connection of residues and assignment of their H^N, N, C_α and C_β atoms.

Side chain assignments are defined via different TOCSY experiments (total correlation spectroscopy). In general such an experiment divides the magnetization over the whole spin system of an amino acid via successive step by step transfer. Depending on the experimental setup the aliphatic carbon resonances of ((H)CC(CO)NH) or the side chain protons (H(CCCO)NH) of residue *i*-1 can be correlated to the backbone amide of amino acid *i*. Intraresidual proton and carbon resonances are correlated via a HCCH-TOCSY. Fig. 1.9 provides an overview.

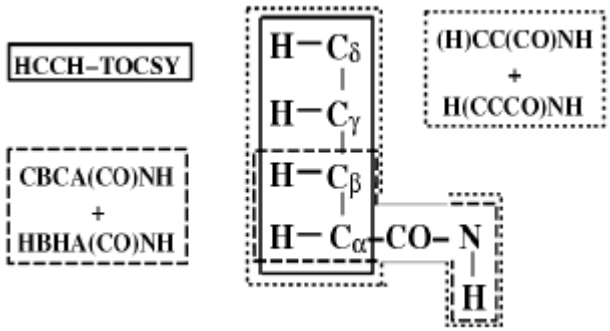

Fig. 6.4: Overview of NMR side chain experiments. Correlated spin system are boxed in the same manner as the associated experiment.

6.4.2 Secondary structure

The knowledge about the chemical shifts of the atoms of a certain residue allows to conclude on the chemical enviorement in which this residue is embedded. A common tool to investigate the secondary structure or backbone conformation of a protein is the secondary chemical shift, which represents the difference of the observed chemical shift to a coiled coil

value. Normally secondary chemical shifts from ^{1}H or ^{13}C shift are used to identify or predict secondary structure elements in proteins.
Another application to determine the secondary structure of polypeptide chains is the analysis of ^{3}J coupling constants of three covalent bounds, which provides information on the geometry of a polypeptide chain. The magnitude of J is a function of the torsion angle Φ and is described by the Karplus relation (Karplus, 1959).

$$J(\Phi) = A\cos^2(\Phi - 60) - B\cos(\Phi - 60) + C$$

where A, B and C are empirical constants and different for every type of torsion angle. Most commonly, the torsion angle Φ of the protein backbone (H^{N}-N-C_{α}-H_{α}) is determined by this method.

6.4.3 Residual dipolar couplings

Residual dipolar coupling (RDC) experiments provide information on the orientation of internuclear, usually one-bond vectors relative to the magnetic field (reviewed by Bax, 2003). Similar RDC values indicate similar orientations. Thus, residual dipolar coupling, do complements the local information given by NOE and J-coupling by restraining all bond orientation to a common frame. The source of this structural information is the direct spin-spin interaction between two nuclei. It depends on the internuclear distance and its orientation to a static magnetic field. In the solid state this leads to large dipolar splittings and linewidth since dipolar couplings of organic macromolecules are in the kHz range. In solution, dipolar couplings of a molecule average to zero. However, in a dilute liquid crystalline medium moderate molecular alignment is achieved, resulting in residual dipolar couplings of a few Hertz. RDC restraints are employed directly in structure refinement or as a judgement of structural quality (Tjandra and Bax, 1997).

6.4.4 Solvent exchange

The amide protons of a protein are exchanged with the surrounding solvent. If the solvent consists of 100% deuterium, this exchange can be monitored by an $^{15}N,^{1}H$-correlation experiment. The rate of exchange of certain residues reflects their accessibility to the solvent and gives information about which parts of the protein are buried or involved in hydrogen bond formation (Huyghues-Despointes et al., 2001). A common application is to compare the exchange of free protein versus a complex. The amides that become protected in the complex, are assumed to be in the binding site.

6.4.5 Structure calculation

The information obtained by the experimental procedure described above (see table 1.2) is supplemented with physically possible values for bond length, bond angles and van der Waals radii of molecules and applied to a simulated annealing protocol, e.g. by using the program ARIA (Linge et al., 2001). The calculation is an iterative process, searching for an energy-minimized structure ensemble (or NMR ensemble) determined by the given experimental data. The quality of the structure is determined by the similarity of the calculated structures as well as by the distribution of dihedral angles in a Ramachandran plot or the Q-factor derived from the RDCs.

6.5 Interaction studies

Compared to other techniques, e.g. isothermal calorimetry, NMR spectroscopy does not only provide binary information about binding or non-binding, but also reveals structural details of the binding process. The most frequently used method is chemical shift perturbation mapping via $^{15}N,^{1}H$-correlation spectra. Thereby the spectra of a free and bound protein are compared by superimposition. Residues involved in binding or structural rearrangements upon binding experience a change in chemical environment and are strongly perturbated. In addition to the mapping of the interaction interface, titration experiments can be carried out, providing information about the interaction kinetics. The appearance of such an NMR spectrum depends on how rapidly the bound and free form of a complex exchange. Weak interactions, with high

K_d values have fast exchange rates compared with the differences in NMR parameters (chemical shift, relaxation rate, etc.) and show a spectrum representing the weighted average of free and bound ligand. This leads to an observable movement of peaks during titration (Fig.6.4). Strong interactions are often in the slow exchange regime, showing separate spectra for both forms and are characterized by an abrupt skip of free-state to bound-state peak shifts.

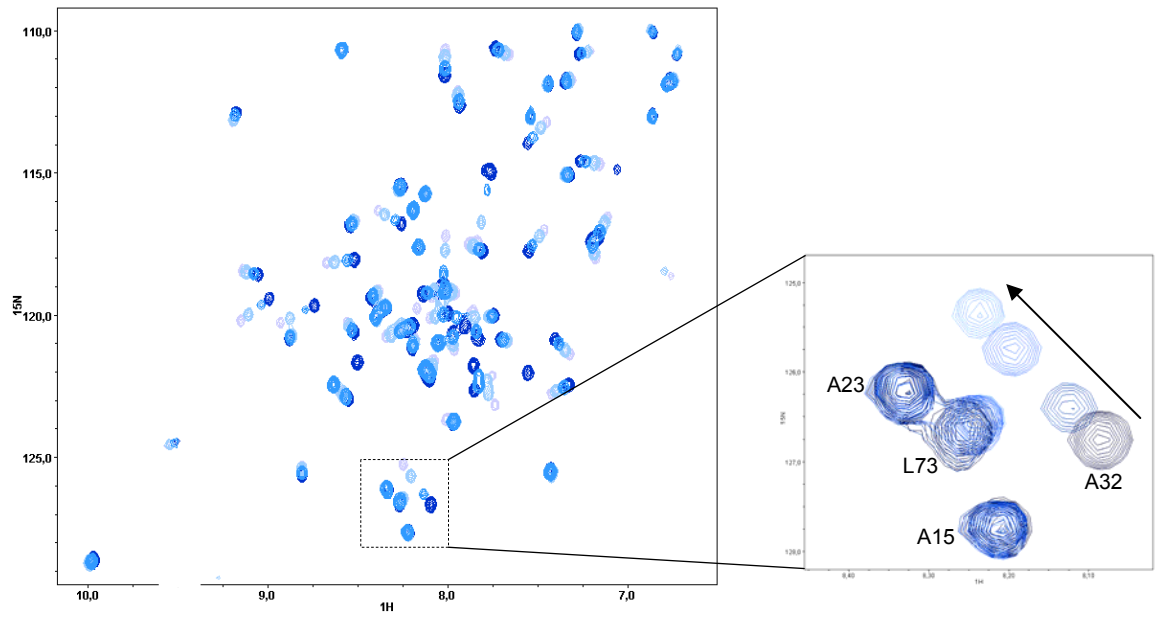

Fig. 6.4: Superimposition of $^{1}H,^{15}N$ correlation spectra of N-terminal Pex14p in complex with increasing Pex19p peptide concentrations. The interaction is in fast exchange on a NMR time scale. Residues involved in ligand binding experience a strong chemical shift perturbation (A32). Residues outside the interaction interface stay stationary (A15, A23, L73).

6.6 References (Appendix)

Bax, A. (2003). Weak alignment offers new NMR opportunities to study protein structure and dynamics. Protein Sci *12*, 1-16.

Cornilescu, G., Delaglio, F., and Bax, A. (1999). Protein backbone angle restraints from searching a database for chemical shift and sequence homology. J Biomol NMR *13*, 289-302.

Huyghues-Despointes, B. M., Pace, C. N., Englander, S. W., and Scholtz, J. M. (2001). Measuring the conformational stability of a protein by hydrogen exchange. Methods Mol Biol *168*, 69-92.

Karplus, M. (1959). J Phys Chem *30*, 11-15.
Kay, L. E. (1998). Protein dynamics from NMR. Biochem Cell Biol *76*, 145-152.

Linge, J. P., O'Donoghue, S. I., and Nilges, M. (2001). Automated assignment of ambiguous nuclear overhauser effects with ARIA. Methods Enzymol *339*, 71-90.

Tjandra, N., and Bax, A. (1997). Measurement of dipolar contributions to 1JCH splittings from magnetic-field dependence of J modulation in two-dimensional NMR spectra. J Magn Reson *124*, 512-515.

Wüthrich, K. (1986). NMR of proteins and nucleic acids Wiley-Interscience.

Zuiderweg, E. R. (2002). Mapping protein-protein interactions in solution by NMR spectroscopy. Biochemistry *41*, 1-7.

7 Appendix II – Additional data

7.1 Mass spectrometry

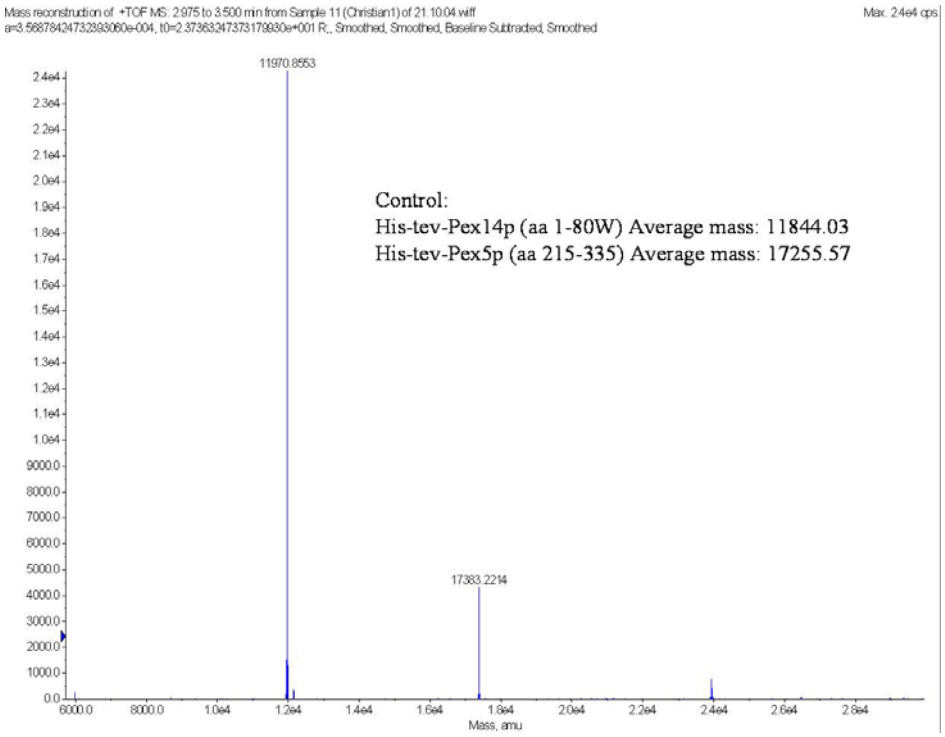

Fig. 7.1 undigested control

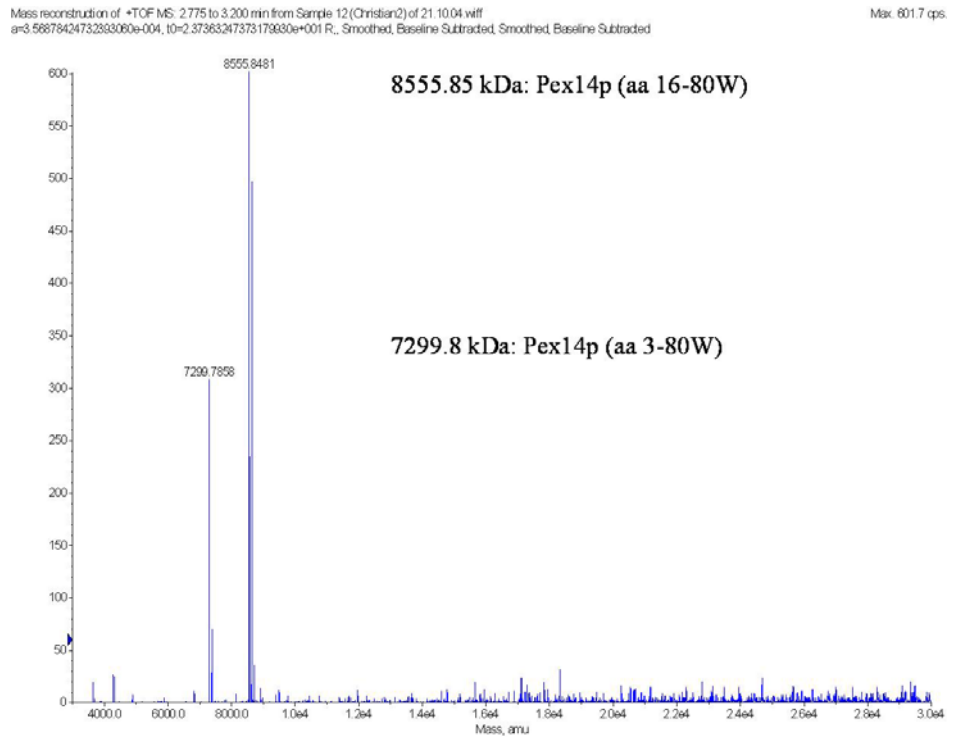

Fig. 7.2: N-terminal digestion

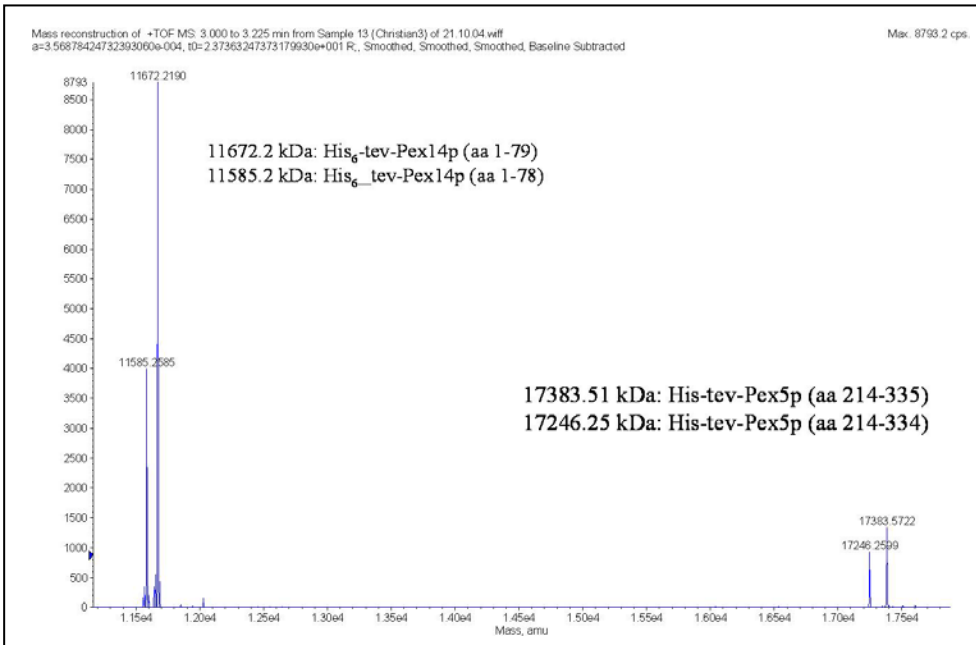

Fig 7.3: C-terminal digestion

7.2 Additional Spectra

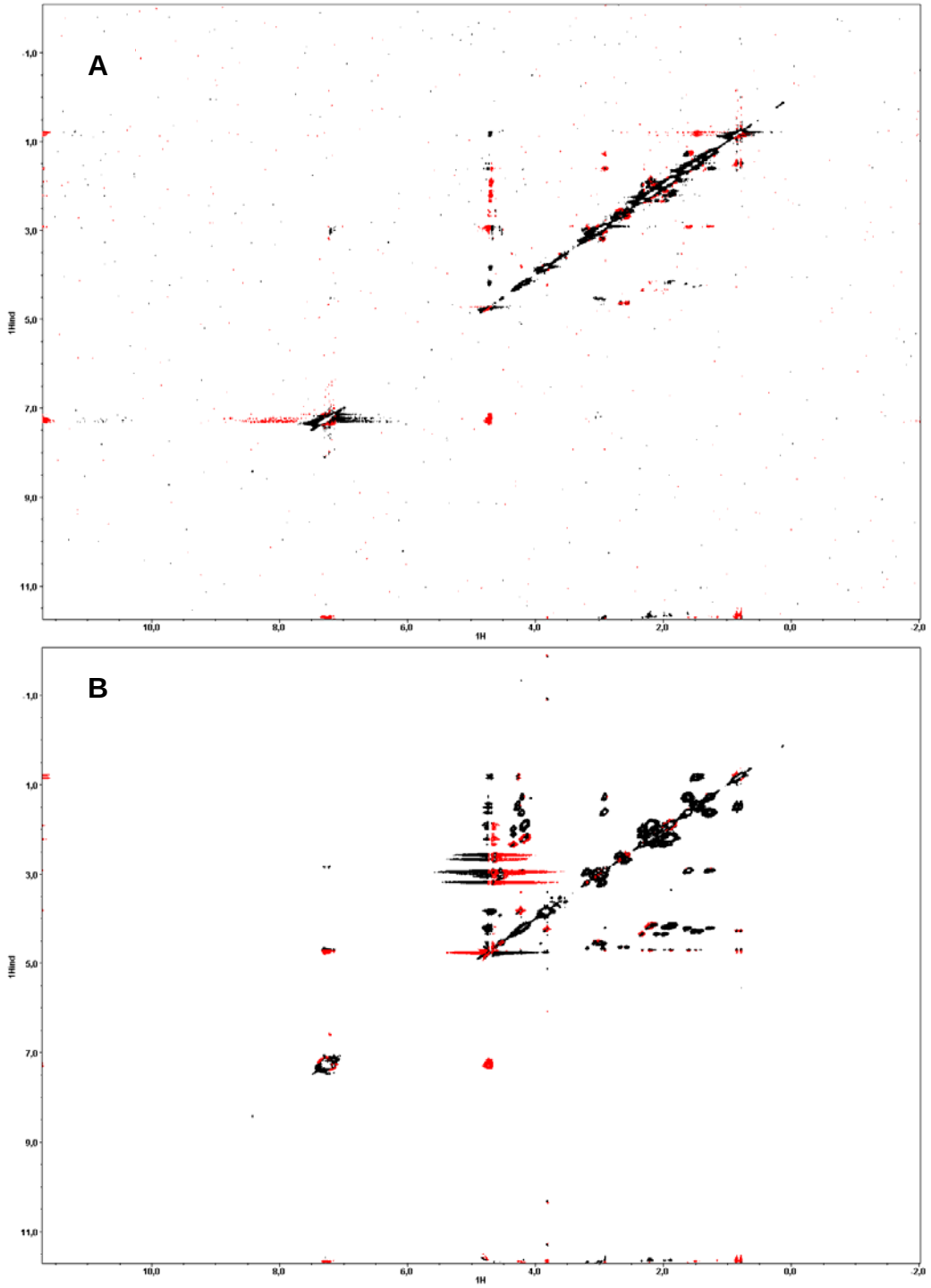

Fig 7.4: $^{1}H^{1}H$ NOESY (A) and TOCSY (B) spectrum of free Pex19p (aa 66-77) in D_2O at 500 MHz and 303K. Mixing times were 500ms (NOESY) and 80ms (TOCSY) respectively. Black color indicates positive, red color negative peak intensities. Only intraresidual NOEs can be observed

Acknowledgements

I am very grateful to MatthiasWilmanns for giving me the opportunity to work in his group, for his contagious enthusiasm and the inspiring discussions. Many thanks go to Michael Sattler for generously hosting me in his laboratory for extended periods and giving me the great opportunity to learn about NMR.

I would like to thank the member my thesis advisory committee, Irmi Sinning, Paul Tucker and Elisa Izaurralde

Special thanks go to our collaborators Wolfgang Schliebs and Marc Fransen who kindly helped with material, useful suggestions and excellent discussions

Many people supported me in different ways during the last years. The members of Michael's lab have always welcomed and helped me, when I was there but often also at a distance. Particular thanks go to Bernd Simon and Cameron McKereth for helping me with various NMR problems and Fabian Filipp. I would like to thank the entire outstation staff, especially Young-Hwa Song, Eleni Mumtsidu and the people from the Pex-team, Nicole Schüller, Kumiko Shiozawa and Will Stanley. Many thanks go to Karen Henning for her friendship and support.

Finally, I would like to thank my family for their love and support.